The synthesis and characterization of novel precursors for the CVD of main group metal phosphides

Apostolico, Leonardo

Award date:
2003

Awarding institution:
University of Bath

THE SYNTHESIS AND CHARACTERIZATION OF NOVEL PRECURSORS FOR THE CVD OF MAIN GROUP METAL PHOSPHIDES

Submitted by Leonardo Apostolico
for the degree of PhD
of the University of Bath
2003

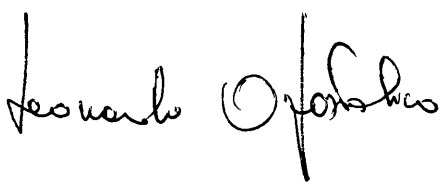

ProQuest LLC
789 East Eisenhower Parkway
P.O. Box 1346
Ann Arbor, MI 48106-1346

to Lorena

ABSTRACT

The syntheses and characterizations of germanium and tin compounds as novel single–source precursors for the deposition and growth of thin films of metal phosphides have been investigated and described in this thesis.

1:1 reactions of germanium(IV) chloride with primary and secondary phosphines have been studied and formation of crystalline salts, *i.e.* $[GeCl_3]^-[CyPH_3]^+$ and $[GeCl_3]^-[Ph_2PH_2]^+$, have been observed. Employment of a large excess of $GeCl_4$, instead, facilitates the complete consumption of phosphine and promote the synthesis of chlorogermyl phosphines $Cl_3GeP(R)H$ which have been investigated and fully characterized. Their suitability as precursors for the CVD of thin films of germanium phosphide is also reported.

The successful syntheses and characterization of organogermyl phosphides from organogermyl chloride ($R_{4-n}GeCl_n$ with n = 1, 2 and R = Ph, Et) and Me_3SiPPh_2 are reported. Decomposition of the materials to germanium phosphide films has been ascertained.

Reactions of tin(IV) halides with primary, secondary and tertiary phosphines are reported. Formation of crystalline salts deriving from redox processes have been ascertained and X–ray diffraction structures have been studied, $[SnI_4]^{2-}[CyPH_3]_2^+$, $[Sn_3I_{12}]^{6-}[Ph_2PH_2]_6^+$, $[SnI_6]^{2-}[Ph_2PH_2]_2^+$, $[SnI_3]^-[Cy_3PI]^+$, $[SnI_5]^-[Cy_3PI]^+$, $[SnCl_5 \cdot THF]^-[Cy_3PH]^+$. In only one case, reaction of $SnCl_4$ with Cy_3P has the formation of an adduct, $SnCl_4 \cdot PCy_3$, been noted and which has been fully characterized and employed as single–source precursor for the deposition of SnP films.

Finally, preparation of Ph_3SnPPh_2 *via* different routes is described. Ph_3SnPPh_2 has been fully characterized and used as precursor for the CVD of tin phosphide. Synthesis of $^tBu_3SnPPh_2$ has been attempted but failed to deliver a pure product that could not be isolated.

All the films produced have been studied by scanning electron microscopy and energy dispersive X–ray analysis.

ACKNOWLEDGEMENTS

Above all, I owe my gratefulness to my supervisor Prof. Kieran Molloy, who has introduced me into the world of *curry* and who has been constantly present throughout my Ph.D. with his guidance and support. There wasn't a single day in which I haven't learnt from him and if now I am a better chemist, I owe it to him. Thank you.

To my colleagues of Lab 1.35, who I have spent many hours of these years with, for the enjoyable time and for their help anytime I needed it. Not to forget all the times we've been out together. In particular to Purvi, for the great time and fun I had to share the lab with her.

To Dr Mike Whittlesey, also my internal, for his assistance and advices with my NMR spectra. To Dr Mary Mahon and Gabi Kociok–Köhn for the crystal structures and data reported in this thesis. To all the technical staff, in particular Alan Carver for the enormous patience he has demonstrated to me and to my *load-in-the-dry-box* samples, and Hugh Perrott for his helpfulness with the SEM and EDAX analyses.

To all my international friends and in particular to Antonella, Hubald (Ubaldo de Gubio) and Karen. We have spent together so many days and nights, dinners and parties. Superb shots of life that will remain impressed in my mind forever.

To my friend Emanuele (Superemanuele) for his unconditional friendship and all the nights out in Bristol. His trips to Bath have been like eating Nutella from the 5Kg jar. "Ma che c'hanno messo dentro...i toni?". To my friend Gabriele (Gabo) for his "failed" attempt to come to Bath, and his funny and hilarious emails all over these years. We'll write a great *best seller*, one day.

To Something Corporate, whose awesome music kept me company during the long days and nights I've been writing this thesis. I had the pleasure to see you live in Bristol and I got to say that you *rock*, guys! And to Christin (ricciolina rossa), who shares with me this passion for their music, for the *fab* person she is. "...and I've taken 18 showers just to pass the time, and the f*****g phone just rang. It wasn't you on the line..."

A Lorena ed alla famiglia Satiri per tutto l'amore e l'affetto che mi hanno constantemente dimostrato. Per le lunghissime ed indimenticabili telefonate e tutto il grande sacrificio che esse hanno significato.

Infine, un immenso grazie alla mia famiglia (mamma, babbo, Stefania, i nonni e Sofia) per il loro sconfinato amore e supporto che non è mai cessato durante questi anni. Ma in particolar modo, per essere la mia FAMIGLIA.

ABBREVIATIONS

AACVD : Aerosol Assisted Chemical Vapor Deposition

APCVD : Atmospheric Pressure Chemical Vapor Deposition

br m : broad multiplet

^{n}Bu : Buthyl

^{t}Bu : Buthyl

CIVPE : Chloride Vapor Phase Epitaxy

Cat : Cation

CN : Coordination Number

CVD : Chemical Vapor Deposition

Cy : cyclohexyl

d : doublet

dbu :1,8-diazabicyclo[5.4.0]undec-7-ene

DCM : dichloromethane

dd :doublet of doublets

dfdh :tetradecafluorononadionate

dpm : dipivaloylmethane

dppe : 1,2 bis(diphenylphosphino)ethane

dppf :1,1 bis(diphenylphosphino)ferrocene

dppm :1,2 bis (diphenylphoshino)methane

depe :1,2 bis(diethlylphosphino)ethane

DLICVD : Direct Liquid Injection Chemical Vapor Deposition

EDAX : Energy Dispersive X-Ray Analysis

Et : Ethyl

hfa	:hexafluoroacetylacetone
HVPE	: Hydride Vapor Phase Epitaxy
LPCVD	: Low Pressure Chemical Vapor Deposition
Me	: Methyl
MOCVD	: Metal Organic Chemical Vapor Deposition
m.p.	: melting point
NMR	: Nuclear Magnetic Resonance
OMVPE	: Organo Metallic Vapor Phase Epitaxy
PACVD	: Plasma Assisted Chemical Vapor Deposition
PECVD	: Plasma Enhanced Chemical Vapor Deposition
Ph	: Phenyl
ppm	: parts per million
iPr	:isopropyl
^{n}Pr	: *normal*-propyl
PVD	: Photochemical Vapor Deposition
s	: singlet
SEM	: Scanning Electron Microscope
THF	: Tetrahydrofuran
TGA	: Thermo Gravimetric Analysis
XPS	: X–ray photoelectron spectroscopy

CONTENTS

CHAPTER ONE

Introduction

1.1 Metal Phosphides

Transition metal–nitrides form some of the most technologically important coatings. Among these, the titanium nitride is often used as a hard coating, diffusion barrier[1] and as solar control coating.[2,3] These nitrides also show similar hardness and wear–resistance properties and have found widespread industrial usages.[4] Despite the fact that metal phosphides have similar physical properties to nitrides – including hardness, wear resistance and reflectance[5] – they have received scant attention.

Almost all metals form phosphides and more than 200 different compounds are known. Their composition range varies broadly between M_3P and MP_3. It is only during the last 40 years that these metal phosphides have begun to be properly characterized and obtained in a quite high state of purity, which has been important to enable the measurement of their properties. The chemical purity of phosphides is important because impurities can have drastic effects on their chemical and physical characteristics, particularly electrical properties. Many of them are high melting point materials and can exhibit a large variation of porosity, which can also affect their properties. The density of metal–rich phosphides is the highest amongst the phosphides and it arises from the presence of the heavy metal atoms and the efficiency with which they pack with the phosphorus atoms in the crystal lattice.

Table 1.1 Melting Points of Some Metal Phosphides (°C)

Compound	mp(°C)	Compound	mp(°C)	Compound	mp(°C)
Fe_3P	1166	Fe_2P	1365	Rh_2P	1500
Cu_3P	1023	Co_2P	1386	Ca_3P_2	1600
Pd_3P	1047	Ni_2P	1110	MnP	1193
Ni_3P	970	Mn_2P	1327	CrP	1800
Mn_3P	1229	Ti_2P	1920	VP	1315
TiP	1100	AlP	1800	GaP	1522
NbP	1729	ReP	1204		

Phosphides show a wide range of crystal structures and differ greatly in their physical and chemical properties. Bond type is often uncertain. They usually have a melting point above 1000°C (Table 1.1), except those with high phosphorus content.

Metal–phosphides can be classified into three types:

Metal–rich phosphides: they are typically hard, brittle with high electrical and thermal conductivity. The transition metal phosphides are dark colored, insoluble in water and dense. These properties are the same shown by the corresponding borides and silicides, to which they are often structurally related. These phosphides of the transition metals have, in general, a common structural feature that is nine–fold (tetrakaidecahedral) arrangement of the metals around the phosphorus atom (Fig 1.1a). The metal phosphorus distances are those typically of covalent bonds and are arranged in various patterns where the metal–metal distances are longer than in the corresponding pure metals.

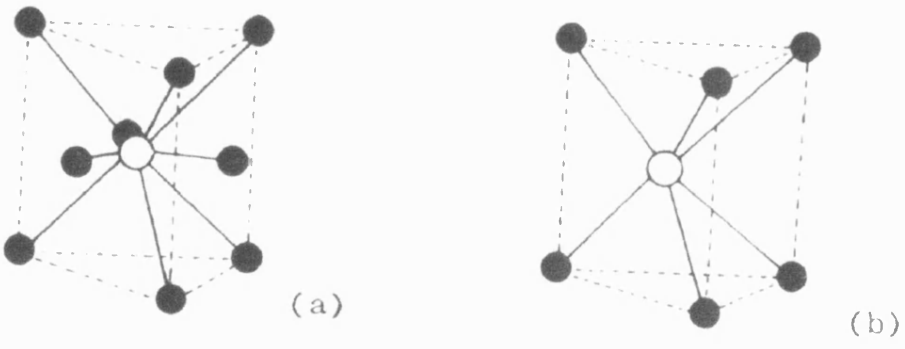

Fig. 1.1 Crystal Structures of the Phosphides. a) Fe_3P fragment, b) Fe_2P fragment. Empty circles represent P and plain circles represent Fe.

There are no covalent P–P linkages. In some other metal–rich phosphides, one or more of the equatorial sites may be unoccupied, resulting in an 8, 7 or 6 coordination of the phosphorus atoms. The 6–fold trigonal prismatic coordination occurs in some monophosphides (Fig. 1.1b). Amongst the

transitional metal phosphides, there are the non–stoichiometric compounds. This phenomenon is supposed to be associated with the vacant lattice sites where P atoms are missing. Palladium phoshides, Pd_3P, can have any composition in the range $Pd_3P_{0.75}$ – $Pd_3P_{1.00}$, and cobalt phosphides in the range Co_2P – $Co_{1.75}P$.

Monophosphides: most of the monophosphides, MP, where M = Ti, V, Cr, Mn, Fe, Co, Ru, W, Zr, Nb, or Ta, are greyish black and have very high melting points and densities. Three types of symmetrical hexagonal structure are found amongst these compounds. The bond is part metallic and part covalent and there is a trigonal prismatic coordination of the phosphorus by the metals. Most of these compounds are hard, chemically inert and resistant to oxidation at high temperature. The MP materials do not only have a trigonal coordination, however, but can also adopt a tetrahedral one, where each atom is coordinated by atoms of the opposite kind in a cubic zinc blend–type structure (Fig. 1.2).

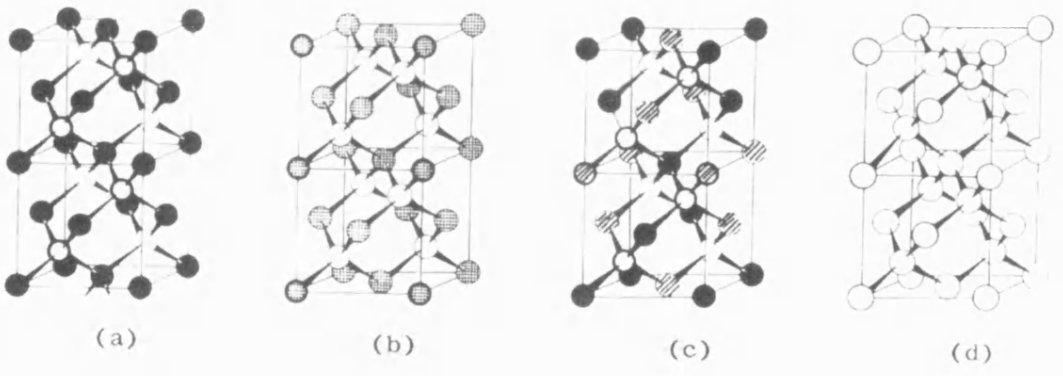

Fig. 1.2 Crystal Structures of Diamond type Phosphides. a) AlP, b) BN, c) $ZnSiP_2$, d) diamond (or silicon).

These MP species are also hard and have high melting points and important semiconductor properties. The difficulties in obtaining these monophosphides with the necessary purity have limited their commercial use.

Finally, monophosphides of the elements Ca, Sr, Y, Sc, and the lanthanides La to Th all crystallize with an ionic–type structure, showing that they are assemblies of anion and cations.

Phosphorus–rich materials: they are potential semiconductors. These compounds contain polymerized P atoms and do not form ions. In their structures each P atom is covalently bonded to at least one other P atom and up to three metal atoms in a tetrahedral configuration. On heating, these compounds lose phosphorus and revert to a monophosphide or a metal–rich phosphide. Semiconductor properties are frequently found amongst these materials.

Dimeric, covalent P–P units are found in PtP_2, NiP_2, SiP_2, FeP_2, OsP_2 and RuP_2. Square four–membered rings of P atoms occur in MP_3 type phosphides where M = Co, Ni, Rh, Pd. Chains of polymerized P atoms are found in Ni_3P_2, Ir_2P_4, Sn_2P_6, PdP_2, NiP_2, ZnP_2, TiP_2 and CdP_2. Some examples are shown in figure 1.3.

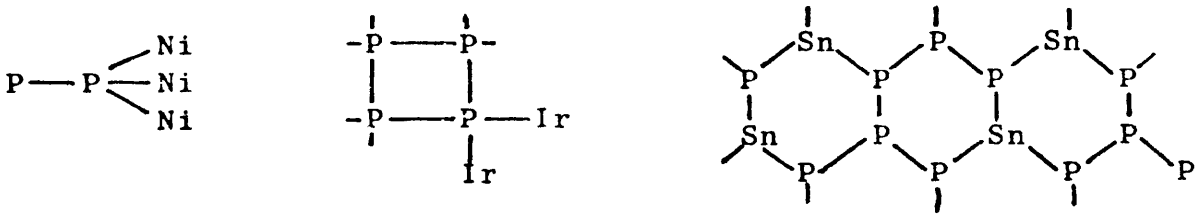

Fig. 1.3 Three example of phosphorus–rich phosphides.

The phosphorus–rich phases are typically thermally and chemical unstable, whereas the metal–rich and monophosphides are usually hard, refractory materials with relatively high electrical conductivities.[6]

1.2 Metal Phosphides Synthesis

The preparation of metal phosphides is a problem in science and engineering at present.[7] Traditionally, these phosphides have been synthesized by elemental combination at high temperatures, by reaction of a metal or metal halide with PH_3 or by thermal decomposition of a higher metal-phosphide. However phosphine (PH_3)[8] used as phosphorus source is difficult to handle because it catches fires in air and is extremely toxic. They can also be made by direct union of the elements *in vacuo* or protective atmosphere under conditions that prevent loss of phosphorus.[9]

$$\mathbf{3Li + P \rightarrow Li_3P} \qquad \textbf{(Eq. 1.1)}$$

In special cases they may be synthesized by reaction of phosphine with an oxide (e.g. $Ga_2O_3 + 2PH_3 \rightarrow 2GaP + 3H_2O$)[10] or metal chloride (e.g. $3ZnCl_2 + 2PH_3 \rightarrow Zn_3P_2 + 6HCl$).[11]

Another synthetic route is the reaction of anhydrous metal halide with sodium phosphide.[12,13]

$$\mathbf{Na_3P + MCl_3 \rightarrow MP + 3NaCl} \qquad \textbf{(Eq. 1.2)}$$

Bulk metal phosphides have been prepared from the reaction of a metal with Ca_3P_2.[14,15] Kaner *et al* have shown that a range of metal phosphides can be made by the solid–state metathesis reaction of MX_4 (M = Ti, Zr, Hf and X = Cl, Br) and Na_3P.[16] The metathesis procedures allow the formation of both the thermodynamically more stable hexagonal phase as well as cubic phases.

1.3 Applications of Metal Phosphides

Transition metal phosphides, MP_x ($x \leq 1$), have attracted attention as commercially and industrially important materials in fields such as wear and corrosion resistant coatings. They are metallic conductors, hard, refractory and in some case resistant to oxidation.[17,18] Despite this, they have found a limited use as catalysts [19] and as diffusion barrier layers in semiconductors.[20]

Currently, despite the fact that metal phosphides are semiconductors with band gap in the range 1.3 – 2.0 eV., only GaP and InP have been extensively studied and have been applied as LEDs, in solar–energy cells, as photovoltaic cells and as field effect transistors. Cu_3P is hard, dense, brittle and electrically conducting. Rh_2P and Ir_2P are hard and inert and the latter has been used for fountain pen tips. Schreibesite, $(Fe, Ni)_3P$, has been found in meteorites and lunar samples and constitutes a rare example of a reduced phosphate mineral. CuP and SnP are used as deoxidants in the preparation of metals and to increase the wear resistance. Fe_3P and Fe_2P, have been utilized to improve the metallurgical properties of steels and they are employed to produce a material known as *ferrophosphorus,* which contains both the species. It is formed as a by–product in the production of elemental phosphorus by the electric furnace method.

1.4 Chemical Vapor Deposition

1.4.1 Introduction

Chemical Vapor Deposition (CVD) can be simply defined as a material synthesis method or process where gaseous species are used and employed in the formation of a solid state material. Thus, the occurrence of the chemical reaction is an essential characteristic of the CVD method.

The growth of thin films by CVD has become one of the most important methods of film formation. The reasons for the rapidly growing importance of CVD in the past decades lie primarily in its versatility for depositing a very large variety of elements and compounds at relatively low temperatures and with a high degree of purity and perfection.[21] It also offers the advantages of mild process conditions, *i.e.* control over microstructure and composition, high deposition rates and possible large scale processing. The chemical vapor deposition process, however, requires the transport of a volatile precursor to a reaction zone where deposition takes place. Once the reaction allows the precursor to decompose on the target material, a deposition has taken place. [22]

Other unique advantages of CVD over other methods of film formation are the relative ease for creating materials of a wide range of accurately controllable stoichiometric composition and layer structures that are difficult or impossible to obtain by other techniques, like sputter deposition, spray pyrolysis, plasma polymerization and ion plating.

For a CVD to provide the desired final material, a suitable precursor must be found *i.e.* the precursor must have the right properties and characteristics. It should have reasonable volatility at a particular temperature, thermally stable over extended periods, and a high purity level. It should also decompose cleanly.

Although the CVD process is quite general, there is a wide range of specialized techniques available which involve variations in the method used for the precursor delivery.

1.4.2 Chemical Vapor Deposition Techniques

In general, chemical vapor deposition is selected for its application as a high throughput, non–line–of–sight and low cost per unit processing technology. The competing technologies which employ high vacuum conditions (e.g.

molecular beam epitaxy) generally have higher cost investment items, and lower throughput per unit time production techniques. Other techniques, such as sputtering, are thought to be inapplicable to large substrate areas. It is the chemical vapor deposition technique which has emerged as the premier candidate for thin film growth for its uniform thickness, elemental composition coverage, large substrate area and non–line–of–sight.

Several chemical vapor deposition techniques have been employed for the growth of a variety of materials. Aerosol–Assisted Chemical Vapor Deposition (AACVD), Low Pressure Chemical Vapor Deposition (LPCVD), Atmospheric Pressure Chemical Vapor Deposition (APCVD), Plasma Chemical Vapor Deposition (PCVD), Photochemical Vapor Deposition (PVD) are the most common and the most used and an explanation of these techniques will be given in the next pages. Other vapor deposition techniques include chloride vapor phase epitaxy (ClVPE), hydride vapor phase epitaxy (HVPE) and organometallic vapor phase epitaxy (OMVPE). Consistent with traditional chemical nomenclature, the term organometallic describes precursors that contain a direct metal–carbon bonding interaction. Widely accepted alternatives, in contrast, include metalorganic as description for any compound in which a metal is bonded to an organic containing ligand for CVD.[22] Each technique has intrinsic strengths and weakness, as well as specific advantages for special applications.

1.4.2.1 Atmospheric and Low Pressure Chemical Vapor Deposition

The change in pressure in chemical vapor deposition is to guarantee either greater uniformity of substrate coating or to increase deposition of a coating on an underlying substrate. Pressure modifications are restricted to the range between a few tenths of a Torr and one atmosphere.[22] While with APCVD is easier to engineer where large scale coverage is required, LPCVD permits use of less volatile precursors.

The deposition of thin films by chemical vapor deposition at atmospheric pressure (APCVD) was a widely accepted process during the seventies when the first equipment for low pressure CVD (LPCVD) was introduced. In the following years LPCVD became the preferred method for chemical vapor deposition of thin films. The reason of this change in methods was mainly due to a superior film quality, greatly reduced processing cost and increased throughput. The fundamentals of films deposition at low pressure are basically the same as for those deposited near atmospheric pressure. The major difference is the rate of mass transfer of the gaseous reactant and by–product species relative to their surface reaction rate to form the film deposit.[21]

Compared to thin films deposited by APCVD, LPCVD films have better thickness uniformity, superior structural integrity with fewer pinholes, better conformability, better step coverage, fewer particulate contaminants and finer surface texture.[23] All these improvements can be directly traced to either the reduction in gas pressure or to the particular design of the process reactor. The higher pressure of the APCVD process promotes gas phase reactions that produce particulates that can readily create defects on the film.[24] In LPCVD, the lower pressure inhibits the gas phase reactions, hence the deposits on the reactor wall are well adherent and do not tend to flake off, which would lead to particles with consequent substrate contamination.

Reactions involving hazardous or toxic vapor phase precursors are operated at reduced pressure from a safety perspective.

1.4.2.2 Aerosol–Assisted Chemical Vapor Deposition

The widely used method of aerosol–assisted chemical vapor deposition (AACVD) is based on flash evaporation of an aerosol. A sweep of a carrier gas is used to transfer an aerosol of a precursor–containing solution into the hot zone of a reactor. This method has been planned for compounds of low volatility and thermal stability. The precursor is dissolved in a solvent and the solution is

atomized or vaporized into a gas carrier stream. The production of the aerosol is due to the use of an ultrasonic technique.[25,26]

The aerosol delivery has several advantages over bubblers or liquid delivery systems. The precursor, being held outside the reactor at room temperature is not subject to premature thermal degradation. Rates of transfer of the aerosol to the evaporator remains constant and this are because the aerosol remains of constant composition with time.[27] This allows reproducible deposition of multi component films with consistent composition. Precursor vaporization occurs without contact with hot surfaces and can therefore be performed at higher temperatures, leading to a higher deposition rate.

The disadvantage is the requirement of pressures near to atmospheric, or higher, enough so that the aerosol droplets do not settle in the reactor before evaporating. A degradation of the film properties and reduced deposition rates may occur when the gas is heated at high temperatures and when high pressures favor gas phase reactions. Incorporation of contaminants from decomposition of the solvent is also possible.

A similar deposition technique is the DLICVD (Direct Liquid Injection Chemical Vapor Deposition), which is now widely used. It consists of a flash evaporation of a pressurized liquid through a fast micro valve. The technique provides high accuracy for the control of the vapor pressure (flow rate), which can be obtained in high values (flash evaporation). The number of injections can determine the thickness of the film. Use of thermally unstable precursors is also allowed when the source container is maintained at room temperature.

1.4.2.3 Plasma Chemical Vapor Deposition

As a deposition method, plasma–enhanced CVD (PECVD), or plasma–assisted CVD (PACVD) has been lengthily investigated and widely applied over the last decade. Prior to that, the plasma process had little commercial success because of the difficulty in controlling it and the complexity of the phenomena

involved. Plasma Enhanced Chemical Vapor Deposition causes the reactive gases to decompose via an electrical glow discharge. The discharge produces high energy electrons that impact with the precursor molecules. This causes films to deposit at lower temperatures.

One of the prime motivating factors in utilizing plasma deposition processes is that the substrate temperature can be kept relatively low, typically 300°C or lower. Conventional CVD processes usually require higher temperatures that may be inappropriate for certain substrate materials or devices structures. Potential advantages of PACVD also include a higher growth rate. Disadvantages may include lack of substrate selectivity, poorer conformality and possibly plasma induced substrate damage.[28]

Plasma are extraordinarily complex mixtures and deposition characteristics depend strongly on gas pressure, flow rate, RF power and frequency, reactor geometry and substrate temperature.

Films deposited by plasma reactions are generally amorphous. The stoichiometry of the film can be made to vary by variation of dominant parameters, such as reactant gas flow ratios. Due to this range in film stoichimetry, it is indeed observed that electrical, mechanical and chemical properties of the deposited film can also vary.

1.4.2.4 Photochemical Vapor Deposition

Photochemical vapor deposition is a direct outgrowth of the ability of short wavelength radiation ($\lambda < \sim 300$nm, $\hbar\nu = 4$eV) to rupture the chemical bonds in most CVD precursors. Photo–induced reactions in the gas phase or at the substrate may enhance film growth rates or quality. Introduction of UV photons into an MOCVD reactor gives the possibility to selectively alter the film growth kinetics.

High frequency radiation, used in CVD processes, has been named photochemical, photosensitized, photo–assisted or, collectively, photo–CVD . A simple fact of chemistry demands that there must be energy adsorption by the molecule in order for radiation to interact with either a vapor phase or a surface moiety.[22] Whatever the wavelength used, important features of photo CVD are the potential for lowering the deposition temperatures, compared with thermal CVD, and the low substrate damage compared with plasma CVD. Another advantage over both thermal and plasma CVD is the possibility of maintaining a well defined reaction volume. Finally, an important feature is that monochromatic radiation offers the potential for minimizing deleterious side reactions.

However, to date, this technique has yet to be fully exploited for commercial use and remains studied only at a research level. This may be due to the perceived lower quality of films deposited.

1.4.3 Precursors for Chemical Vapor Deposition

The factors that influence the preference of a particular precursor molecule for CVD are complex and depend on the application and the properties being considered. Some microelectronic applications require smooth surfaces, low deposition temperatures and high purity films. These conditions may not be important for other coating applications, where impurities are not disadvantageous and high deposition temperatures can be accepted.

The following properties are amongst those that must be considered when selecting materials as a good CVD precursor:

a) Good volatility to enable transport to the reactor and achieve high deposition rates.

b) Good thermal stability during its evaporation and transport in the gas phase.

c) It should decompose cleanly on pyrolysis without contamination of the growing film.

d) High level of purity.

e) It constitutes an advantage if it is not–toxic and non–pyrophoric, to enable easier handling.

f) Stable, to enable easier storage.

g) Liquid precursors are the most favorable to ensure reproducible delivery rates, but are less easy to purify than solids.

h) Availability in consistent quantity and quality at low cost.

Volatility is one of the most important properties of a precursor. It is important to achieve a reasonably high volatility to allow an adequate transport of the precursor to the deposit zone. High volatility can be achieved by introducing weak intermolecular interactions, a minimization of the polarity, minimization of the polarizability, dipoles and suppression of intermolecular hydrogen bonds. Higher vapor pressure sources are preferred to lower pressure ones. Therefore, in general, a low electro negativity difference should be present within the precursor. This results in a more covalent, hence, less ionic bonding interaction, which provides a lower dipole moment to the molecules. In general, the lower the dipole moment, the lower the intermolecular attractive forces, and the lower the latent heat of vaporization.[22] Although volatility, along with purity and clean decomposition routes have been the fundamental requirements for precursors, advances in the design of precursor delivery systems are drawing the attention to compounds that only fulfill the latter two requirements, so that chemists can concentrate only on the design of precursors without the added problem of volatility.[27]

It is known that the presence of bulky ligands in the precursor influences the volatility of the precursor itself. A systematic study on the alkoxides has established that the steric effect of the alkyl group has a controlling influence on the volatility of the metal alkoxides. Alkoxides containing less bulky group (methyl and ethyl) proved to be oligomers (e.g., dimers, trimers and tetramers)

due to the bridging property of the alkoxide group, which can be bonded through its oxygen to two or three metals.[29] Some oligomeric metal alkoxides retain their structure in the vapor phase and much more energy is required to vaporize a trimer or a dimer rather that a monomer. Alkoxyboranes, which are monomeric, $B(OR)_3$, are more volatile than aluminum alkoxides that are oligomers, $Al_4(OR)_{12}$, and alkoxysilanes, $Si(OR)_4$, are more volatile than the oligomeric titanium tetralkoxides, $[Ti(OR)_4]_n$. The monomeric metal alkoxides can be prevented by steric hindrance from intermolecular bond formation (bridging) by utilizing very bulky alkyl groups. The *tert*-alkyl groups are the best to prevent bridging and promoting higher volatility.[30]

Using fluorinated ligands is possible to get a higher volatility: the substitution of fluorinated ligands diminishes the hydrogen bonds and then fluorides are more difficult to polarize due to the minimizing of dipole–dipole interactions between molecules. $Ba(hfa)_2$[31] and $Ba(dfdh)_2$,[32] are an example of fluorinated precursors, with groups containing many lone pairs that repulse, and they ease reduction of intermolecular attraction. However, fluorinated ligands may lead to fluorine incorporation.

The use of Group 2 elements (Ca, Sr, Ba) has proven to be problematic for MOCVD due to the low volatility, poor reproducible stoichiometries and thermal stability; this is caused by the small charge – to – radius ratio. The large coordination sphere of these elements allows oligomerization to take place, so the coordination sites have to be saturated.[33] The low oxidation state prevents coordinating further β-diketoneate ligands on to the metal center so neutral ligands are required. As neutral ligand, polyethers (also called glymes) can provide the additional donor atoms (Fig. 1.4a and 1.4b). These consist of the OCH_2CH_2 repeat unit. The number of OCH_2CH_2 units as well as the R and R' end groups are both important for volatility by producing monomers, e.g. $Ba(hfa)_2$·pentaglyme, rather than oligomeric $[Ba(dpm)_2]_4$.

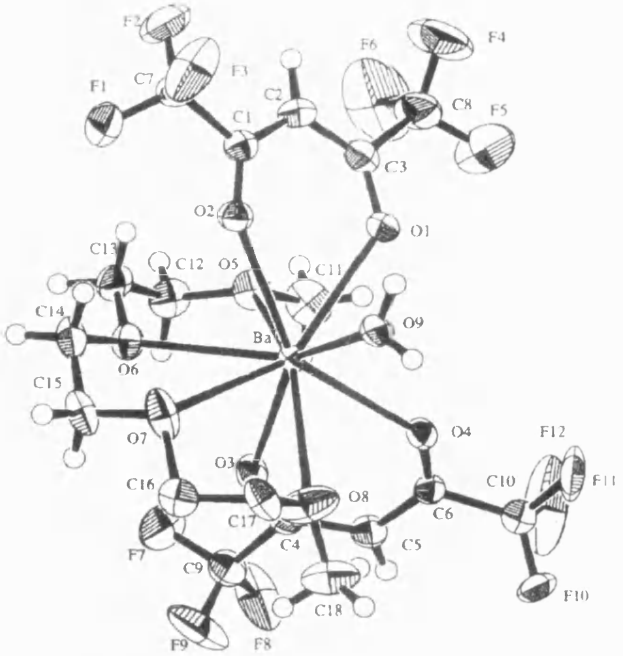

Fig. 1.4a Perspective view of the newly developed $Ba(hfa)_2$·triglyme·H_2O illustrating the atomic numbering scheme. H atoms omitted for clarity.

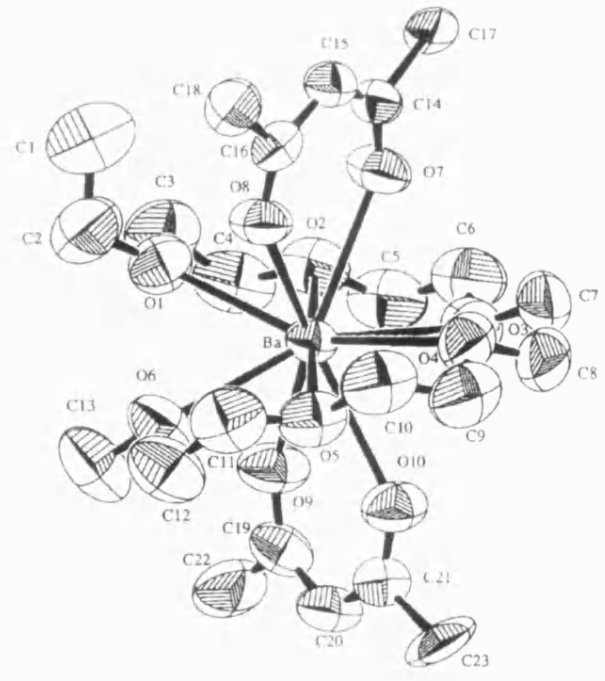

Fig. 1.4a Perspective view of the newly developed $Ba(hfa)_2$·triglyme·H_2O illustrating the atomic numbering scheme. H and F atoms omitted for clarity.

The use of new precursors designed for MOCVD processes has resulted in significant process improvement. Precursor properties and decomposition characteristic have been modified and improved, by chelating β–diketonate ligands or donor functionalized alkoxide groups.[34] To date, only commercially available ligands have been used for the synthesis for precursors. In the future, it is most likely that we will see the growing use of designed ligands to tune precursor properties in order to have films with the desired properties.

A significant problem with the use of organometallic compounds for CVD is the potential presence of the impurities in the final film, *i.e.* carbon incorporation. From a practical point of view, MOCVD precursors must often satisfy the conditions of producing films of extreme purity. It is of primary importance in controlling the optical and electrical properties that determine in turn their technological usefulness. The use of these precursors can convey high quality and novel properties to semiconductor materials. To minimize impurity incorporation, ligands that give volatile by–product that is easy to desorb from the surface, are preferred. Traditionally, the alkyl groups attached to the metal center have to be relatively small with just few carbon atoms. Ethyl or tertiary butyl groups, although bulky and contributing to minimize molecule aggregation, have the potential to incorporate carbon in the growing film. However, they are often chosen because they undergo a β–hydrogen elimination mechanism that cleaves the metal–carbon bond, since this is the weakest bond in the molecule. In the β–elimination reaction hydrogen, a metal alkyl complex is converted into a metal hydride and either a cooordinated or free alkene. The mechanism proposed is shown in figure 1.5.

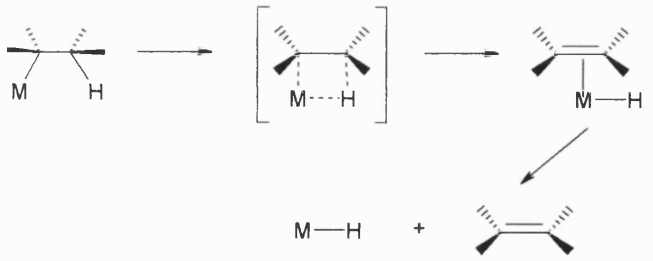

Fig.1.5 β-Hydrogen elimination pathway

The reaction is thought to proceed through a planar, four co–ordinate metal–alkene hydride intermediate. The hydrogen atom on a β-carbon of a co–ordinated alkyl group is then transferred to the metal centre, forming a hydrido-metal alkene complex. This complex can, in turn, lose either an alkene by dissociation or displacement or an alkane by a reductive elimination step.

Toxicity issues are also crucial in the choice of the CVD precursor and are the major problem relating to the use of PH_3 (560 mg/m^3 is lethal in 60 minutes, 2.8 g phosphine/m^3 is lethal in a short time) and AsH_3 (0.6 mg/kg/d is lethal in few hours) in CVD.

The general observation that the best quality material corresponds to the highest purity of precursors has stimulated efforts designed at finding very efficient purification methods and clean preparative routes.[35] One method for their purification is by the so–called adduct route, where in general the precursors form an adduct characterized by a coordination bond rather than a covalent one; generally a coordination bond shows a strength lower than a covalent bond. Combination of trimethyl or triethyl derivates of Al, Ga and In (e.g., Me_3Ga, Me_3In and Et_3Al) with Lewis bases of the type R_3P (e.g., Me_3P, Et_3P and Ph_3P) and R_3As (e.g., Ph_3As, Me_3As) give products that, due to the saturation of the coordination of the central metal, are more resistant to hydrolytic decomposition and oxygen attack than the metal alkyls (e.g., Me_3GaPMe_3). Also, since they contain P and As in addition to the metal, it was estimated that these molecules could act as single–source precursors for metal pnictides and thus avoid the need for AsH_3 and PH_3 as separate precursors. Solid adducts are both more stable but crucially are easier to purify (by crystallization).

1.4.4 Dual and Single – Source Precursors

The MOCVD process is quite complex and involves both gas–phase and surface reactions (catalysis). It consist of several steps:

a) Evaporation of reagents (precursors),

b) pyrolysis of precursors and reaction of decomposition fragments to give the desired material and

c) elimination of side reactions and unwanted products (e.g. carbon).

The growth of GaAs from trimethylgallium ($GaMe_3$) and arsine (AsH_3) precursors in a carrier gas at atmospheric pressure can be given as an example of dual–source CVD, where one precursor is used for each component, as is shown in the following examples.

$$\mathbf{AsH_3 + GaMe_3 \rightarrow GaAs + 3CH_4} \qquad \textbf{(Eq. 1.3)}$$

Further examples of dual–source approach are.

$$\mathbf{H_2S + Me_2Zn \rightarrow ZnS + 2CH_4} \qquad \textbf{(Eq. 1.4)}$$

$$\mathbf{PH_3 + Me_3In \rightarrow InP + 3CH_4} \qquad \textbf{(Eq. 1.5)}$$

In principle the precursors must be extremely pure and characterized by suitable volatility and by pyrolytic decomposition mode leading to the formation of only one solid compound (e.g. InP). The other side product must be gaseous at the reaction temperature in order to be easily eliminated form the system.[36] Trimethyl and triethyl derivates of Al, Ga and In in combination with PH_3, AsH_3 and SbH_3 have been employed for the preparation of III – V semiconductor materials.

Limitation of this method can be serious, especially the need of relatively high temperatures to volatilize material. Chemical transport can lower the optimum growth temperature, but the carrier itself may be a problem. For compound semiconductors a major problem is often that non–stoichiometry

results from the high growth temperature required.[37] Other problems may occur from matching the vapor pressures of each component as they have different volatilities. Limitations are also given by pre–reactions, *i.e.* the two precursors react before reaching the substrate.

The concept of the single–source precursors is relatively new, considering that only in the last ten years has been seen a significant increase in this field. The concept is relatively simple compared to the huge amount of potential it offers.

The precursor contains all the required constituents of the film and during the vapor deposition process all the undesired materials are lost to give the coating with a particular stoichiometry, hence the term single–source.

Use of a single–source precursor technique for film deposition has several advantages.

a) No separate dopants are required; in this way the procedure has less parameters to take into consideration and to perfect.
b) Increase the film reproducibility.
c) Costs are important: less material means less cost.
d) The precursor can be engineered to produce a specific film, rather than relying on separate dopants to achieve the correct dopant concentration.
e) No problem of pre–reaction.

But, with the single–source technique, there could be some possible problems.

a) It may not be possible to synthesize a compound containing all the required elements in their specific ratios.

b) Precursor composition does not always transfer directly to resultant film stoichiometry.

c) A cost problem. It would be extremely expensive to adapt existing large scale production plants to a new technology.

As an example of single–source versus a dual–source approach, we can choose the formation of the InP film. Me_3In reacts with PH_3 giving InP and CH_4, in a dual–source approach. The same compound can be obtained by using the single–source precursor Me_2InPR_2. The advantages using a single–source approach are:

a) The stoichiometry of the precursor can be retained in the film.

b) The precursor delivery film can be simplified.

c) Obtaining a better homogeneity because the elements are pre mixed at the molecular level

There has been a vast increase in the amount of research conducted on single–source precursors in recent years. Example of the single–source precursors used to produce thin film has been explored recently [e.g., $Me_3GaP(^tBu)H_2$, $Me_2InP(^tBu_2)_2$, Me_2InNMe_3, $Cd(S_2PMe_2)_2$, $Et_2InS_2CNEt_2$, $MeZn(Se_2CNEt_2)$].[38-41] Metal chalcogenide complexes have attracted the attention of single source methods [e.g., $Zn(S_2COCHMe_2)_2$][42,43] and group 13–antimonides [e.g., $Et_3GaSb(SiMe_3)_3$ and $(MeSiCH_2)_3InSb(SiMe_3)_3$].[44]

Heterobimetallic complexes have also been developed as single–source precursors to both mixed metal[45] and mixed metal oxide films.[46] It can therefore been seen what enormous potential there is for the future in this exciting new field of chemical vapor deposition.

1.5 Metal Phosphides Thin-Film

The limited disposal of phosphorus–containing precursors is one of the reasons why there has been a lack of development in making metal phosphides thin film coatings.

Adducts involving primary and/or secondary phosphines which facilitate the elimination of hydrogen halide during the film growth process are particularly important. In many cases the approach is dual–source, in which a key assumption is the formation, at some point in the CVD process, of a P:→M donor interaction which survives the thermal decomposition which removes ancillary groups and delivers the two bonded components to the substrate. In other cases, pre–formed adducts are used in which the P:→M interaction is establish *a priori*.

Previously in this chapter, the differences between dual and single source precursors have been stated. It has been found that wherever is possible, the single–source precursor approach has to be preferred to the dual–source one. Single source precursors, which contain pre–formed M–P bonds, could offer several potential advantages over the dual–source routes, including lower deposition temperatures and easier handling of the precursor. To our knowledge, the first single–source precursor to TiP thin films to be reported has been the adduct material $TiCl_4(PH_2Cy)_2$[47] which enabled growth of $TiP_{1.1}$ films on glass and silicon substrates at 400–600°C by LPCVD (low pressure chemical vapor deposition). The authors stated that the single source route is preferable because of control of film stoichiometry and the difficulties associated with dual source CVD.[48]

Niobium phosphide (NbP)[49] and chromium phosphides (CrP)[50,51] have been produced by single–source precursors using LPCVD [e.g., $(CyPH_2)_4Nb_2Cl_8$ and $Cr(CO)_5(PH_3)$]. Molybdenum and tungsten analogues also afforded films under low pressure conditions at 200–350°C.[51]

While titanium nitride coatings have been synthesized from a range of single and dual–source precursors,[52-56] titanium phosphide coatings have, in contrast, seen very little exploration. Thin films of TiP have been prepared by chemical vapor deposition (CVD) involving the gas phase reaction of $TiCl_4$ and PCl_3 under an atmosphere of hydrogen and argon at 850–1050°C.[17,18] This route requires high reaction temperatures that in turn limits the choice of substrate used in the film deposition process. Sasaki prepared films of composition TiP through Ti_4P_3 by reacting titanium plates with phosphorus at 650–900°C.[57]

Motojima and co workers have successfully reported the preparation of films of the early transition metals; TiP, β–NbP, β–TaP, MoP and WP [18] have been made by using the dual–source precursors system consisting of the respective metal chloride, phosphorus trichloride at 350 – 500°C.

More recently, the first dual–source APCVD (atmospheric pressure CVD) route to TiP coating on glass from the reaction of TiC_4 and three RPH_2 ($^tBuPH_2$, Ph, Cy) at 500-600 °C, has been reported.[58] This synthesis has offered a facile route to high quality TiP coatings, giving fast growth rates and can be readily adapted to coating large substrate from commercially available reagents. These thin films are silver, slightly phosphorus–rich, electrically conducting and largely impervious to attack by common solvents. They are also hydrophobic and have metallic properties, according to electrical conductivity measurements.

In a recent work,[59] thin films of TiP have been achieved using precursors from the synthesis of $TiCl_4$ and several phosphines ($CyPH_2$, Cy_2PH, PCy_3, dppm). From the work, also results that the complexes with primary and secondary phosphines ($CyPH_2$, Cy_2PH) are superior titanium phosphides precursors.

As phosphorus source, $(Me_3Si)_3P$ has been used in the dual–source CVD reaction with $TiCl_4$ leading to the deposition of titanium phosphides film of highly

purity.[60] The film is hard, chemically resistant and shows metallic–like conductivity and reflectance.

Formation of molybdenum phosphate (MoP) [61] from the reaction of $MoCl_5$ and $CyPH_2$, by APCVD, has been reported recently and shows a new route to thin films of molybdenum phosphides.

InP thin film can be achieved using the new precursors pentamethylcyclopentadienylindium(I) and phosphorus at low temperatures.[62]

Being stimulated by this lack of a low cost route to a material with potentially important commercial applications, TaP thin film has been produced using APCVD techniques.[63] Both crystalline and amorphous forms could be grown dependent on the substrate temperature. The ease of film production, the low temperature of deposition combined with the inherent advantages of the CVD methodology have also been noticed.

Reactions of SnX_4 (X = Cl, Br) with substituted phosphines ($PCyH_2$, PCy_2H, PCy_3 or $PhPH_2$) under atmospheric pressure deposition (APCVD) give rise to films of tin phosphides with a range of stoichiometry ($SnP_{0.40}$ – $SnP_{1.33}$). These films have shown good surface coverage and they are all electrical insulators.[64]

Most recently, the first chemical deposition has been attempted [65] using GeX_4 (X = Cl and Br) and cyclohexylphosphine under atmospheric pressure. Germanium phosphide films with a range of stoichiometry (Ge_3P – GeP_2) could be obtained.

It is quite surprising that no systematic studies have been done and the same is for their bulk synthesis by molecular precursor routes: only InP and GaP have an extensive literature.[62,66-75] The technological potential and the general properties of the thin film form of the phosphides are still largely unknown and it is quite unexpected considering that they have similar physical properties to the corresponding nitrides

Metal phosphides thin films have also been prepared by different techniques. Homogeneous amorphous germanium phosphide films, with several compositions, have been synthesized for the first time using the technique of pulsed plasma deposition.[76] The use of tantalum phosphide as a diffusion barrier layer in semiconductor devices has also been reported and a film of it has been fabricated by high–frequency sputtering from a powdered TaP source.[77]

1.6 Aim

The main aim of this research work has been to achieve the growth and formation, by single–source precursors, of thin films of composition M_xP_y (where M = Ge and Sn) using the chemical vapor deposition (CVD) technique. As previously reported, formation of germanium and tin phosphide films have been achieved only by dual–source technique.[64,65] In general, not much is known about germanium phosphide[78] and tin phosphide.[79] More recently, research has been focused on ternary germanium and tin phosphide. $CdGeP_2$ and $MnGeP_2$ have been growth as ferromagnetic semiconductor,[80] as well as $CuGe_2P_3$.[81] Tin phosphide selenide ($Sn_2P_2Se_6$) is a ferroelectric semiconductor [82] and few more ternary phosphides of tin are known, i.e. $ZnSnP_2$,[83] $HgSnP_{14}$, [84] Cu_4SnP_{10},[85] $Ba_3Sn_2P_4$, [86] Ni_2SnP,[87] $CdSnP_2$. [88]

Although germanium and tin are adjacent in Group 14, their physical and chemical characteristics are often very different. While germanium presents characteristic similar to silicon, tin is more closely related to lead (*i.e.* ionization energies, electronegativities and electrical resistivity). The chemistry of these elements also can be very different. It is known that the group oxidation state is generally +4, but while for Ge the +4 is the predominant state (although in the +2 state Ge has some stable compound), Sn has the characteristic to switch easily from +2 to +4. The M–X covalent bond strength decreases as the atomic number of M increases, so the formation of four bonds cannot provide enough

energy to stabilize the +4 oxidation state with the result that at lead not all Pb–X bonds are capable of supplying the energy required to stabilize the Pb(IV) state with respect to Pb(II). The increase stability of lower oxidation states for heavier atoms of the *p-block*, is known as the *inert pair effect* and can be thought as a competition between the electron promotion energies and bond strengths.

For this purpose work has been focused on the synthesis and full characterization of a variety of novel phosphorus containing organotin (IV) and germanium (IV) compounds, to avoid the use of the extremely toxic PH_3 in CVD experiments. The reason why such metals have been chosen lies in the fact that, except for the Group 13 phosphides (GaP and InP), little research has been carried out on the formation and properties of films of the main-group phosphides.

CHAPTER TWO

Reactions of $GeCl_4$ with Primary and Secondary Phosphines

2.1 Introduction

One of the key compound classes which can be used to deposit metal phosphides are phosphine adducts of metal halides, particularly adducts involving primary and/or secondary phosphines which facilitate the elimination of hydrogen halide during the film growth process. In many cases the approach is dual–source, in which the assumption is the formation, at some point in the CVD process, of a P:→M donor interaction which survives the thermal decomposition which removes ancillary groups and delivers the two bonded components to the substrate e.g. deposition of TiP from $TiCl_4/PCl_3$ vapor at 1050°C.[18] In other cases, pre–formed adducts are used in which the P:→M interaction is established *a priori* e.g. $TiCl_4.CyPH_2$.[47]

The coordination chemistry of Ge(II) and Ge(IV) halides with phosphorus as a donor ligand has received relatively little attention. One of the earliest studies regarding the coordination chemistry of germanium[89] reports that treating Ge(II) iodide with a triaryl or trialkyl phosphine, the corresponding reaction is:

$$\mathbf{GeI_2 + PR_3 \rightarrow GeI_2(PR_3)} \qquad \textbf{(Eq. 2.1)}$$

($R = Ph_3$, Ph_2Me, Ph_2Et, Ph_2Bu^n, Ph_2H or Bu_3^n)

These products were found to be air–sensitive, yellow solids, turning to red as soon as they were exposed to the atmosphere. The first to be crystallographically characterized was $GeCl_2(PPh_3)$ revealing a trigonal pyramidal geometry for the germanium.[90]

Further work with Ge(II) halides revealed that alkylbis(trichlorogermyl)phosphanes could be formed by insertion of dichlorogermylene into P–Cl bonds of alkyldichlorophosphanes under mild

conditions.[91] Depending on the organic substituents and the reaction conditions, this reaction leads to mixtures of products that contain $RP(H)GeCl_3$, diphosphanes $R(H)PP(H)GeCl_3$ and $R(Cl)PPGeCl_3$, cyclophosphanes and Ge–P heterocycles such as $(RP)_3(GeCl_2)_2$ and $(RP)_4GeCl_2$ (Fig. 2.1)

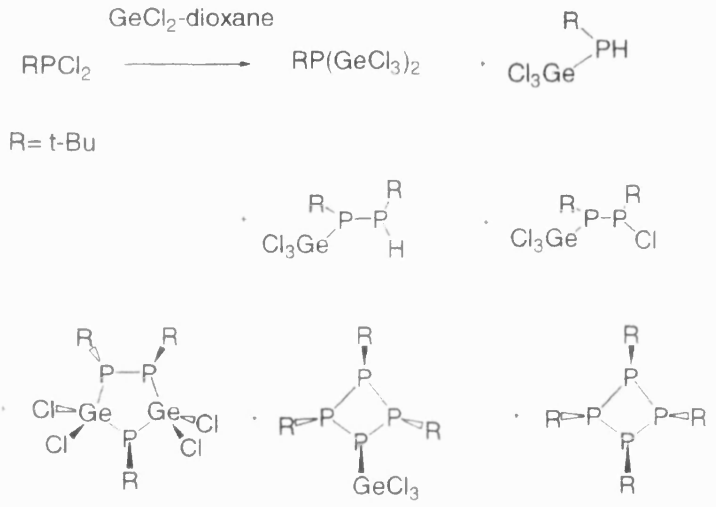

Fig. 2.1 Reaction and products of $RPCl_2$ with $GeCl_2$-dioxane complex

The reaction – both 1:1 and 1:2 ratio – of 1,2–bis(diphenylphosphino)ethane (dppe) with $GeCl_2$·dioxane gave both the 1:1 and 1:2 adducts. The 1:1 adduct has been crystallographically characterized.

$$\textbf{dppe + GeI}_2\textbf{-dioxane} \rightarrow \textbf{GeCl}_2\textbf{·(dppe)} \qquad \textbf{(Eq. 2.2)}$$

$$\textbf{dppe + 2GeI}_2\textbf{-dioxane} \rightarrow \textbf{(GeCl}_2\textbf{)}_2\textbf{·(dppe)} \qquad \textbf{(Eq. 2.3)}$$

Du Mont *et al.* reported the synthesis of the adduct $(^tBu_3P)GeCl_2$ in high yield from reaction between organophosphines and either $GeCl_2$-dioxane and $GeCl_2$.

$$\textbf{GeCl}_2\textbf{-dioxane + }^{\textbf{t}}\textbf{Bu}_3\textbf{P} \rightarrow \textbf{Cl}_2\textbf{GeP}^{\textbf{t}}\textbf{Bu}_3 \qquad \textbf{(Eq. 2.4)}$$

$$GeCl_2 + {}^tBu_3P \rightarrow Cl_2GeP^tBu_3 \qquad \textbf{(Eq. 2.5)}$$

It was noticed that these germyl compounds, when put in contact with HCl, had their Ge–P bonds cleaved, giving phosphonium salts of the type $[{}^tBu_3PH]^+ [GeCl_3]^-$.[92]

Since no formal studies had been carried out concerning analogous complexes of germanium (IV) halides, in the early 70's a few scientists reported the formation of some 1:1 and 2:1 trimethylphosphine adducts of $GeCl_4$.[93] They reported the formation of $GeCl_4(PMe_3)_2$ and assigned it a *trans*–octahedral structure based on IR data.[94] They also noted that using an excess of $GeCl_4$, only the 1:1 complex, and not the 2:1, was formed. The same has been found for the reaction of $GeBr_4$ with PMe_3, which resulted in a 1:1 complex – $GeBr_4(PMe_3)$ – and no evidence for the 2:1 adduct.

It is now known that these interpretations are incorrect. In fact, the reaction of $GeBr_4$ with bulky tertiary phosphines results in a redox reaction.[95-97]

$$GeBr_4 + R_3P \rightarrow [GeBr_3]^-[R_3PBr]^+ \qquad \textbf{(Eq.2.6)}$$

The product of this reaction contains an anionic Ge(II) species.

From these studies, it initially appeared that the reaction of Ge(IV) halides with tertiary phosphines of low steric bulk forms Ge(IV) adducts, whereas with bulky tertiary phosphines a redox reaction takes place to give the ionic complex that contains Ge(II).

To solve this controversy, a recent study has been carried out on the reaction between $GeCl_4$ and a wide range of tertiary phosphines, in both 1:1 and 1:2 ratio.[98]

In both cases, only products with Ge:P in a 1:1 ratio were formed with no evidence for the 1:2 stoichiometry.

$$GeCl_4 + nR_3P \rightarrow GeCl_4(PR_3)_n \qquad \textbf{(Eq. 2.7)}$$

(R = Me, Et, Pr^n, Bu^n, Bu^t, C_6H_{11}, $C_6H_{11}CH_2$, Me_2N, Et_2N, $^nPr_2N$, Ph_2Et)

This work clearly describes and shows that all the complexes of formula $GeCl_4(PR_3)$ are the ionic species $[GeCl_3]^-[R_3PCl]^+$ and contain germanium (II) and not germanium (IV), no matter what the steric bulk of PR_3 (Fig. 2.2). The ionic species is formed by reductive halide transfer from germanium to phosphorus.

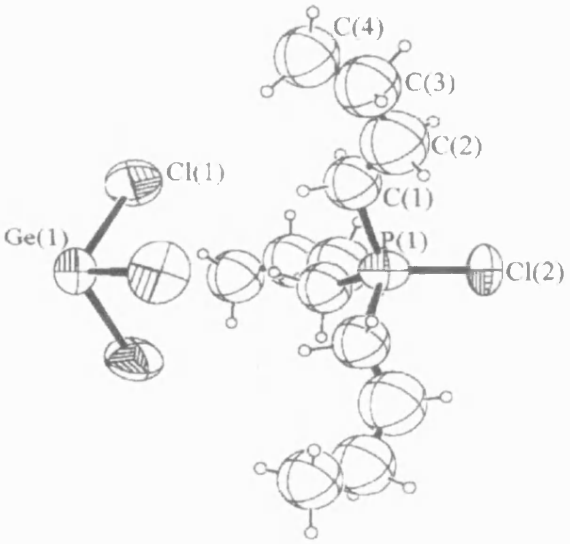

Fig. 2.2 The crystal structure of the ionic Germanium(II) complex $[GeCl_3]^-[Bu^n{}_3PCl]^+$. Selected bond lengths (Å) and angles (°) for $[GeCl_3]^-[Bu^n{}_3PCl]^+$: Ge(1)–Cl(1) 2.230(9), Cl(2)–P(1) 1.82(2), P(1)–C(1) 1.83(4), Cl(1)–Ge(1)–Cl(1) 96.1(4), C(1)–P(1)–Cl(1) 106(1), C(1)–P(1)–Cl(2), 113(1).

The anion, shown in figure 2.2, exhibits angles and lengths consistent with other previously crystallographically characterized complexes containing the $[GeCl_3]^-$ anion. The cation, however, exhibits a very short *d*(P–Cl) [1.82(2) Å] which

is shorter than for the compound PCl_5 [1.903(2) Å]. Furthermore, in this ionic complex no cation–anion interactions are present and it is in contrast to the only other crystallographically characterized compound of this type, $[GeBr_3]^-[Pr^i_3PBr]^+$.[98]

In the late 1970s Du Mont and Schumann reported the synthesis of halogermyl phosphines from the reaction of GeX_4 (X = Cl and Br) with Ph_2PSiMe_3. They ascertained that the products of these reactions were not adducts, but a mixture of two products, *i.e.* R_2PGeX_3 and $R_2(X)PGeX_2$. ^{31}P NMR as well as ^1H NMR was given as proof of the occurred formation of the products.[99]

$$\mathbf{GeX_4 + R_2PSiMe_3 \rightarrow R_2PGeX_3 + Me_3SiCl} \qquad \textbf{(Eq. 2.8)}$$

$$\mathbf{GeX_4 + R_2PSiMe_3 \rightarrow R_2P(X)GeX_2 + Me_3SiCl} \qquad \textbf{(Eq. 2.9)}$$

In order to more understand the viability of growing GeP films from germanium halides and primary and secondary phosphines, a fundamental appraisal of the reaction chemistry of $GeCl_4$ with both $CyPH_2$ and $PhPH_2$, as representative of primary phosphines and with Ph_2PH as representative of secondary phosphines, has been undertaken.

2.2 Results and Discussion

2.2.1 Reaction of $GeCl_4$ and $CyPH_2$ (1:1)

The 1:1 reaction of $GeCl_4$ and $CyPH_2$ in diethyl ether at room temperature and under argon generates a white precipitate after a few minutes. The amount of precipitate is dependant on the volume of solvent used, *i.e.* the precipitated products are soluble to some extent in diethyl ether.

The ^{31}P NMR of the solid precipitate consists of two signals, a triplet at 24.1 ppm (J = 505 Hz) and a doublet at -60.2 ppm (J = 188 Hz) (Fig. 2.3). The ^{31}P NMR of the filtrate (Fig. 2.4) shows the same doublet (δ = -61.2 ppm, J = 194 Hz) along with a series of minor peaks. From both NMR samples crystals were isolated which X–ray diffraction shows to be the salt $[GeCl_3]^-[CyPH_3]^+$(**1**) (Fig. 2.5); after cannula filtration and redissolution of these crystals the ^{31}P NMR spectrum appears at 24.5 ppm, identical to the triplet species present in the initial precipitate.

The doublet at *ca.* -60 ppm, present in both precipitate and filtrate, is assigned to $CyP(H)GeCl_3$ (**2**), by comparison with data for $^{i}PrP(H)GeCl_3$ (δ = -56 ppm, J = 191 Hz)[91] and related species.[100] The remaining material in the initial precipitate is clearly related to $[GeCl_3]^-[CyPH_3]^+$, but the triplet structure implies only two hydrogens are attached to phosphorus. The low–field ^{31}P shift implies an involvement of the phosphorus lone pair in bonding, thus we propose $CyH_2P{:}\rightarrow GeCl_2$ (**3**) as the second component of the precipitate.

Microanalysis of the precipitate (C = 26.5; H = 4.84%) corresponds well with a 1:1 ratio of $CyH_2P{:}\rightarrow GeCl_2$ and $CyP(H)GeCl_3$ (C, 26.2; H, 4.81%). Furthermore, $^{t}Bu_3P{:}\rightarrow GeCl_2$ has a similar ^{31}P chemical shift (35.6 ppm) and is known to react with HCl to form $[GeCl_3]^-[^{t}Bu_3PH]^+$.[96]

The following mechanism of formation of these products (Scheme 1) is proposed. It would seem reasonable that the initial step is the formation of the adduct $R_3P{:}\rightarrow GeCl_4$, which, when none of the substituents on phosphorus is hydrogen, undergoes halide transfer to yield $[GeCl_3]^-[R_3PCl]^+$.[98] However, when at least one hydrogen is present loss of HCl dominates and $Cy(H)PGeCl_3$ is the major product.[100] The requirement for formation of $[GeCl_3]^-[CyPH_3]^+$, which ultimately forms from both the filtrate and after redissolution of the initial precipitate, seems to be $GeCl_2$, which can combine with HCl and $CyPH_2$. Since $Cy(H)PGeCl_3$ is common to both components of the reaction, it is suggested that it is this material can give rise to $GeCl_2$, presumably along with CyP(H)Cl. Adduct formation can

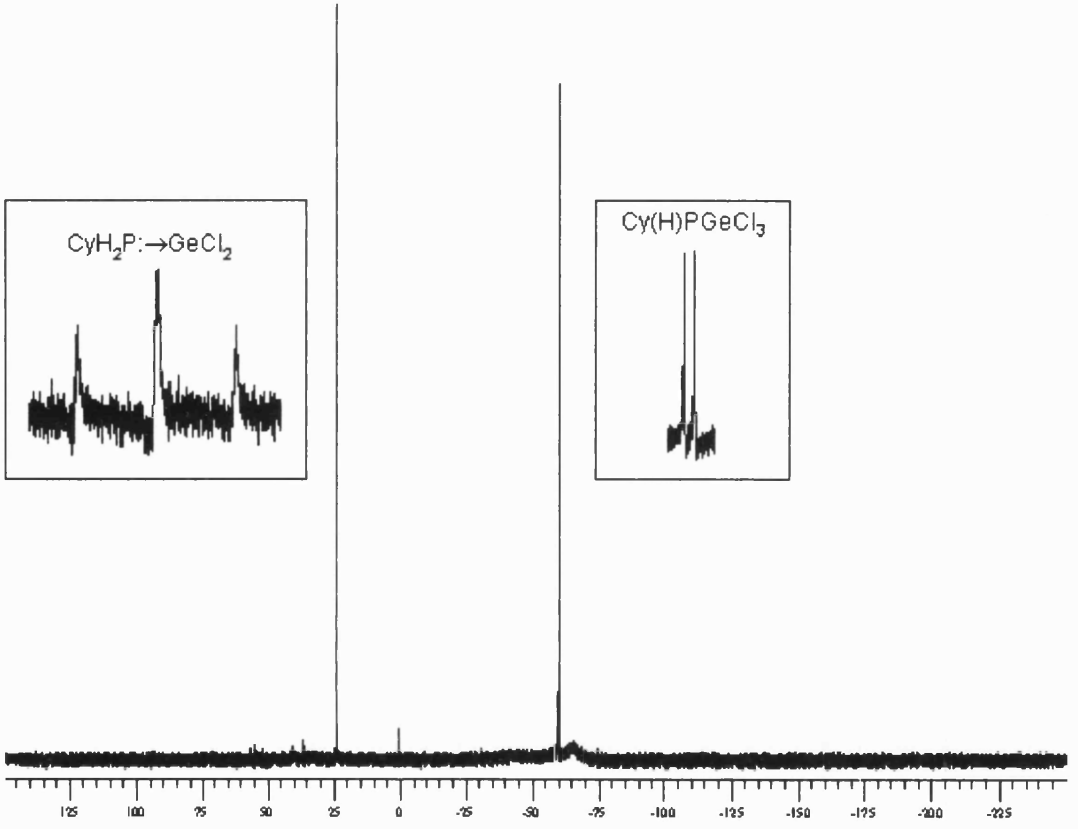

Fig. 2.3 The $^{31}P\{^{1}H\}$ NMR spectra of the precipitate from the reaction of $GeCl_4$ and $CyPH_2$. Insets show the non-decoupled spectra.

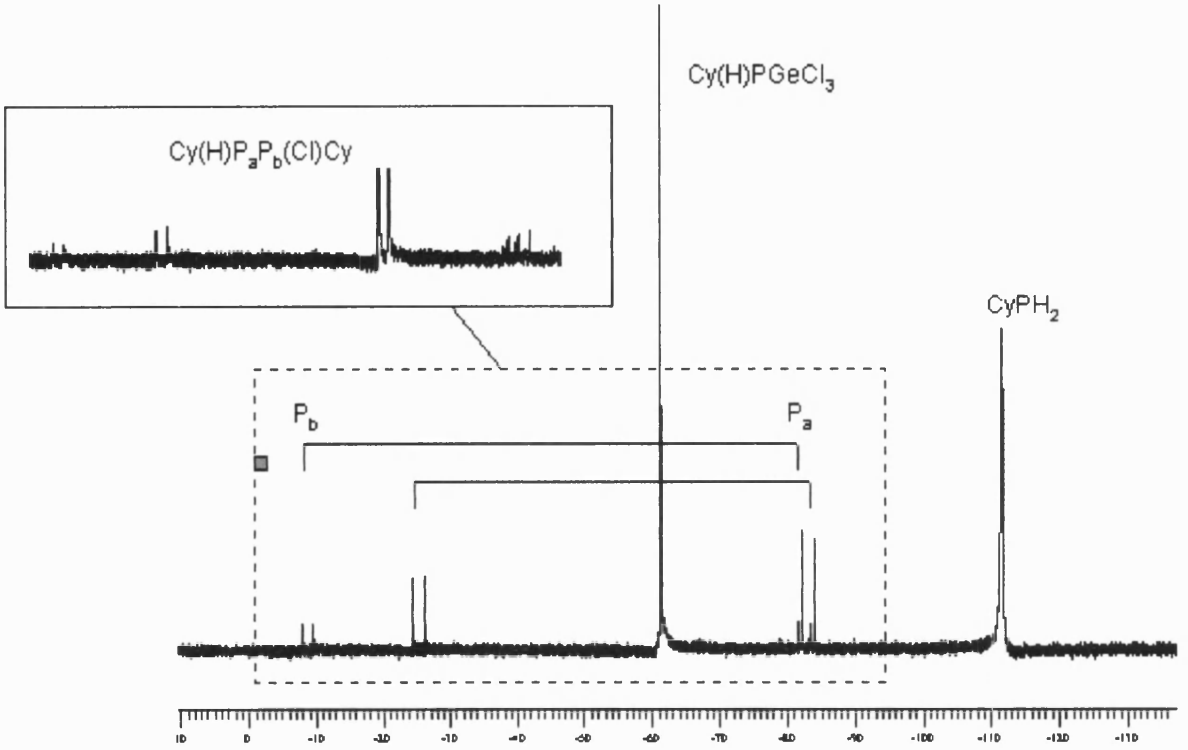

Fig. 2.4 The $^{31}P\{^{1}H\}$ NMR spectra of the filtrate from the reaction of $GeCl_4$ and $CyPH_2$. Insets show the non-decoupled spectra.

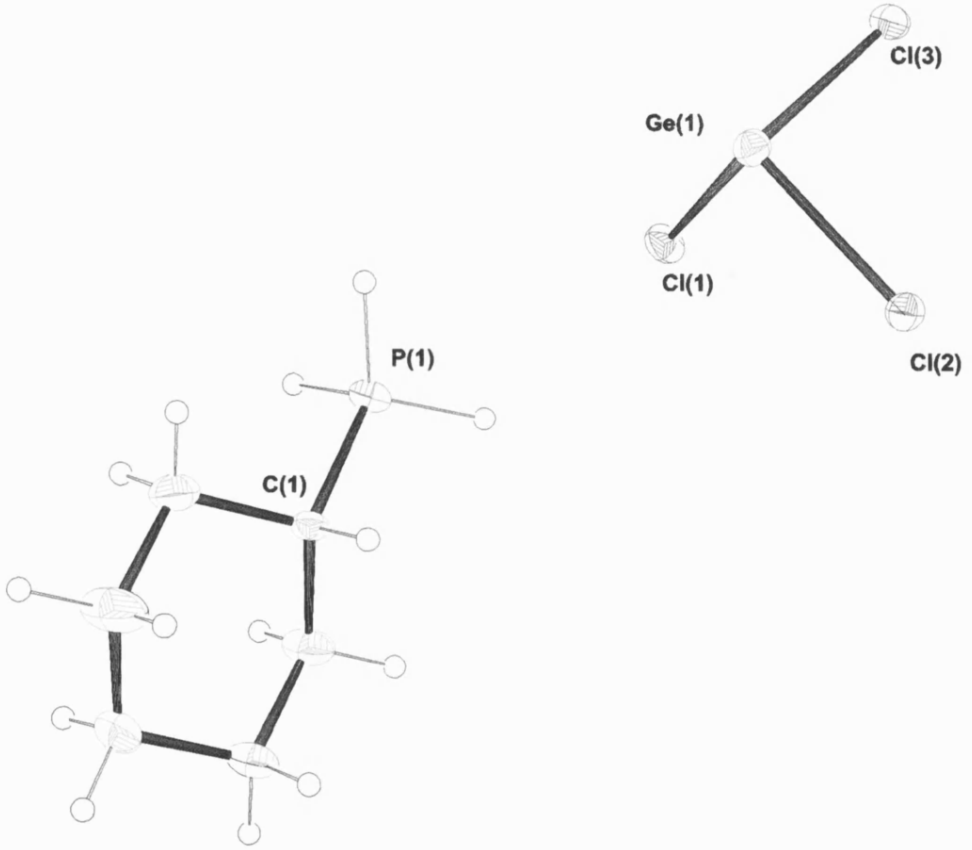

Fig 2.5 ORTEP plot of $[GeCl_3]^-[CyPH_3]^+$ (**1**).Thermal ellipsoids are at the 30% probability level. Selected metrical data: Ge(1)–Cl(1) 2.3091(8), Ge(1)–Cl(2) 2.3264(8), Ge(1)–Cl(3) 2.3571(8), P(1)–H(1A) 1.358(18), P(1)–H(1B) 1.359(18), P(1)–H(1C) 1.371(18), P(1)–C(1) 1.802(3) Å; Cl(1)–Ge(1)–Cl(2) 95.80(3), Cl(1)–Ge(1)–Cl(3) 93.86(3), Cl(2)–Ge(1)–Cl(3) 94.58(3), H(1A)–P(1)–H(1B) 109(2), H(1A)–P(1)–H(1C) 112(2), H(1B)–P(1)–H(1C) 106(2), H(1A)–P(1)–C(1) 112.4(17), H(1B)–P(1)–C(1) 106.7(15), H(1C)–P(1)–C(1)110.8(15), C(6)–C(1)–C(2)111.2(3)°. The hydrogen atoms on bonded to the phosphorus are in calculated positions.

then take place between unreacted $CyPH_2$ and $GeCl_2$, which, when HCl is present, can generate the salt shown in Fig. 2.5.

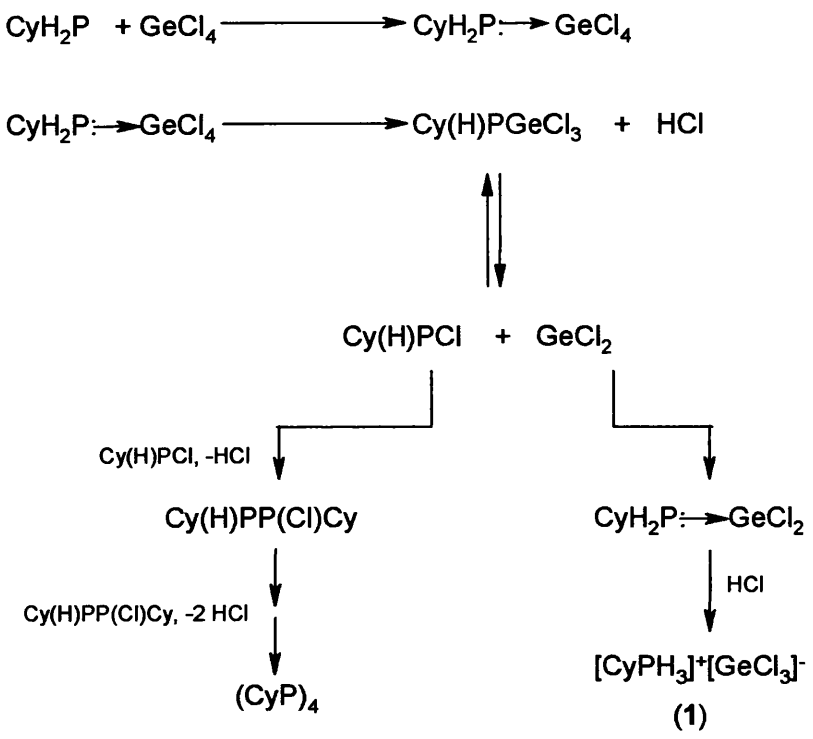

Scheme 1

Halophosphines, RP(H)X, are known to be generally unstable and lose HCl, except when R is bulky[100,101] or CF_3,[102] and lead to the formation of the corresponding cyclophosphines. The minor products seen in Fig. 2.4 can be assigned to Cy(H)PP(Cl)Cy, arising from coupling of CyP(H)Cl with elimination of HCl, although analogous species arising from $GeCl_2$ insertion, *i.e.* Cy(H)PP($GeCl_3$)Cy, cannot be excluded. The doublet at -83.1 ppm [J(PP): 218 Hz] in the $^{31}P\{^1H\}$ spectrum becomes a doublet of doublets on ^1H coupling [J(PH):194 Hz], while the doublet at -25.4 ppm [J(PP): 218 Hz] is not coupled to hydrogen. As

pointed out by du Mont,[91,96] the phosphorus centers in such species are chiral and both RR/SS and RS/SR diastereoisomers are possible, which we suggest gives rise to the minor signals at -82.5 ppm [d, J(PP): 206 Hz; signals too weak on $\{^1H\}$ decoupling to measure J(PH)] and -8.6 ppm [d, J(PP): 206 Hz]. Further coupling of Cy(H)PP(Cl)Cy with loss of HCl will lead to cyclophosphines as noted above and a crystal of $(CyP)_4$ has been isolated from the reaction filtrate. This crystal has identical cell parameters to those available in the literature[103] and no ^{31}P NMR signals which could be attributed to such a species.

The structure shown in Figure 2.5 is, apparently, the only second structurally characterized example of a primary phosphonium cation. The cation is tetrahedral with no obvious trends in the distribution of bond angles about the phosphorus. In the solid state, the anions form chains linked by weak Ge···Cl(1′) interactions (3.856 Å) supported by hydrogen bonds involving H(1B) and H(1C) which bridge adjacent anions [H(1B)-Cl(3): 2.604; H(1C)-Cl(3′): 2.753 Å]. Chains are cross-linked by additional hydrogen bonds involving H(1A) and Cl(1) (2.815 Å) (Fig. 2.6). Cl(2) does not involve itself in any intermolecular interactions < 3Å. The structure of $[GeCl_3]^-[^iPrPH_3]^+$ has previously been reported by Du Mont[91] and the presence of chains of $[GeCl_3]^-$ anions noted (Ge···Cl: 3.721 – 4.096 Å), but no comments were made on any anion–cation interactions.

2.2.2 Reaction of $GeCl_4$ and $CyPH_2$ (4:1)

When $CyPH_2$ is reacted with a large excess of $GeCl_4$ in toluene and under argon, Cy(H)P$GeCl_3$ (**2**) is produced quantitatively in the form of a white precipitate, which was separated by filtration from the solution (excess $GeCl_4$ and toluene). This reaction is presumably due to the rapid consumption of phosphine by the metal halide such that no free phosphine is available for reaction with, for example, HCl, which is the case when a 1:1 reaction is carried out.

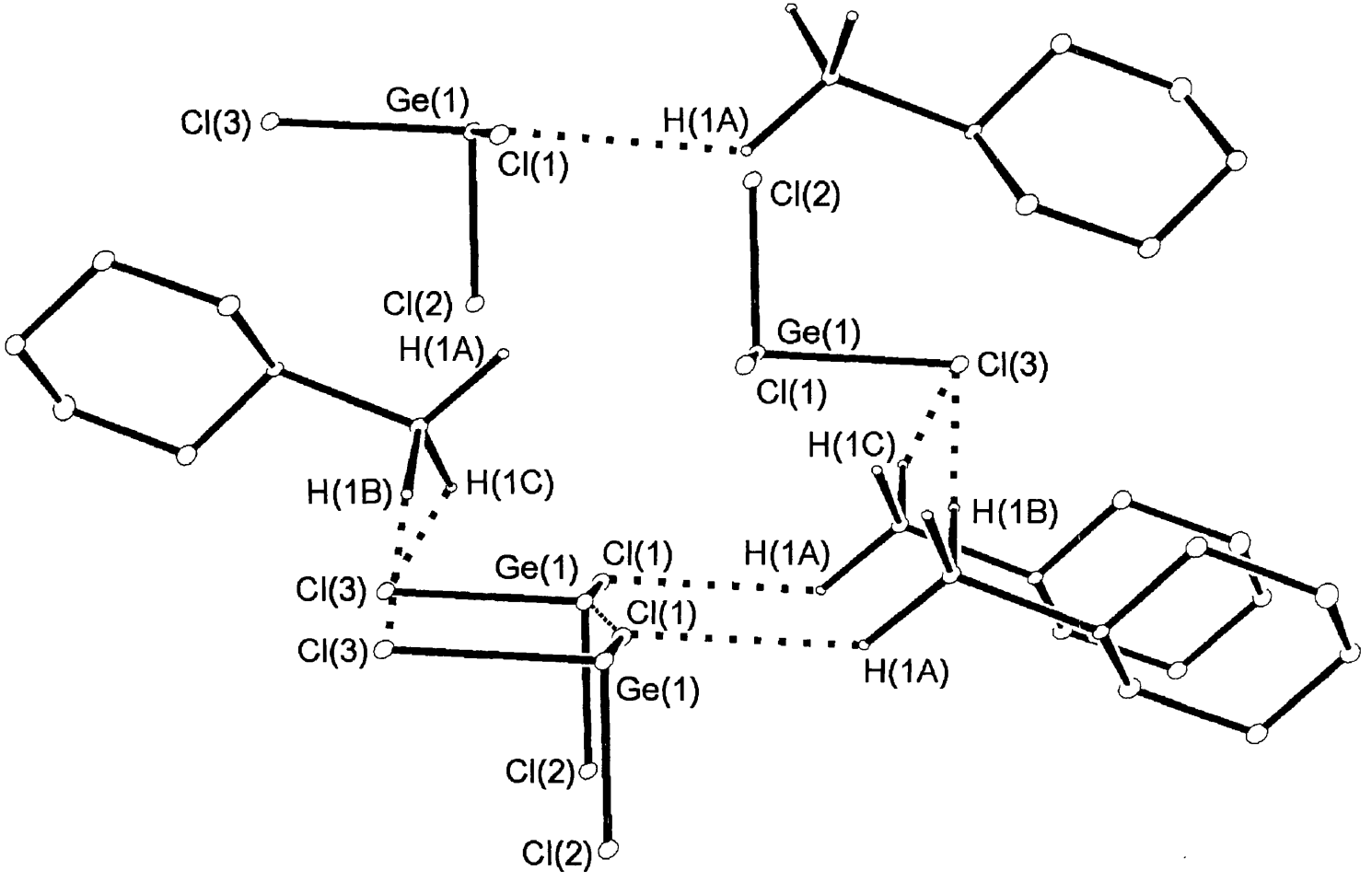

Fig. 2.6 The lattice structure of $[GeCl_3]^-[CyPH_3]^+$ (**1**).

$$CyPH_2 + xsGeCl_4 \rightarrow Cy(H)PGeCl_3 + HCl \qquad \textbf{(Eq. 2.10)}$$

(2)

Microanalysis of **2** (C = 24.8; H = 4.27%) obtained from this reaction corresponds well with the formation of $CyP(H)GeCl_3$ (C = 24.5; H = 4.1 %).

Couret *et al.* reported, in the attempt to produce diphosphine compounds, that trichlorogermyl phosphines could be synthesized by heating a dioxane solution of dichlorogermylene–dioxane complex[104] and a dichlorophosphine at reflux. The reaction gives, unexpectedly, the trichlorogermyl phosphines in a variable yield, depending on the substituent R.

$$RPCl_2 + GeCl_2{\cdot}C_4H_8O_2 \rightarrow R(H)PGeCl_3 \qquad \textbf{(Eq. 2.11)}$$

The yield of the Eq. 2.10 is 28% and the melting point of **2** is 40 – 42°C. Such a value is of particular importance for volatility implications. It is known that volatility is one of the most significant properties of a precursor to allow an adequate transport of the precursor to the deposition zone.

Tests done on compound **2** have shown that it also has a certain degree of stability. ^{31}P NMR of a solution of $CyP(H)GeCl_3$ left open to air for 5 minutes does show the same doublet at -60.2 ppm and no evidence for oxidation products. The same result has been ascertained on solid 2 left exposed to air for 5 minutes and then redissolved. However, it was noticed that exposure to air for one day and repeated dissolution of **2**, using different solvents, lead to the possible formation of $CyP(H)(O)GeCl_3$. The IR spectrum of the aged material includes a band at 1057 cm^{-1}, similar to values reported in literature for $\nu(P{=}O)$, *e.g.* $\nu(P{=}O)$ of $Ph_3P(O)H$ is 1193 cm^{-1} and is shifted to lower frequency when it coordinates to metals.[105] ^{31}P

NMR of the oxidized compound shown a doublet at +24.6 ppm, consistent with a +5 state for the phosphorus.

As expected, operating with an excess of the germanium tetrahalide, the ^{31}P NMR of the solid precipitate, redissolved in toluene, consists a doublet at -60.2 (d, J_{P-H}= 188 Hz) as previously reported for the 1:1 reaction. $^{13}C\{^1H\}$ NMR shows doublets at δ = 35.1 ppm (d, $^3J_{C-P}$ = 8.4 Hz), 34.0 ppm (d, $^2J_{C-P}$ = 16.7 Hz) and 31.3 ppm (d, $^1J_{C-P}$ = 17.7 Hz); and a broad singlet at 26.6 ppm. The doublets are referred to interactions between phosphorus and the cyclohexyl carbons. ^1H NMR presents a doublet of doublet, δ = 4.1 ppm (dd, J_{H-P} = 188 Hz, J_{H-H} = 4.6Hz) and several peaks between 1.8 and 2.6 ppm (br, m, 11 H).

Cy(H)PGeCl$_3$ (**2**) has been studied using thermal gravimetric analysis (TGA) in order to have an indication of the temperature at which the decomposition of this compound may be expected to begin. The data also suggest information concerning the relative stability of the compound. The analysis has been carried out at atmospheric pressure under a N_2 flow. The decomposition curve of the compound (Fig. 2.7) shows the loss of the cyclohexyl and the three Cl atoms between 70 and 550°C, and it would be pure speculation to say what have been eliminated, *i.e.* CyH, Cl_2, CyCl or HCl. It is clear from the picture that in the final step, over 550°C, a species with mass corresponding to GeP is formed (observed 33.6, theoretical 31.4%).

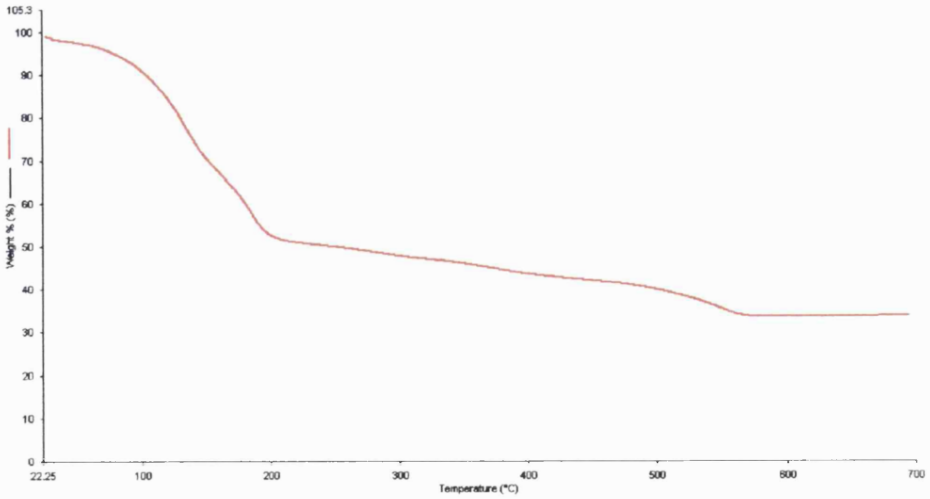

Fig. 2.7 TGA of $Cy(H)PGeCl_3$

2.2.3 CVD studies of $Cy(H)PGeCl_3$

$Cy(H)PGeCl_3$ has been tested as a precursor for its suitability to produce germanium phosphide films under CVD conditions. Experiments have taken place by either LPCVD or AACVD under a nitrogen flow. The films formed were examined by scanning electron microscopy (SEM) and were sputtered with carbon in order to avoid charging and to improve the secondary electron image quality.

Films have been grown by AACVD (Appendix Two) using a solution of $Cy(H)PGeCl_3$ in toluene and deposited on standard borosilicate glass slides at 500°C. The films are strongly adherent to the glass, are generally transparent and show typical refringence patterns. At positions further from the vapor inlet, some depositions showed a gray cloudiness that could be due to amorphous carbon.

The transparent films grown by AACVD (Fig 2.8) are amorphous to X–rays, though EDAX (Fig. 2.9) is able to confirm the presence of both germanium and phosphorus. However, there is also considerable amounts of oxygen associated with the films, and the atomic ratio of the elements is uniformly ca. Ge 24: P 11: O

64 atom percent (ranges over several sites: Ge 24.1 – 24.5: P 10.6 – 11.4: O 64.5 – 64.8). A small amount of silicon from the underlying glass was also noted. The presence of a large amount of oxygen could be associated with either GeO_2 or $Ge_3(PO_4)_4$ /$Ge_3(PO_4)_2$. However, a band gap measurement of 1.1 eV, extrapolated from the electronic spectrum of the film, is consistent with the presence of either GeP or Ge_2P_3.[106,107]

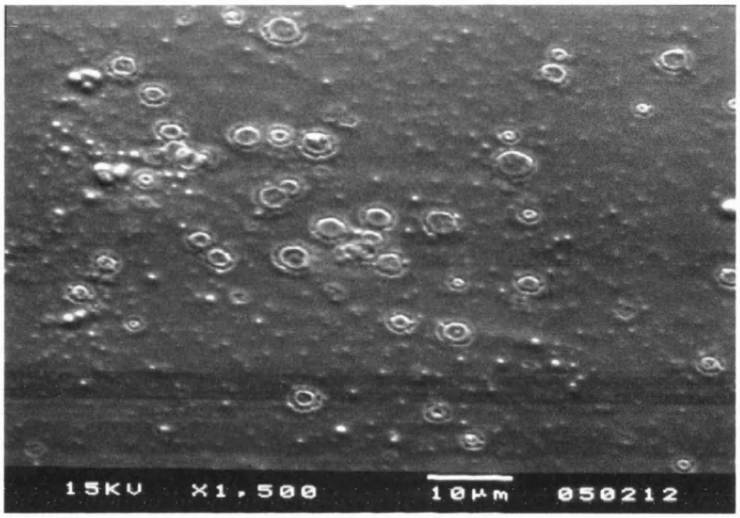

Fig. 2.8 SEM (15 kV) of film grown by AACVD from Cy(H)PGeCl$_3$ at 500°C

Due to the presence of oxygen in the film grown by AACVD, deposition has also been carried out using the same precursor (**2**) under LPCVD conditions (Fig. 2.10). The material, approximately 1.5 g, has been used to deposit on standard borosilicate glass slides at 500°C and has produced a transparent film with refringence patterns and a slight haze. The precursor was held at low pressure and heated in a tube furnace, 50°C, until evaporation was completed. External to the furnace, the deposition substrate (glass slide) was placed and heated by a ceramic infra–red heater to the preferred decomposition temperature (Appendix Two).

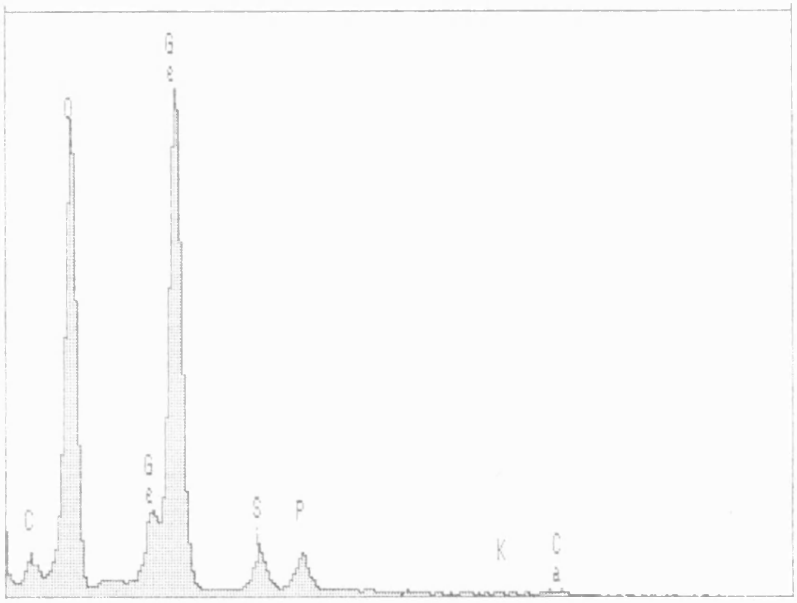

Fig. 2.9 EDAX (10 kV) of film grown by AACVD from $Cy(H)PGeCl_3$ at 500°C

The film is amorphous to X–rays and EDAX (Fig. 2.11) provides an accurate quantitative analysis showing the presence of both germanium and phosphorus as well as a considerable amount of oxygen. The atomic ratio found for this film is regularly *ca.*: Ge 18: P 15: O 67 atom percent and the ranges over different positions are: Ge 17.8 – 17.9: P 14.1 – 14.6: O 67.3 –67.7. As it has been seen previously, the presence of a large amount of oxygen could be associated with either GeO_2 or $Ge_3(PO_4)_4$ /$Ge_3(PO_4)_2$.

However, as the depth profile for the oxygen shows in Figure 2.12, the oxygen levels decrease with etching, suggesting that the oxidation occurs after the film has been deposited. It is thought that CVD of the precursor produces a film of GeP, also confirmed by the almost 1:1 ratio of Ge:P, in the form of small particles spread over the whole of the substrate. Only after the film is exposed to air, a large percentage of the GeP is converted into $Ge_3(PO_4)_4$ /$Ge_3(PO_4)_2$. Particles of these substances contribute to expand the volume of the particles providing a homogeneous film over the substrate.

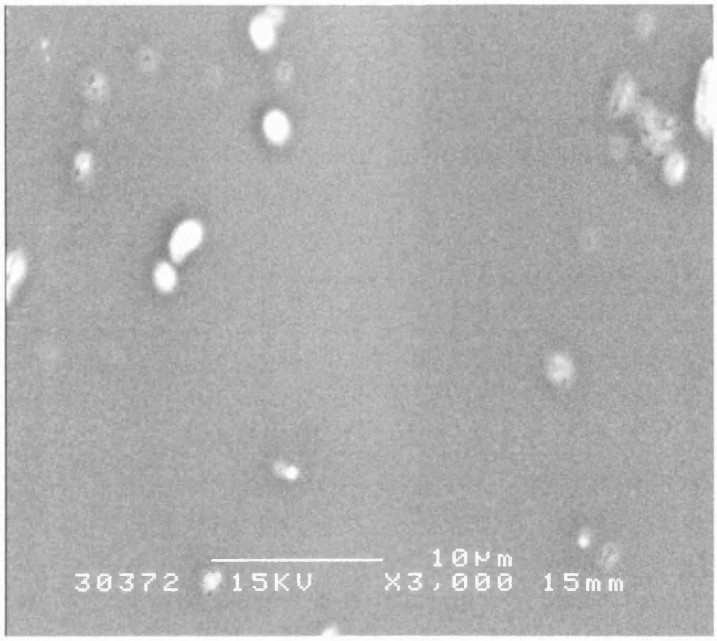

Fig. 2.10 SEM (15 kV) of film grown by LPCVD from Cy(H)PGeCl$_3$ at 500°C

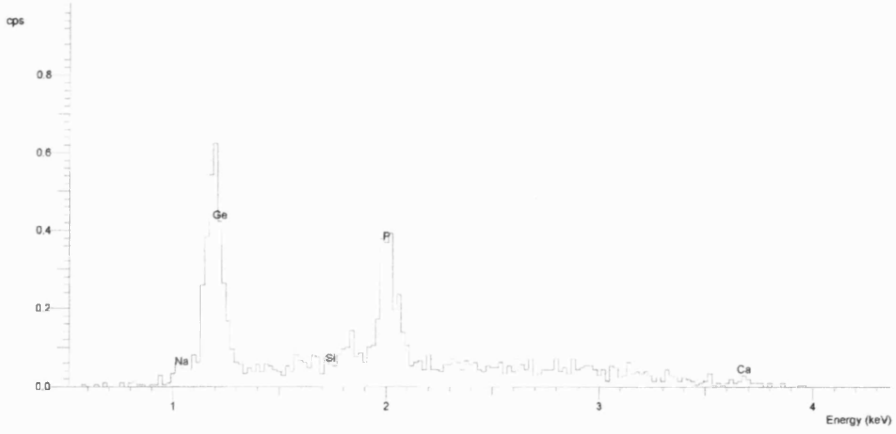

Fig. 2.11 EDAX (4 kV) of film grown by LPCVD from Cy(H)PGeCl$_3$ at 500°C

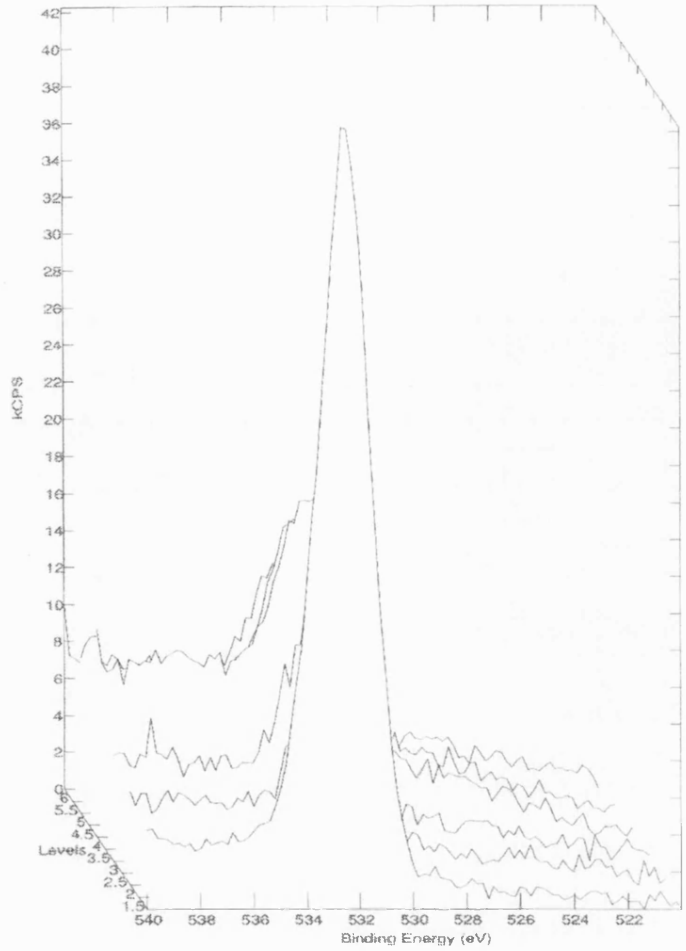

Fig. 2.12 XPS of film grown by LPCVD from $Cy(H)PGeCl_3$ at 500°C

2.2.4 Reaction of $GeCl_4$ and $PhPH_2$ (4:1)

An excess of $GeCl_4$ has been made react with $PhPH_2$. The reaction, carried out in absence of solvent and under argon, has been left stirring for 30 minutes and produced $Ph(H)PGeCl_3$ (**4**) quantitatively in form of a white solid which has been separated by cannula filtration from the excess of $GeCl_4$.

$$\mathbf{xsGeCl_4 + PhPH_2 \rightarrow Ph(H)PGeCl_3 + HCl} \qquad \textbf{(Eq. 2.12)}$$

(4)

Microanalysis of the precipitate (C = 25.0; H = 2.1 %) obtained from this reaction corresponds well with the formation of $PhP(H)GeCl_3$ (C = 25.2; H = 2.25%).

The melting point of the product shows a value in the range of 69 – 72 °C as reported in literature.[100] Such value is of particular importance for volatility implications.

^{31}P NMR of **4**, dissolved in toluene, has been recorded and it consists of a doublet at –65.7 ppm (J_{P-H} = 200.5 Hz),[100] along with a series of minor peaks, that probably arise from a series of coupling products as already seen for the reaction of $GeCl_4$ with $CyPH_2$. $^{13}C\{^1H\}$ NMR presents a doublet at δ = 124.2 ppm (d, $^1J_{H-P}$= 19.6 Hz), a second doublet at δ = 136.8 ppm (d, $^2J_{C-P}$= 17.6 Hz), a third doublet at δ = 135.8 ppm (d, $^3J_{C-P}$= 15.09 Hz) and a singlet at δ = 131.6 ppm (s). These peaks arise from the interaction between phosphorus and the carbons of the phenyl ring. ^1H NMR presents a doublet at δ = 4.8 ppm (J_{H-P}= 200.5 Hz).

In Figure 2.13 the thermal decomposition of $Ph(H)PGeCl_3$ is shown. TGA analysis shows decomposition of the product starts at approximately 80°C and it is effectively over by 200°C. Weight loss observed at 187°C corresponds to GeP (found 35.8%, theoretical 35.9%).

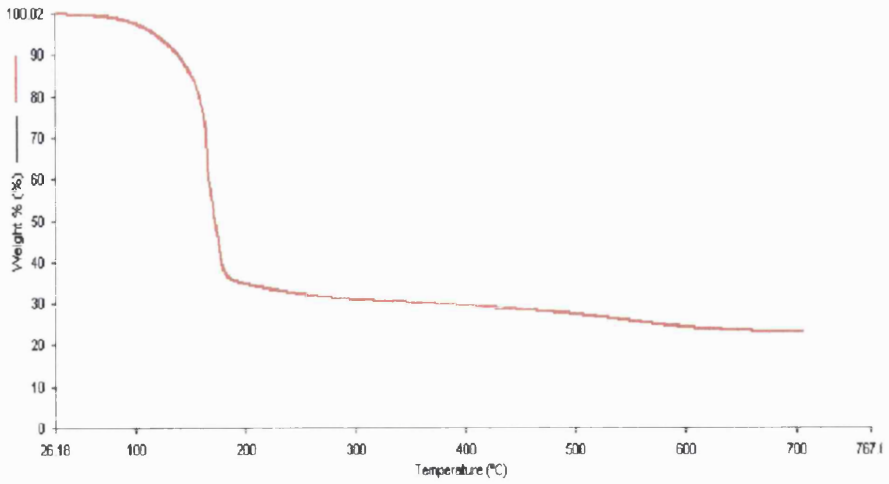

Fig. 2.13 TGA of $Ph(H)PGeCl_3$

2.2.5 CVD studies of $Ph(H)PGeCl_3$

$Ph(H)PGeCl_3$ (**4**) has been tested as a potential CVD precursor for its suitability to produce germanium phosphide films under LPCVD condition (see Appendix Two for apparatus details).

The precursor, approximately 0.85 g, has been used to deposite films on standard borosilicate glass slides at 500°C, producing a transparent film with refringence patterns and a slight haze. The film was examined by scanning electron microscopy (Fig. 2.14).

EDAX (Fig. 2.15) indicates that the average germanium – phosphorus composition across the whole surfaces is uniformly: Ge 12: P 17. However, there is again considerable amounts of oxygen associated with the films and the atomic ratio, express in percent, found for this film is Ge 12: P 17: O 70. It has been also observed that the ranges over several spots are: Ge 11.7 – 12.1: P 16.5 – 17.3: O 70.7 – 71.5. As it has been seen previously for the LPCVD of **2**, **the** existence of a large amount of oxygen is likely to be due to a post oxidation reaction which

produce $Ge_3(PO_4)_4$ /$Ge_3(PO_4)_2$. It is thought that the film produced after the deposition of **4** is subjected to the same process that has seen involved **2**.

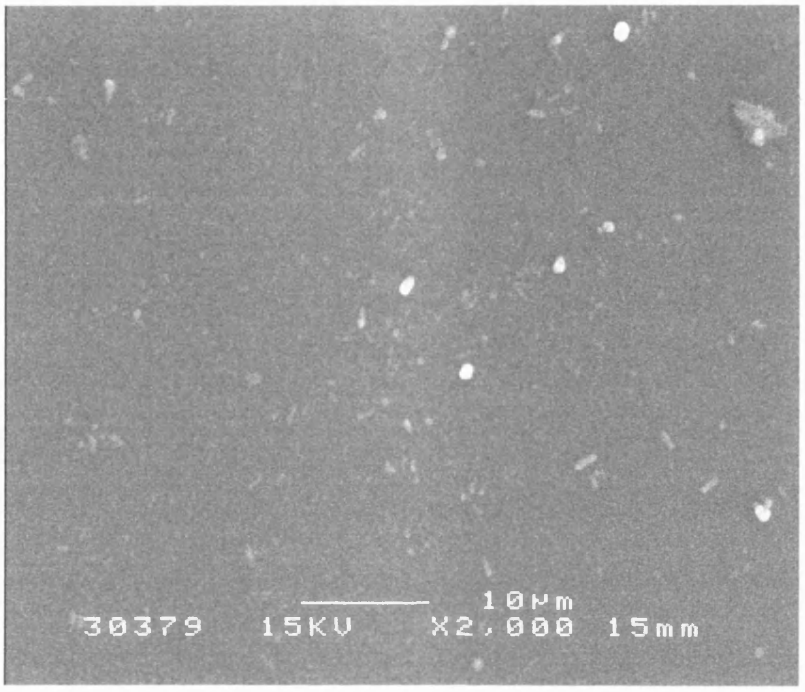

Fig. 2.14 SEM (15 kV) of film grown by LPCVD from $Ph(H)PGeCl_3$ at 500°C

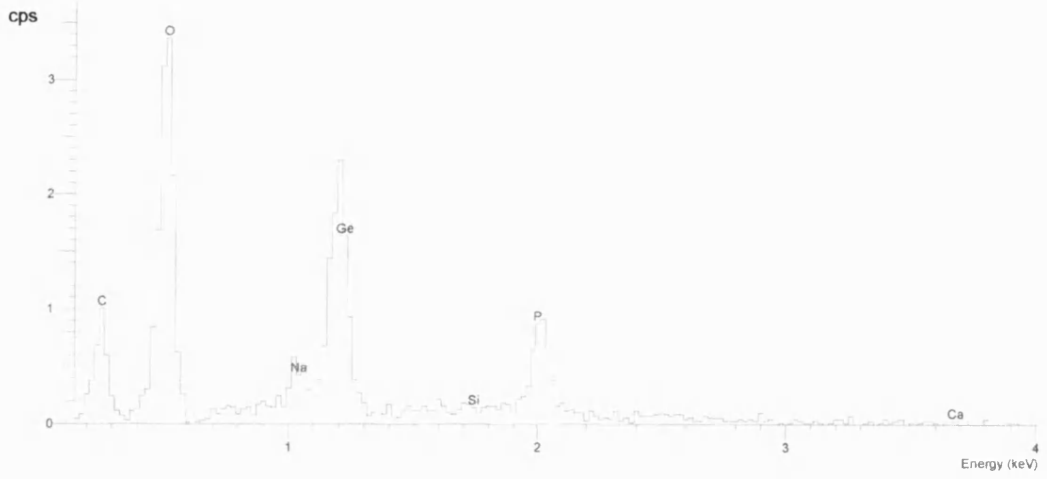

Fig. 2.15 EDAX (4 kV) of film grown by LPCVD from $Ph(H)PGeCl_3$ at 500°C

2.2.6 Reaction of $GeCl_4$ and Ph_2PH (1:1)

In a similar manner to the 1:1 reaction of $GeCl_4$ with $CyPH_2$, a 1:1 reaction of $GeCl_4$ with the secondary phosphine Ph_2PH yields a solid precipitate but this turns to an oil on drying *in vacuo*. The ^{31}P NMR of this oil ($CDCl_3$) is a doublet (J = 532 Hz) at 29.5 ppm, data which parallel those for the precipitate obtained from $CyPH_2$ / $GeCl_4$ and which are hence assigned to $Ph_2(H)P:\rightarrow GeCl_2$ (**5**). Microanalysis of the oil is consistent with this formulation [Found (calc.) for $C_{12}H_{11}Cl_2PGe$: C = 44.7(43.7); H = 3.52(3.37)%]. The $\{^1H\}^{31}P$ NMR spectrum of the reaction filtrate (Et_2O) is dominated by a singlet at 80.2 ppm, with very minor resonances at 5.3 (unidentified) and -40.8 ppm (broad, probably Ph_2PH). The major soluble product appears to be Ph_2PCl from the lack of any $^1J(PH)$ coupling. An authentic sample of this compound has δ = 84.0 ppm ($CDCl_3$), while others have report it as 78.7 ppm (C_6H_6).[108]

From the filtrate of the reaction mixture a product, which x-ray crystallography reveals to be $[GeCl_3]^-[Ph_2PH_2]^+$ (**6**) (Fig. 2.16), has been isolated.

$[GeCl_3]^-[Ph_2PH_2]^+$appears to have limited stability, as dissolution of the crystals in $CDCl_3$ yields a ^{31}P NMR spectrum comprising in excess of a dozen peaks. The largest of these is, however, a triplet (J = 509 Hz) at 25.7 ppm which is consistent with the $[Ph_2PH_2]^+$ cation. The only data available for comparison relates to that for $[Ph_2PH_2]^+[AlCl_4]^-$, which has δ = -22.8 ppm and J = 508 Hz.[108]

While the reaction described above is reproducible in terms of the NMR spectra of the solid precipitate and the filtrate, crystals of $[GeCl_3]^-[Ph_2PH_2]^+$ have only been obtained from the reaction filtrate on one occasion.

The reactions involved when Ph_2PH and $GeCl_4$ are mixed in 1:1 ratio parallel the sequence for the reaction of $CyPH_2$ and $GeCl_4$ (Scheme 1), save for the fact

that Ph_2PCl is more stable than Cy(H)PCl and no P–P containing by–products are observed.

In the structure shown in Figure 2.17, the Ge–Cl bonds are unexceptional [2.3017(6) – 2.3158(6) Å] but do not show the close intermolecular Ge···Cl interactions (< 4Å) which have been observed in both **1** and other salts containing this anion.[109] The cation is tetrahedral with the widest angles being between carbon atoms [(C(1)–P(1)–C(7): 114.40(9)°], as is the case in the only other structural report on secondary phosphonium cation, $[AlCl_4]^-[Me_2PH_2]^+$, prepared from Me_2PH, HCl and $AlCl_3$.[110] The P–H groups of the cation are opposite the basal Cl_3 plane of the anion (*i.e.* the lone pair on germanium points away from the cation) resulting in close intra– [H(1B)–Cl(1): 2.688Å] and inter–molecular hydrogen bonds [H(1A)–Cl(2)': 2.524 Å]. In addition, there are close contacts of a similar magnitude involving the anion and C–H groups, *i.e.* H(6)–Cl(2)': 2.685 Å.

2.2.7 Reaction of $GeCl_4$ and Ph_2PH (4:1)

It has been previously seen in 2.2.1 that the mechanism proposed for the 1:1 reaction of $GeCl_4$ and Ph_2PH is similar to that already proposed for a 1:1 reaction of the $GeCl_4$ with $CyPH_2$. Consequently, several attempts of reacting $GeCl_4$ with Ph_2PH in a 4:1 ratio have been carried out. The synthesis, with the aim of synthesizing Ph_2PGeCl_3 by loss of HCl, did not lead to the formation of the expected product. In the majority of the attempts tried, the $^{31}P\{^1H\}$ NMR, in (Et_2O), of the precipitate formed suggested a mixture of species. The main peak, a singlet has δ = 83.0 ppm, has been assigned to Ph_2PCl, and an unidentified species at 8.6 ppm. Only in one occasion did the $^{31}P(^1H)$ NMR, in toluene, of the precipitate show, as major resonance, a doublet [29.3 ppm (J_{P-H}= 532 Hz)] could arise from $Ph_2(H)P:\rightarrow GeCl_2$ (**5**).

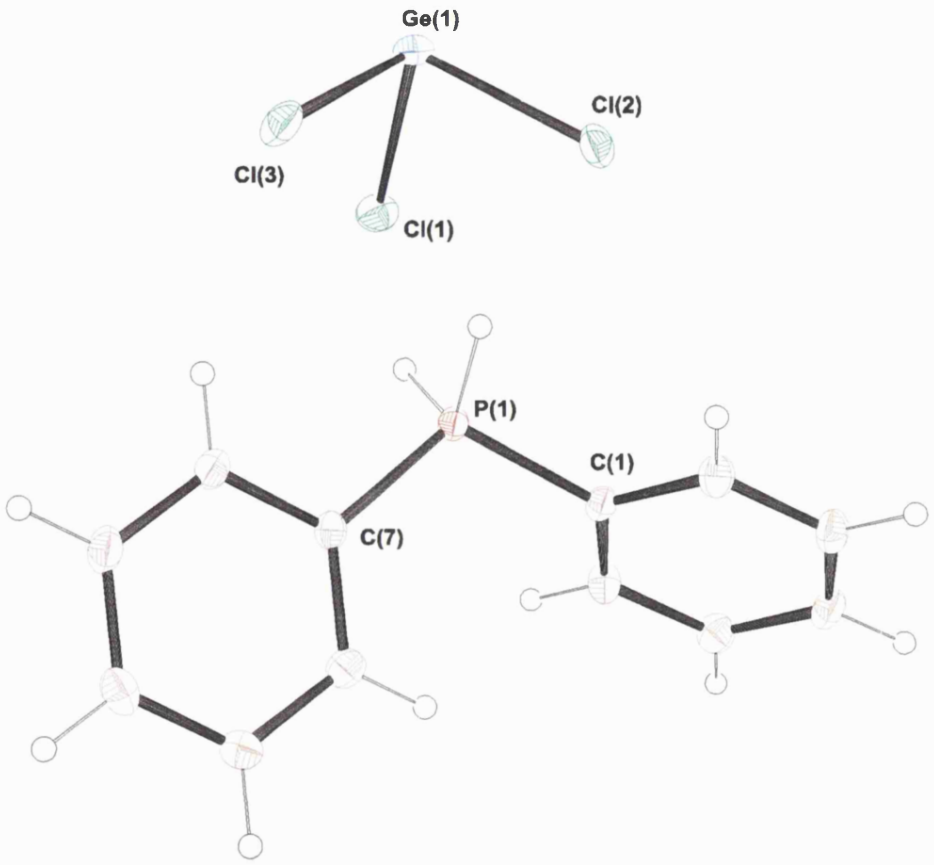

Figure 2.16 ORTEP plot of $[GeCl_3]^-[Ph_2PH_2]^+$ (**6**). Thermal ellipsoids are at the 30% probability level. Selected metrical data: Ge(1)–Cl(1) 2.3017(6), Ge(1)–Cl(2) 2.3158(6), Ge(1)–Cl(3) 2.3078(6), P(1)–H(1A) 1.323(16), P(1)–H(1B) 1.368(16), P(1)–C(1) 1.786(2), P(1)–C(7) 1.790(2) Å; Cl(1)–Ge(1)–Cl(2) 92.22(2), Cl(1)–Ge(1)–Cl(3) 95.88(2), Cl(2)–Ge(1)–Cl(3) 95.16(2), H(1A)–P(1)–H(1B) 107.4(15), H(1A)–P(1)–C(1) 107.5(11), H(1B)–P(1)–C(1) 110.2(10), H(1A)–P(1)–C(7) 107.7(11), H(1B)–P(1)–C(7) 109.4(11), C(1)–P(1)–C(7)114.40(9)°. The hydrogen atoms on bonded to the phosphorus are in calculated positions.

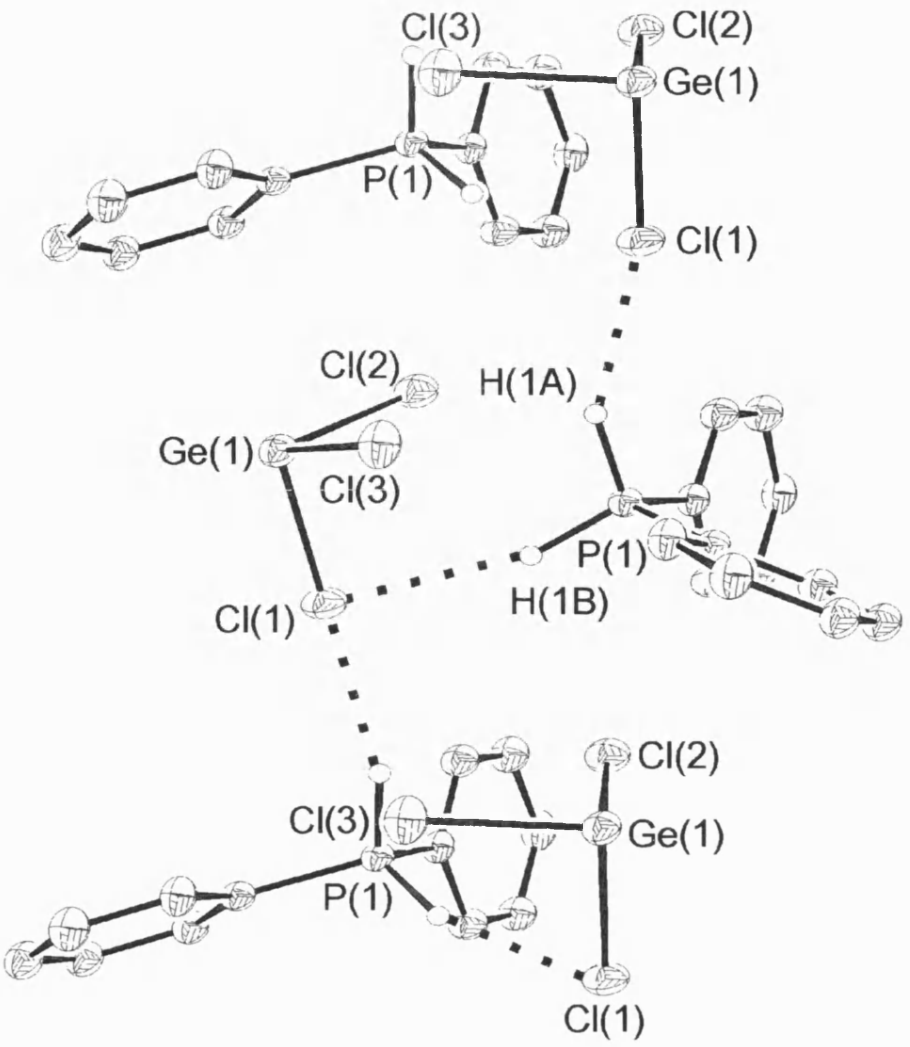

Figure 2.17 The lattice structure of $[GeCl_3]^-[Ph_2PH_2]^+$ (**6**).

2.3 Conclusions

Reaction of Ge(IV) chloride with primary and secondary phosphines does not lead to the production of phosphine adducts as expected but a mixture of products is obtained, among those $[GeCl_3]^-[CyPH_3]^+$ (**1**) and $[GeCl_3]^-[Ph_2PH_2]^+$ (**6**) have been isolated and crystallographically studied. Only when an excess of the germanium chloride is employed, have chlorogermyl phosphine been obtained. As examples of these, $CyP(H)GeCl_3$ (**2**) and $Ph(H)PGeCl_3$ (**4**) have been synthesized and fully characterized. Their suitability as single–source

precursors for the chemical deposition of GeP films have also been investigated. Results show that germanium phosphide in a 1:1 ratio has been deposited, but the films incur a post oxidation deposition that possibly converts the phosphide to phosphate.

2.4 Experimental Section

2.4.1 Synthesis of $Cy(H)PGeCl_3$ from $GeCl_4$ and $CyPH_2$ (1:1)

A Schlenk tube was charged with diethyl ether (30 ml) and cyclohexylphosphine (0.34 ml, 2.57 mmol) added. Germanium tetrachloride (0.30 ml, 2.57 mmol) was slowly added via syringe with continuous stirring of the solution. A white precipitate formed within a few minutes, though stirring was continued for up to 2 h. The precipitate and supernatant were separated by cannula filtration.

Microanalysis:

Found (calc.) for 1:1 $C_6H_{13}PCl_2Ge$ and $C_6H_{12}PCl_3Ge$ (**3**) and (**2**): C 26.2 (26.5)%; H 4.81 (4.84)%.

^{31}P NMR [δ (ppm), $CDCl_3$]:

precipitate: -60.2 [d, PH in $CyP(H)GeCl_3$], J_{P-H} = 188 Hz; 24.1 [t, PH_2 in $CyPH_2\rightarrow$:$GeCl_2$], J_{P-H} = 505 Hz.

supernatant: -61.2 [d, PH]; -111.6 [t, PH_2 in $CyPH_2$]; -83.1 [dd, PH in Cy<u>P</u>(H)–P(Cl)Cy (RR/SS or RS/SR)]; -25.4 [d, PCl in CyP(H)–<u>P</u>(Cl)Cy (RR/SS or RS/SR)]; -82.5 [dd, PH in Cy<u>P</u>(H)–P(Cl)Cy (RR/SS or RS/SR)]; -8.6 [d, PCl in CyP(H)–<u>P</u>(Cl)Cy (RR/SS or RS/SR)].

2.4.2 Synthesis of $Cy(H)PGeCl_3$ from $GeCl_4$ and $CyPH_2$ (4:1)

A solution of cyclohexylphosphine (0.48ml, 3.6 mmol) in toluene (10 ml) was stirred in an argon-filled Schlenk tube and $GeCl_4$ (1.66 ml, 14.5 mmol) added by syringe. Stirring was continued for 30 min during which time a white precipitate had formed. The precipitated product was then isolated by cannula filtration and then dried under vacuum; yield (0.30 g, 28%); m.p. 40 – 42 °C.

Microanalysis:

Found (calc.) for $C_6H_{12}PCl_3Ge$ (**2**): C 24.8 (24.5)%; H 4.27 (4.1)%.

^{31}P NMR [δ (ppm), $CDCl_3$]:

-60.2 [d, PH in $CyP(H)GeCl_3$], J_{P-H} = 188 Hz.

$^{13}C\{^1H\}$ NMR [δ (ppm), $CDCl_3$]:

35.1 [d, PC in $CyP(H)GeCl_3$], $^1J_{C-P}$ = 8.4 Hz; 34.0 ppm [d, PC$\underline{C}$ in $CyP(H)GeCl_3$], $^2J_{C-P}$ = 16.7 Hz; 31.3 ppm [d, PCC$\underline{C}$ in $CyP(H)GeCl_3$], $^3J_{C-P}$ = 17.7 Hz; 26.6 [s, PCCC$\underline{C}$ in $CyP(H)GeCl_3$].

^1H NMR [δ (ppm), $CDCl_3$]:

4.08 [dd], J_{H-P} = 188 Hz, J_{H-H} = 4.6Hz; 1.8 – 2.6 ppm (br m, 11 H, C_6H_{11}).

2.4.3 Synthesis of $Ph(H)PGeCl_3$ from $GeCl_4$ and $PhPH_2$ (4:1)

A solution of phenylphosphine (1.00 ml, 9.1 mmol) was stirred in an argon-filled Schlenk tube and $GeCl_4$ (4.41 ml, 36.0 mmol) added by syringe. Stirring was continued for 30 min during which time a white precipitate had formed. The precipitated product was then isolated by cannula filtration and then dried under vacuum; mp 69 – 72°C (Lit: 69-72°C).[100]

Microanalysis:

Found (calc.) for $C_6H_6PCl_3Ge$ (**4**): C 25.0 (25.2)%; H 2.1 (2.25)%.

^{31}P NMR [δ (ppm), $CDCl_3$]:

-65.7 [d, PH in $PhP(H)GeCl_3$] J_{P-H} = 200.5Hz.

$^{13}C\{^1H\}$ NMR [δ (ppm), $CDCl_3$]:

136.8 [d, PC in $PhP(H)GeCl_3$], $^1J_{P-C}$ =17.4Hz; 135.8 [d, PC<u>C</u> in $PhP(H)GeCl_3$], $^2J_{P-C}$ =15.1Hz; 124.2 [d, PCC<u>C</u> in $PhP(H)GeCl_3$], $^3J_{P-C}$ = 19.6Hz; 131.6[s, PCCC<u>C</u> in $PhP(H)GeCl_3$].

^1H NMR [δ (ppm), $CDCl_3$]:

4.84 [d, HP in $PhP(H)GeCl_3$], J_{P-H} = 200.5 Hz.

2.4.4 Reaction of $GeCl_4$ and Ph_2PH (1:1)

Using the methodology described for $GeCl_4/CyPH_2$, diphenyl phosphine (0.89 ml, 5.14 mmol) and $GeCl_4$ (0.6 ml, 5.14 mmol) were reacted in diethyl ether (30 ml) to yield a solid ($Ph_2PHGeCl_2$) that turned to oil on isolation.

Microanalysis:

Found (calc.) for $C_{12}H_{11}Cl_2Pge$ (**5**): C 44.7(44.3)%; H 3.52(3.37)%

^{31}P NMR [δ (ppm), $CDCl_3$]:

precipitate: 29.5 [d, PH in $Ph_2P(H)GeCl_2$], J_{P-H}=532Hz.

supernatant: 80.2 ppm (s); 5.3 ppm (s); -40.8 ppm (broad, probably Ph_2PH); 25.7 [t, H in $Ph_2PH_2^+$].

2.4.5 Reaction of $GeCl_4$ and Ph_2PH (4:1)

A solution of diphenylphosphine (1.00 ml, 1.07 g, 5.7 mmol) in toluene (20 ml) was stirred in an argon-filled Schlenk tube and $GeCl_4$ (2.62 ml, 4.9 g, 23 mmol) added by syringe. Stirring was continued for

30 mins during which time a white precipitate had formed. The solution was frozen using an acetone / CO_2 bath and any HCl removed under vacuum. After warming to room temperature, the precipitated product was isolated by cannula filtration, washed with hexane and dried under vacuum.

^{31}P NMR [δ (ppm), $CDCl_3$]:

29.5 [d, PH], J_{P-H}=532Hz; 83.0 ppm (s); 8.6 ppm (s).

2.4.6 AACVD

Films were grown using aerosol-assisted chemical vapor deposition (AACVD) on standard borosilicate glass slides under a N_2 atmosphere at 1 bar pressure, using a horizontal cold wall reactor; details of the reactor assembly have been given in Appendix Two. Glass substrates were cleaned prior to use by washing with water and soap, then acetone and subsequently dried in air.

2.4.6.1 AACVD of CyP(H)$GeCl_3$

The precursor was delivered in the gas phase as an aerosol of the compound dissolved in 30 ml of toluene and swept into the reactor using N_2 as the carrier gas. The precursor was consumed over a period of 20 mins. The reactor temperature was 500°C.

2.4.7 LPCVD

Films were grown on standard borosilicate glass slides using low pressure chemical vapor deposition (LPCVD); details of the reactor assembly have been given in Appendix Two. Glass substrates were cleaned prior to use by washing with water and soap, then acetone and subsequently dried in air.

2.4.7.1 LPCVD of $CyP(H)GeCl_3$

Approximately 0.85 g. of the complex was used. The precursor was held at 50°C for 2 hour at low pressure (ca.0.1 mmHg) to allow the complete evaporation. At the same time, external to the furnace, the substrate (glass slides) were placed and independently heated
at 500°C by a ceramic infrared heater. Once the deposition was ascertained, films were left to cool under low pressure.

2.4.7.2 CVD of $PhP(H)GeCl_3$

Approximately 1.5 g. of the complex was used. The precursor was held at 50°C for 1 hour at low pressure (ca.0.1 mmHg) to allow the complete evaporation. At the same time, external to the furnace, the substrate (glass slides) were placed and independently heated at 500°C by a ceramic infrared heater. Once the deposition was ascertained, films were left to cool under low pressure.

CHAPTER THREE

Reactions of Organogermylchloride with $Ph_2PSi(CH_3)_3$

3.1 Introduction

Reactions of organometallic halides with organophosphines have been under investigation since the beginning of the 1960s, when it was known that derivatives of all Group 14 metals formed covalent bonds to phosphorus.[111-113] In particular, for the purpose of this project, attention has been focused on reactions involving the formation of organotin and organogermyl phosphides.

The first ever example of an organogermane containing germanium bonded to phosphorus was reported in the early 1960s:[114] diphenyl(triethylgermyl)phosphorus, Et_3GePPh_2, was synthesized from Ph_2PLi and Et_3GeBr.

This pioneering work on organogermanium compounds was followed by another work[115] where the syntheses of thermally stable complexes, R_3GePPh_2 and $R_2Ge(PPh_2)_2$, from lithium diphenylphosphide and the organohalogenogermanes, R_3GeX and R_2GeX_2, were reported. This work, although claiming the syntheses of these materials, did not provide complete spectroscopic and/or crystallographic evidences to prove the preparation of the above mentioned compounds. The work also stated that on increasing the number of halogens attached to germanium, the reaction with lithium diphenylphosphide showed complications and none of the expected products were isolated.

Schumann and co workers[116-118] later reported the synthesis of an organogermanium phosphide. The reaction was carried out using diphenyldichlorogermane and phenylphosphine in the presence of triethylamine and it yielded bis(diphenylchlorogermyl)phenylphosphine. They also reported formation of several organogermanium phosphides using $(CH_3)_3SiPPh_2$ with different organohalogenogermane reagents.

$$\mathbf{2\ Ph_2GeCl_2 + PhPH_2 + 2\ Et_3N \rightarrow (Ph_2GeCl)_2PPh + 2\ Et_3N{\cdot}HCl} \qquad \textbf{(Eq. 3.1)}$$

$$Me_3GeCl + Ph_2PSiMe_3 \rightarrow Me_3GePPh_2 + Me_3SiCl \qquad \textbf{(Eq. 3.2)}$$

Since these early studies, no significant further work has been undertaken. Hence, with this project, attempts have been made to produce and characterize organogermylphosphines that can be used to deposit germanium phosphides. The employment of such precursors is the first attempt to grow GeP films from this class of material.

3.2 Results and Discussion

3.2.1 Reaction of Et_3GeCl and $Ph_2PSi(CH_3)_3$ (1:1)

There is no report in the literature of the reaction between Et_3GeCl and $Ph_2PSi(CH_3)_3$ to prepare Et_3GePPh_2 (**7**). Previous literature[115,117] reported the synthesis of **7** using either another phosphorus source (*i.e.* Ph_2PLi) or another organogenogermanium halide (*i.e.* Et_3GeBr). The reaction has been carried out under argon in the absence of solvent; the reaction was left stirring for 30 minutes and heated using a warm water bath. Et_3GePPh_2 (**7**), which resulted as a colorless liquid,[115] was then isolated and separated from the trimethylsilylchloride produced under vacuum.

$$Et_3GeCl + Ph_2PSi(CH_3)_3 \rightarrow Et_3GePPh_2 + Me_3SiCl \qquad \textbf{(Eq. 3.3)}$$
$$\textbf{(7)}$$

Microanalysis of a sample of the liquid product obtained from this reaction (C = 61.9; H = 7.15%) corresponds well with the formation of Et_3GePPh_2 (C = 62.6; H = 7.27%).

Evidence for the formation of Et_3GePPh_2 is also given by NMR spectroscopy. ^{31}P NMR ($CDCl_3$) shows a singlet at -52.4 ppm, which differs from the ^{31}P NMR ($CDCl_3$) for $Ph_2PSi(CH_3)_3$ that is a singlet at -55.5 ppm. ^1H NMR also confirms the formation of the product; there are several peaks between 1.04 and 1.61 ppm (br m, 15 H) that have assigned to the hydrogens of the ethyl groups and other several peaks between 7.18 and 8.2 ppm (br, m, 10 H) assigned to the hydrogens of the phenyl groups. No signals due to CH_3 groups remain in the ^1H spectrum.

$^{13}C\{^1H\}$ NMR ($CDCl_3$) presents information for the interaction between phosphorus and the carbons of the phenyl groups as doublet at δ = 135.7 ppm (d, $^1J_{C-P}$ = 20.38 Hz), 132.7 ppm (d, $^2J_{C-P}$ = 17.4 Hz), 127.3 ppm (d, $^3J_{C-P}$ = 6.8 Hz) and a singlet at 126.3 ppm for the *para*-carbon. The ethyl groups shows two doublets: the CH_2 doublet is at 4.98 ppm (d, $^2J_{C-P}$ = 8.3 Hz), while the CH_3 doublet is at 8.5 ppm (d, $^3J_{C-P}$= 3.6 Hz). 135° DEPT was used to distinguish the doublets belonging to CH_2 and CH_3. This is also consistent with the fact that the J_{C-P} for CH_2, which is closer to the phosphorus, is bigger that the J_{C-P} for the CH_3 groups.

In order to study the decomposition pathway of compound **7** to assess its suitability as CVD precursor, thermal gravimetric analysis (TGA) has been carried out. Figure 3.1 shows essentially complete evaporation of the product by 450°C (residue *ca* 3%). The compound proves to be extremely volatile.

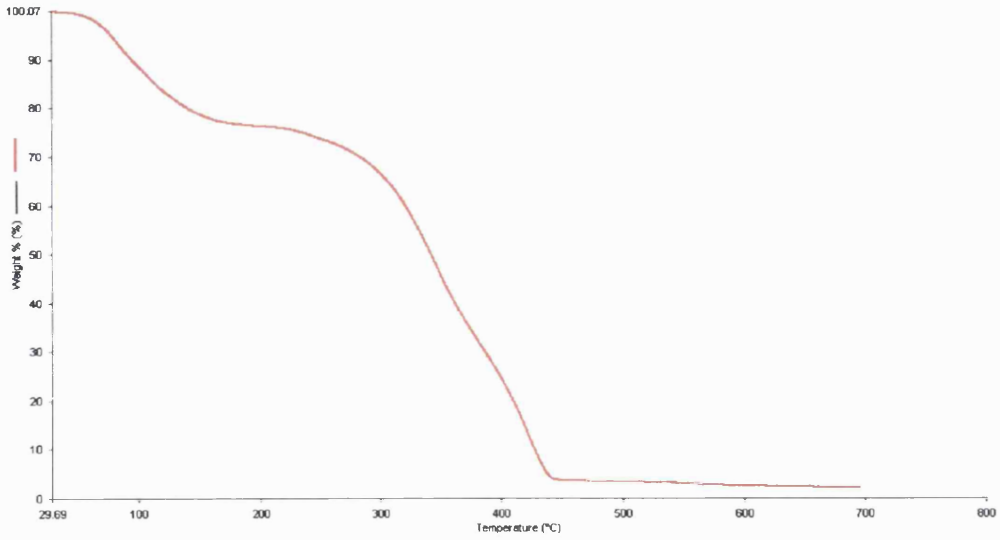

Fig. 3.1 TGA of Et_3GePPh_2

3.2.2 CVD studies of Et_3GePPh_2

Et_3GePPh_2 has been tested as a potential CVD precursor for its suitability to produce germanium phosphide films under LPCVD condition (see Appendix Two for the apparatus details).

Films using the liquid precursor **7**, approximately 0.65 ml, have been produced by LPCVD and deposited on standard borosilicate glass slides at both 450 and 550°C, producing transparent films with refringence patterns and a slight haze. The films were examined by scanning electron microscopy and shown in Figures 3.2a, 3.2b and 3.3. Isolated particles of diameter *ca* 15 μm are seen. It is also possible to see that increasing the temperature from 450 to 550°C, the number of particles diminishes. In particular, at 450°C the particles are very close to each other to form lines.

EDAX of the film deposited at 450°C (Fig. 3.5) provides an accurate quantitative analysis of the sample, validating the presence of both germanium and phosphorus. However, the film is contaminated with oxygen. The atomic

ratio found for this film is uniformly *ca.* Ge 14: P 15: O 71 atom percent, while the range over few sites are: Ge 13.0 – 13.8: P 14.5 – 16.4: O 70.2 – 71.8.

EDAX of the film deposited at 550°C (Fig. 3.4) confirms the presence of both germanium and phosphorus in almost 1:1 ratio, together with high value of oxygen. EDAX also shows the atomic ratio for the three elements are identical to what has been found for the deposition at 450°C. The EDAX result shows a homogenous composition over a number of points: Ge 14: P 15: O 71 atom percent.

As previously reported for CVD using precursor $Cy(H)PGeCl_3$ (**2**) as precursor, it is thought likely that the high value of oxygen is due to a number of species generated by a post oxidation reaction which converts the GeP into either GeO_2 or Ge(II)/Ge(IV) phosphates.

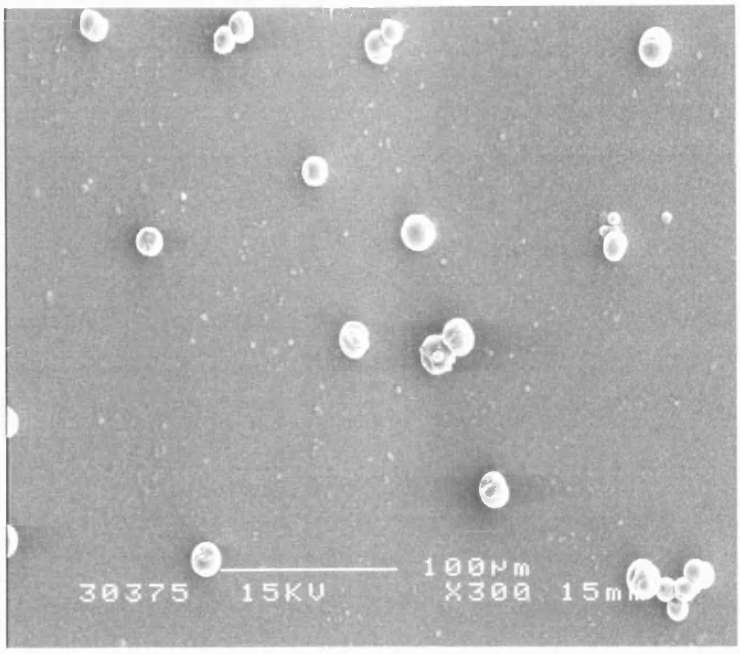

Fig. 3.2a SEM (15 kV) of film grown by LPCVD from Et_3GePPh_2 at 550°C

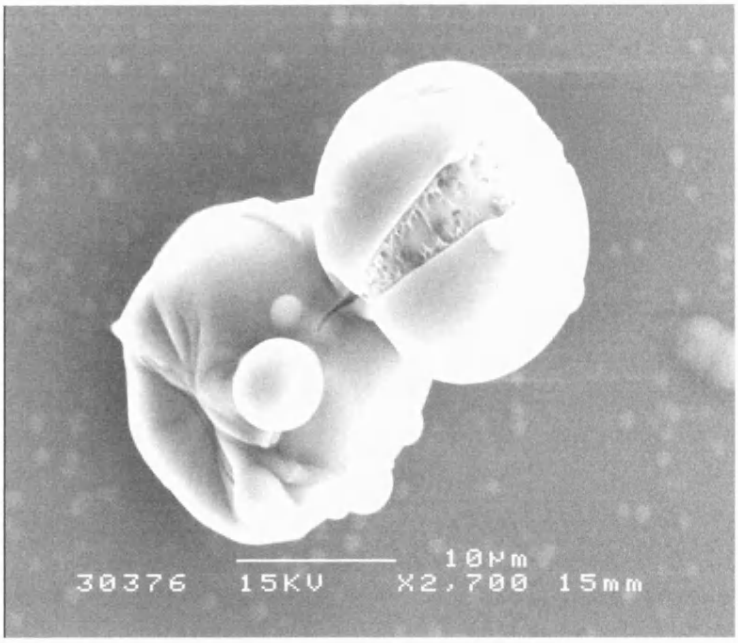

Fig. 3.2b SEM (15 kV) of particules of film grown by LPCVD from Et_3GePPh_2 at 550°C

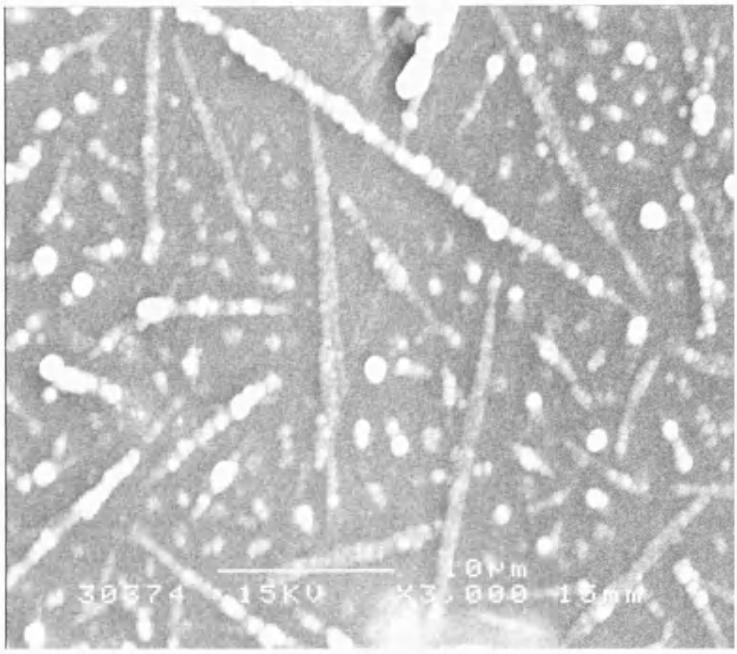

Fig. 3.3 SEM (15 kV) of film grown by LPCVD from Et_3GePPh_2 at 450°C

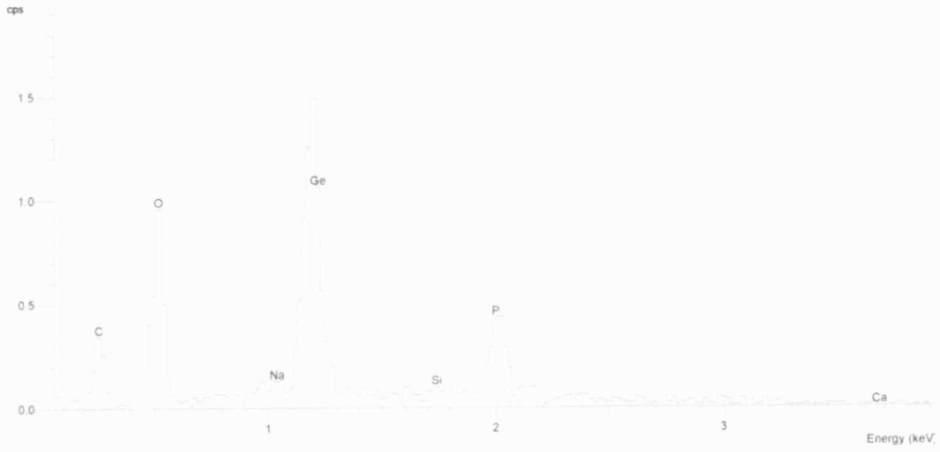

Fig. 3.4 EDAX (4 kV)of film grown by LPCVD from Et_3GePPh_2 at 550°C

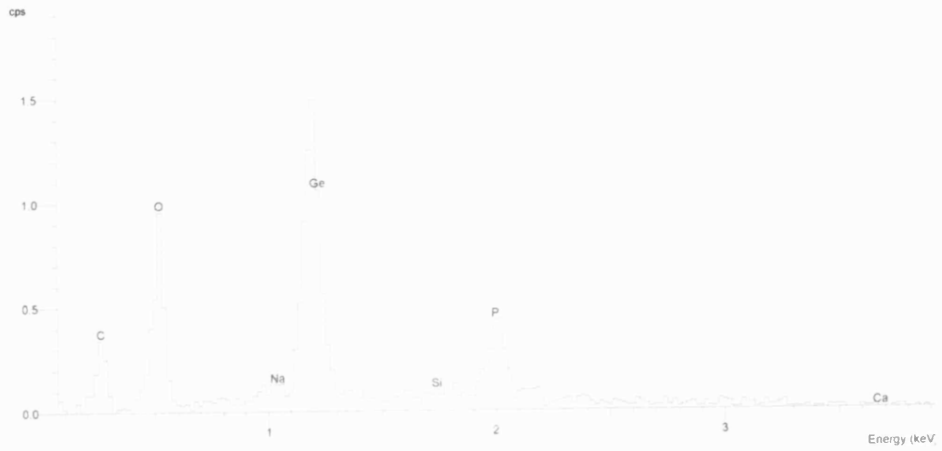

Fig. 3.5 EDAX (4 kV) of film grown by LPCVD from Et_3GePPh_2 at 450°C

3.2.3 Reaction of Et_2GeCl_2 and $Ph_2PSi(CH_3)_3$ (1:2)

Reaction of E_2GeCl_2 with $Ph_2PSi(CH_3)_3$ has been attempted in a 1:2 ratio. The product, a colorless liquid thought initially to be $Et_2Ge(PPh_2)_2$, has been produced under argon in absence of solvent after stirring the reagents for 30 minutes. Trimethylsilyl chloride, which is also produced in this reaction, has been removed under vacuum to obtain the $Et_2Ge(PPh_2)_2$.

$$\mathbf{Et_2GeCl + 2Ph_2PSi(CH_3)_3 \rightarrow Et_2Ge(PPh_2)_2 + Me_3SiCl} \qquad \textbf{(Eq. 3.4)}$$

Microanalysis of the liquid [found (calc.)% C = 54.0 (66.9)%; H = 5.75 (5.98)%] does not match with a formulation of $Et_2Ge(PPh_2)_2$. However, if a 1:1 ratio of the reagents is taken into consideration, the microanalysis is perfectly consistent with formation of $Et_2Ge(Cl)PPh_2$ (**8**) as shown in equation 3.5 [found (calc)% C = 54.0 (54.7)%; H = 5.75 (5.70)%].

$$\mathbf{Et_2GeCl_2 + Ph_2PSi(CH_3)_3 \rightarrow Et_2Ge(Cl)PPh_2 + Me_3SiCl} \qquad \textbf{(Eq. 3.5)}$$

(**8**)

^{31}P NMR ($CDCl_3$) exhibits a singlet at -44.0 ppm, a value that is close to that seen for **7** and similar compounds.[117] ^{1}H NMR ($CDCl_3$) shows several peaks between 1.4 and 0.9 ppm (br m, 10 H) that have been assigned to the ethyl groups, and between 8.03 and 6.9 ppm (br, m, 10 H) that have been assigned to the phenyl groups. The integrals are also consistent with $Et_2Ge(Cl)PPh_2$ and not with $Et_2Ge(PPh_2)_2$. $^{13}C\{^{1}H\}$ NMR ($CDCl_3$) for the carbons of the ethyl group presents two doublets: one belongs to CH_2 and has δ = 11.6 (d, $^{2}J_{C-P}$ = 5.5 Hz), and the other one belongs to CH_3 and has δ = 7.5 ppm (d, $^{3}J_{C-P}$ = 2.3 Hz). ^{13}C NMR presents evidence for the interaction between phosphorus and the carbons of the phenyl groups as doublets at δ = 132.3 ppm (d, $^{1}J_{C-P}$ = 19.6 Hz), 132.8 ppm (d, $^{2}J_{C-P}$ = 18.1 Hz), 127.6 ppm (d, $^{3}J_{C-P}$ = 6.8 Hz) and a singlet, δ = 126.6 ppm.

Having previously analyzed the TGA of the diphenyl(triethylgermyl)phosphine, the same behavior might be expected for the diphenyl(diethylchlorogermyl)phosphine. In fact, the thermal gravimetric analysis (Fig. 3.6) for this compound exhibits a curve similar in shape to that seen (Fig. 3.1). The final residual mass has a weight of just 2.8% of the total. $Et_2Ge(Cl)PPh_2$ is evidently extremely volatile.

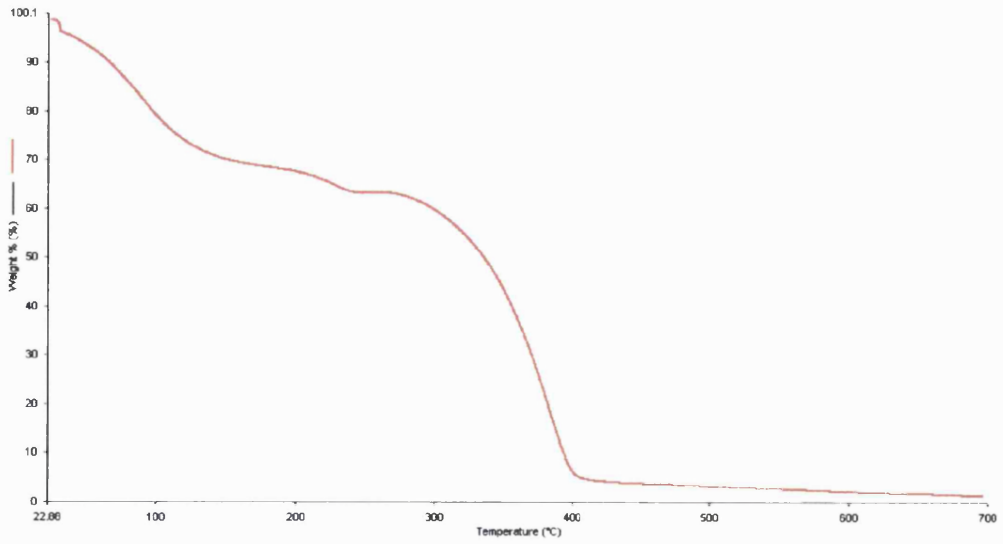

Fig. 3.6 TGA of $Et_2Ge(Cl)PPh_2$

3.2.4 CVD studies of $Et_2Ge(Cl)PPh_2$

$Et_2Ge(Cl)PPh_2$ has been evaluated as a potential CVD precursor for its suitability to produce germanium phosphide films under CVD condition (see Appendix Two for the apparatus details).

Films using the liquid precursor **8**, approximately 0.65 ml, have been produced by LPCVD and deposited on standard borosilicate glass slides at 450, 500 and 550°C producing transparent films with refringence patterns and a slight haze. The films have been examined by SEM and are presented in Figures 3.7a–c. What is evident from the SEM pictures is that the number of particles present in the films decreases as the temperature rises. The particles observed are all above the film surface and, while their size ranges from 0.4 to 1.0 μm in Figure 3.7a, the particles size in Fig. 3.7b and 3.7c varies from 4.3 to 21.7 μm.

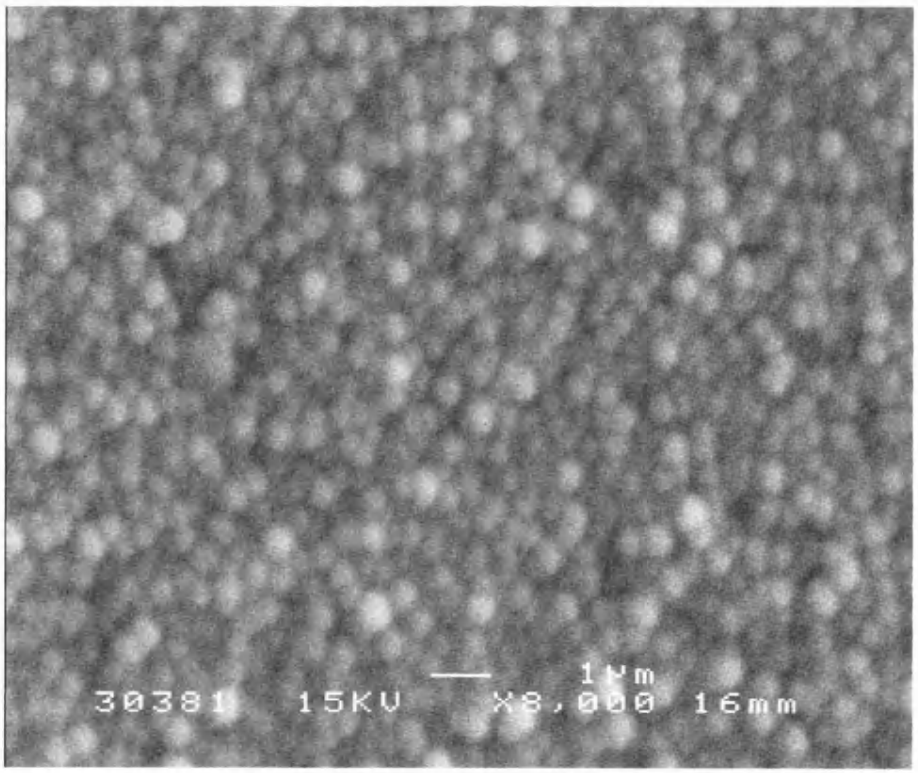

Fig. 3.7a SEM (15 kV) of film grown by LPCVD from $Et_2Ge(Cl)PPh_2$ at 450°C

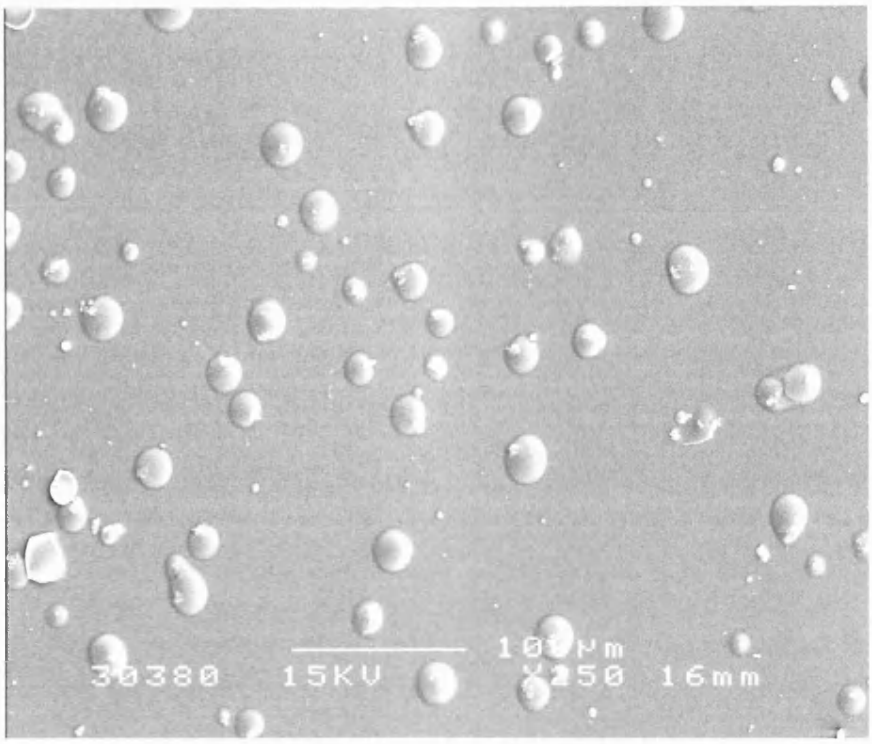

Fig. 3.7b SEM (15 kV) of film grown by LPCVD from $Et_2Ge(Cl)PPh_2$ at 500°C

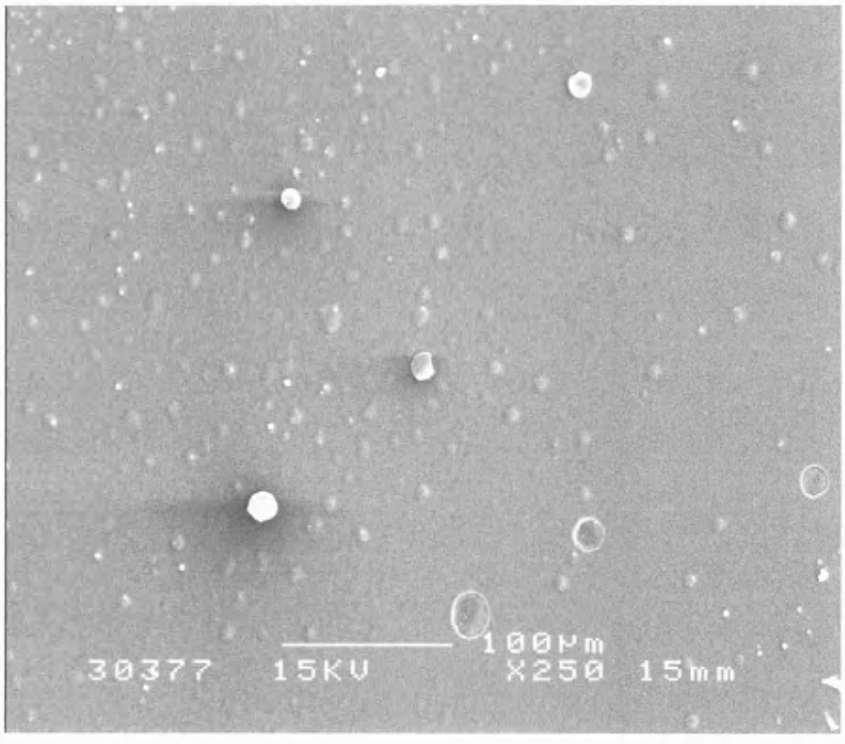

Fig. 3.7c SEM (15 kV) of film grown by LPCVD from $Et_2Ge(Cl)PPh_2$ at 550°C

EDAX of the films (Fig. 3.8–3.10) are summarized in Table 3.1. The presence of a large amount of oxygen is it thought to be associated with either GeO_2 or $Ge_3(PO_4)_4/Ge_3(PO_4)_2$ produced by an oxidation occurred after the films have been deposited. The germanium phosphide present in the films has been partially converted either in to germanium phosphates or germanium oxide. It is also evident that, while the level of oxygen remains constant, the percentage of germanium drops with the increase of temperature.

Table 3.1 EDAX for $Et_2Ge(Cl)PPh_2$.

T (°)	Ge (atom %)	P (atom %)	O (atom %)
450°C	14	13	72
500°C	13	17	70
550°C	7	20	73

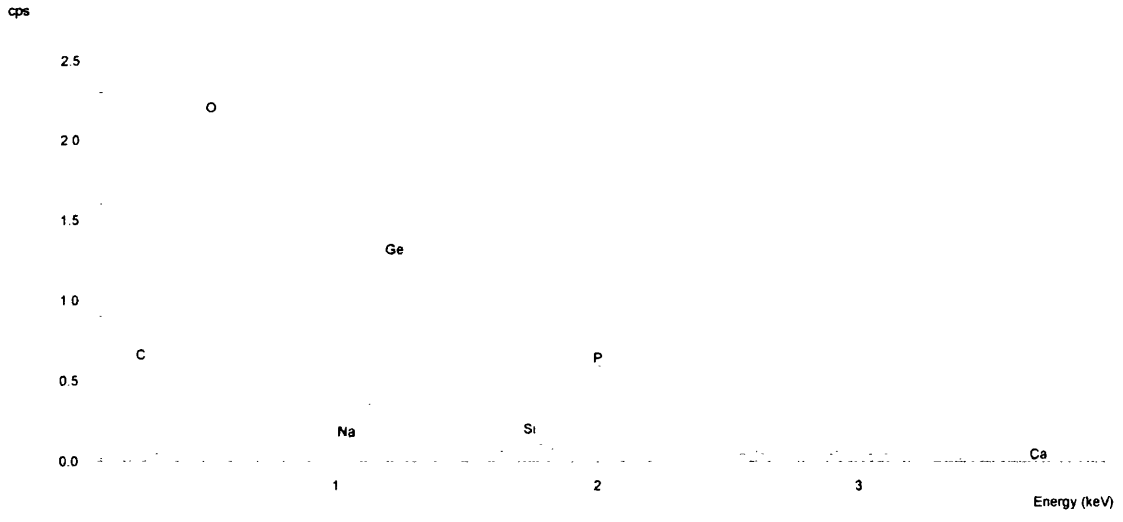

Fig. 3.8 EDAX (4 kV) of film grown by LPCVD from $Et_2Ge(Cl)PPh_2$ at 450°C

Fig. 3.9 EDAX (4 kV) of film grown by LPCVD from $Et_2Ge(Cl)PPh_2$ at 500°C

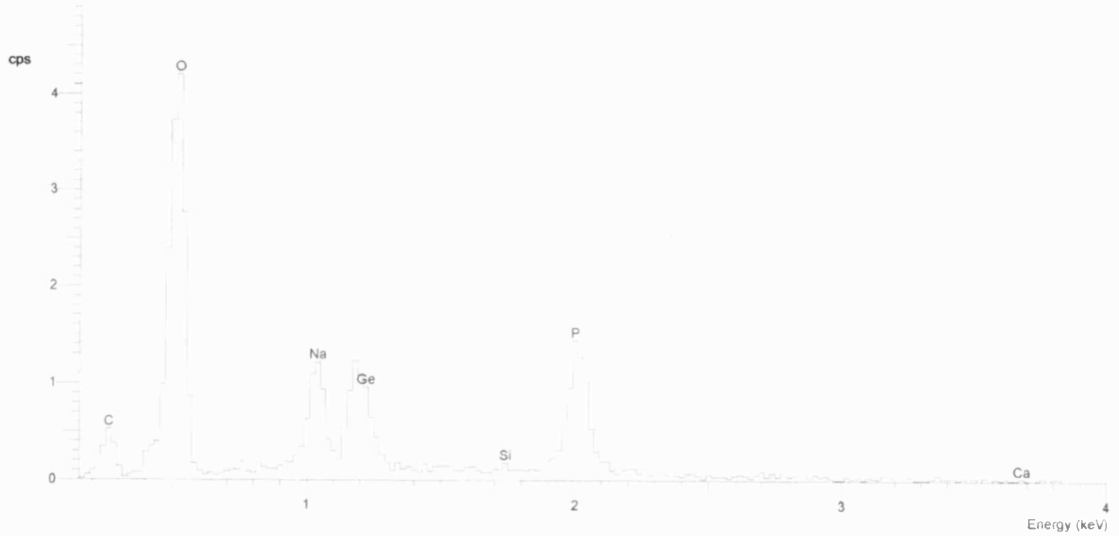

Fig. 3.10 EDAX (4 kV) of film grown by LPCVD from $Et_2Ge(Cl)PPh_2$ at 550°C.

3.2.5 Reaction of Ph_3GeCl and $Ph_2PSi(CH_3)_3$ (1:1)

The synthesis of Ph_3GePPh_2 has been attempted by reacting Ph_3GeCl with diphenylphosphine in the presence of dbu (1,8-diazabicyclo[5.4.0]undec–

7–ene), a base which helps formation of the Ge–P bond:[119] the presence of a nitrogen atom in the base provides a lone pair which facilitates and promotes the reaction by binding a molecule of HCl produced from the reagents.

$$Ph_3GeCl + Ph_2PH + dbu \rightarrow Ph_3GePPh_2 + dbuH^+Cl^- \quad \textbf{(Eq. 3.6)}$$

(9)

The reaction mixture, after all the reagents gave been added, is a colorless liquid whose ^{31}P NMR ($CDCl_3$) shows a doublet (main peak) at -39.1 ppm and which has been assigned to Ph_2PH.[120] The second, smaller peak, is a singlet at -51.3 ppm which has been assigned to Ph_3GePPh_2 (**9**). The appearance of the spectrum was unchanged after heating the NMR tube in a warm water bath for 15 h.

In previous reaction, *i.e.* Eq 3.3 and 3.5, use of $Ph_2PSi(CH_3)_3$ has been reported to produce organogermylphosphines using different organogermanium chlorides. Having seen that those syntheses were successful and that reaction with dbu was not a complete success, attempts to produce Ph_3GePPh_2 have been carried out employing $Ph_2PSi(CH_3)_3$. The reaction has been carried out in dichloromethane adding the diphenyl(trimethylsilyl)phosphine to the organogermanium halide. The solution, left stirring for 3 hours under a constant flow of argon, remained colorless and clear. The solvent and Me_3SiCl produced have been removed under vacuum generating a white solid.

$$Ph_3GeCl + Ph_2PSi(CH_3)_3 \rightarrow Ph_3GePPh_2 + Me_3SiCl \quad \textbf{(Eq. 3.7)}$$

(9)

Microanalysis of a sample of the compound formed from this reaction (C = 72.6; H = 5.41%) corresponds well with the formation of Ph_3GePPh_2 (C = 73.5; H = 5.1%).

^{31}P NMR ($CDCl_3$) shows a singlet, δ = -51.3 ppm as previously reported for (**9**) prepared from Eq.3.6. $^{13}C\{^1H\}$ NMR presents doublets at δ = 134.6 ppm (d,

$^{2}J_{C-P}$ = 8.30 Hz),133.8 ppm (d, $^{3}J_{C-P}$ = 2.26 Hz), 132.7 ppm (d, $^{1}J_{C-P}$ = 18.12 Hz) and a singlet, δ = +132.3 ppm. These peaks arise from the interaction of phosphorus with the carbons of the phenyl groups. ^{1}H shows several peaks from 6.89 ppm to 7.42 ppm (br m, 25 H).

It has been seen that the thermal decomposition of diphenyl(triethylgermyl)phosphine and diphenyl(diethylchlorogermyl)phosphine shows how these two compounds are extremely volatile. The TGA curve for **9** (Fig. 3.10) present a final mass of 1.96 % of the total weight. It means that is also particularly volatile.

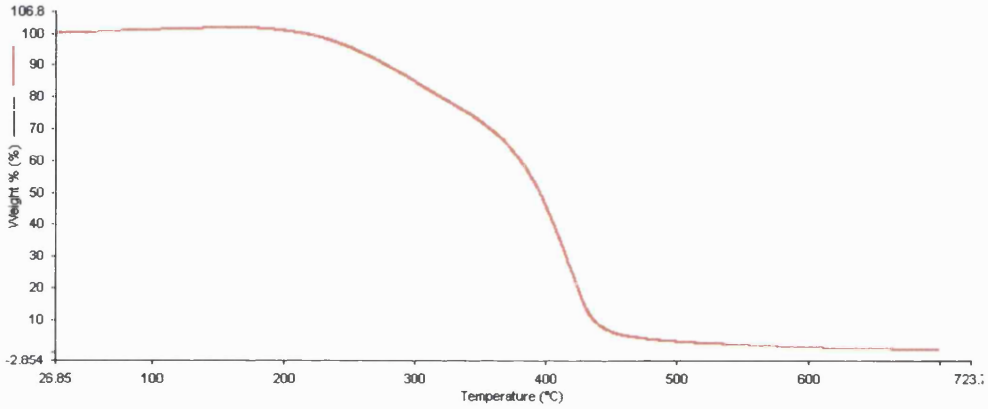

Fig. 3.10 TGA of Ph_3GePPh_2

3.2.6 CVD studies of Ph_3GePPh_2

Ph_3GePPh_2 has been used as potential CVD precursor for its suitability to produce germanium phosphide films under CVD condition, using either a purpose–built low pressure CVD and an aerosol–assisted CVD reactors, whose apparatus details are reported in Appendix Two.

Films using the solid precursor **9**, approximately 0.30 g, have been produced by AACVD and LPCVD and deposited on standard borosilicate glass slides at 500°C producing transparent films with a slight haze. The films were

examined and are presented in Figures 3.11 and 3.12. As it is clear to see from these pictures, **9** do not generate the same kind of particles when deposited with different techniques. While the SEM picture obtained from the AACVD shows square shaped particles with an average side size of 1 μm, the SEM acquired from low pressure deposition shows isolated particles of irregular shape and different size.

The films were also analyzed (EDAX) which shows that the films are all rich in phosphorus, while there is no evidence for the presence of germanium.

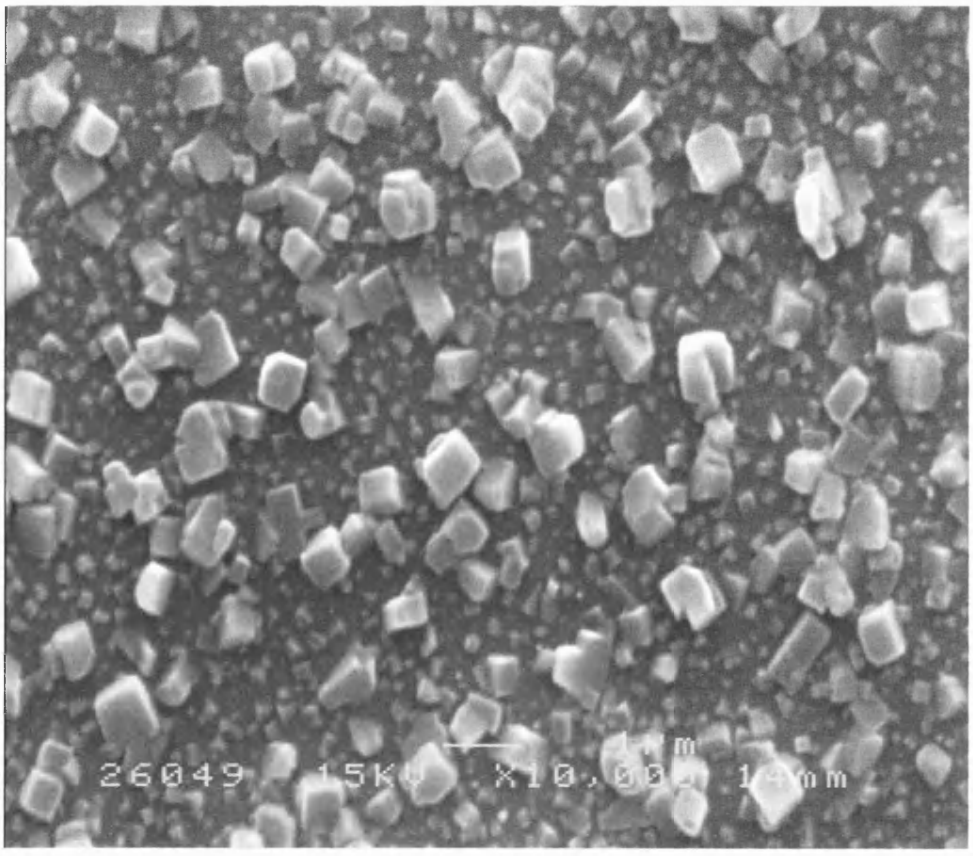

Fig. 3.11 SEM (15 kV) of film grown by AACVD from Ph_3GePPh_2 at 500°C

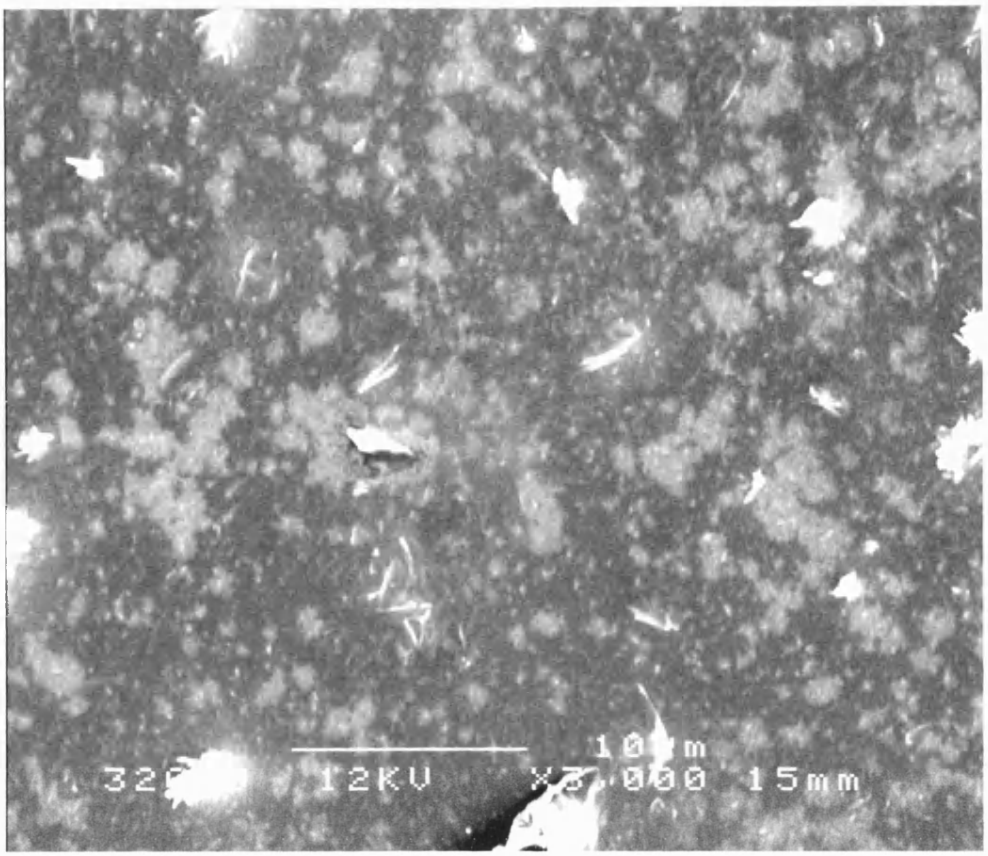

Fig. 3.12 SEM (15 kV) of film grown by LPCVD from Ph_3GePPh_2 at 500°C

3.3 Conclusions

Reactions of different organogermanium chlorides with diphenyl(trimethyl)silyl phosphine have been attempted and the corresponding organogermanium phosphides successfully obtained have been studied and fully characterized. Compounds Et_3GePPh_2 (**7**), $Et_2Ge(Cl)PPh_2$ (**8**) and Ph_3GePPh_2 (**9**) have been also tested as precursors for the deposition of GeP films over a glass substrate and, except **9** which deposited a film containing only phosphorus, precursors **7** and **8** have deposited germanium and phosphorus in a 1:1 ratio. However, the large presence of oxygen in the films has been ascribed to a post oxidation deposition reaction.

3.4 Experimental Section

3.4.1 Synthsis of Et_3GePPh_2 from Et_3GeCl and $Ph_2PSi(CH_3)_3$ (1:1)

To a solution of diphenyl(trimethylsilyl)phosphine (0.75 ml, 2.93 mmol), in an argon-filled Schlenk tube, triethylchlorogermane (0.48 ml, 2.93 mmol) was added by syringe. Stirring was continued for 30 minutes in a warm water bath. Triethylgermyldiphenylphosphine was isolated by leaving the reaction mixture under vacuum for 5 minutes to remove the trimethylsilyl chloride formed.

Microanalysis:

Found (calc.) for $C_{18}H_{25}PGe$ (**7**): C 61.9 (62.6)%; H 7.15 (7.25)%

^{31}P NMR [δ (ppm), $CDCl_3$]:

-52.4 ppm [s].

^{13}C NMR [δ (ppm), $CDCl_3$]:

135.7 ppm [d, PC], $^1J_{C-P}$ = 20.4 Hz; 132.7 ppm [d, PC<u>C</u>], $^2J_{C-P}$ = 17.4 Hz; 127.3 ppm [d, PCC<u>C</u>], $^3J_{C-P}$ = 6.8 Hz; 126.3 ppm [s, PCCC<u>C</u>]; 5.0 ppm [d, PGe<u>C</u>], $^2J_{C-P}$ = 8.3 Hz; 8.5 ppm [d, PGeC<u>C</u>,], $^3J_{C-P}$ = 3.6Hz.

^1H NMR [δ (ppm), $CDCl_3$]:

1.04 – 1.6 ppm (br m, 15 H, in C_2H_5);

7.18 – 8.2 ppm (br m, 10 H, in C_6H_5).

3.4.2 Synthesis of $Et_2Ge(Cl)PPh_2$ from Et_2GeCl_2 and $Ph_2PSi(CH_3)_3$ (1:2)

To a solution of diphenyl(trimethylsilyl)phosphine (0.60 ml, 2.34 mmol), in an argon-filled Schlenk tube, diethyldichlorogermane (0.172 ml, 1.17 mmol) has been added by syringe . Stirring was continued for 30 minutes in a warm water bath. Diethylchlorogermyldiphenylphosphine was isolated by leaving the reaction mixture

under vacuum for 5 minutes to remove the diphenyl(trimethylsilyl)phosphine in excess and the trimethylsilyl chloride formed.

Microanalysis:

Found (calc.) for $C_{16}H_{20}ClPGe$ (**8**): C 54.0 (54.7)%; H 5.75 (5.70)%

^{31}P NMR [δ (ppm), $CDCl_3$]:

-44.0 ppm [s]

$^{13}C\{^1H\}$ NMR [δ (ppm), $CDCl_3$]:

132.3 ppm [d, PC], $^1J_{C-P}$ = 19.6 Hz; 132.8 ppm [d, PC<u>C</u>], $^2J_{C-P}$ = 18.1 Hz; 127.6 ppm [d, PCC<u>C</u>], $^3J_{C-P}$ = 6.8 Hz; 126.6 ppm [s, PCCC<u>C</u>]; 11.6 ppm [d, PGe<u>C</u>], $^2J_{C-P}$= 5.5 Hz; 7.5 ppm [d, PGeC<u>C</u>], $^3J_{C-P}$ = 2.3 Hz.

^1H NMR [δ (ppm), $CDCl_3$]:

0.9 – 1.4 ppm [br m, 10 H, $(C_2H_5)Ge$]; 8.03 – 6.9 ppm [br m, 10 H, $P(C_6H_5)_2$].

3.4.3 Synthesis of Ph_3GePPh_2 from Ph_3GeCl and $Ph_2PSi(CH_3)_3$ (1:1)

$Ph_2PSi(CH_3)_3$ (0.4 ml, 1.56 mmol) has been added to a solution of Ph_3GePPh_2 (0.53 gr, 1.56 mmol) in dichloromethane (10 ml) prepared in an argon filled Schlenk tube. The colorless and clear reaction mixture was left stirring for three hours and then a white solid was obtained by removing the solvent under vacuum. The solid material was dried for two hours.

Microanalysis:

Found (calc.) for $C_{30}H_{25}PGe$ (**9**): C 72.6 (73.5)%; H 5.41 (5.10)%

^{31}P NMR [δ (ppm), $CDCl_3$]:

-51.3 ppm (s).

$^{13}C\{^1H\}$ NMR [δ (ppm), $CDCl_3$]:

132.7 ppm [d,PC], $^1J_{C-P}$ = 18.1 Hz; 134.6 ppm [d, PC<u>C</u>], $^2J_{C-P}$ = 8.3 Hz; 133.8 ppm [d, PCC<u>C</u>], $^3J_{C-P}$ = 2.3 Hz; 132.3 ppm [s, PCCC<u>C</u>].

^1H NMR [δ (ppm), $CDCl_3$]:

6.89 – 7.42 ppm (br m, 25 H, in C_6H_5).

3.3.4 LPCVD

Films were grown on standard borosilicate glass slides using low pressure chemical vapor deposition (LPCVD); details of the reactor assembly have been given in Appendix Two. Glass substrates were cleaned prior to use by washing with water and soap, then acetone and subsequently dried in air. To prevent the precursor from air contamination, it has been stored in Young NMR tube packed with argon and then injected into the reaction tube under a flow of argon atmosphere.

3.3.4.1 CVD of Et_3GePPh_2

Approximately 0.65 ml of the complex was used. The precursor was held at 180°C for 1 hour at low pressure (*ca.* 0.1 mmHg) to allow the complete evaporation. At the same time, external to the furnace, the substrate (a glass slide) were placed and independently heated at temperature of either 450 or 550°C by a ceramic infrared heater. Once the deposition was completed, films were left to cool under low pressure.

3.3.4.2 CVD of $Et_2Ge(Cl)PPh_2$

Approximately 0.65 ml of the complex was used. The precursor was held at 200°C for 2 hour at low pressure (ca.0.1 mmHg) to allow the complete evaporation. At the same time, external to the furnace, the substrate (a glass slide) was placed and independently heated at temperatures of either 450, 500 or 550°C by a ceramic infrared heater. Once the deposition was completed, films were left to cool under low pressure.

3.3.4.3 CVD of Ph_3GePPh_2

Approximately 0.31 g. of the complex was used. The precursor was held at 150°C for 1 hour at low pressure (ca.0.1 mmHg) to allow the complete evaporation. At the same time, external to the furnace, the substrate (a glass slide) were placed and independently heated at temperature of 500°C by a ceramic infrared heater. Once the deposition was completed, films were left to cool under low pressure.

CHAPTER FOUR

Reactions of Sn(II) and Sn(IV) Halides with Primary, Secondary and Tertiary Phosphines

4.1 Introduction

In contrast to tin tetrahalides and germanium tetrahalides, no extensive work has been carried out to investigate the formation of tin dihalide adducts with phosphorus donors, which are potential precursors for tin phosphide. Only two reports have appeared in the literature and both involve tertiary phosphines. The first one, dated 1969, reports the syntheses of 5 different adducts of tin(II) halides with triphenyl phosphine and *n*-tributylphosphine, as well as their Mössbauer parameters.[121] The second work was published by Du Mont *et al.* in the mid 1970s. They reported the reaction of tri-*tert*-butylphosphine with tin(II) chloride and bromide and the formation of the corresponding adduct.[92]

$$SnX_2 + {}^tBu_3P \rightarrow {}^tBu_3PSnX_2 \qquad \textbf{(Eq. 4.1)}$$

(x = Cl, Br)

Since the late 1960s, researchers started to investigate the synthesis of tin tetrahalide adducts, in particular those involving $SnCl_4$, with tertiary phosphines. Such studies were assisted by I.R.[122,123] and ^{119}Sn Mössbauer[124-126] data (Table 4.1) and only in a few cases by ^{31}P NMR[127] and ^{119}Sn NMR.[128]

Tab 4.1 Mössbauer Parameters for Tin Complexes

Compound	δ (mms^{-1})	ΔE_Q (mms^{-1})
$SnCl_4PPh_3$[a]	0.82	0
$SnCl_4{\cdot}2(PPh_3)$[a]	0.78	0
$SnCl_4{\cdot}2(PPh_2Me)$[a]	0.79	0.57
$SnCl_4{\cdot}2(PPhEt_2)$[a]	0.86	1.04
$SnCl_4{\cdot}2(Et_3P)$[a]	0.84	1.15
$SnCl_4{\cdot}2(PBu^n{}_3)$[a]	0.87	1.06
$SnCl_4{\cdot}PCy_3$[b]	0.49	0.36
$SnCl_4{\cdot}2(PPr^n{}_3)$[b]	0.89	0.95
$SnCl_4{\cdot}2(Ph_2PCH_2CH_2PPh_2)$[a]	0.69	0

[a] Cunnungham, Frazer, Donaldson, J.Chem. Soc.(A), 2049, 1971,
[b]Carty, Hinsperger, Mihichuk, Sharma, Inorg. Chem, 2573, 9, 1970

Only 4 such adducts have been crystallographically characterized (Table 4.2). The first adduct isolated was $SnCl_4{\cdot}2(PEt_3)$ in 1973[129] which confirmed previous works,[93,130] where a *trans*–P_2SnCl_4 structure was identified (Fig. 4.1). In recent years, only three more tin(IV) adducts have been crystallographically characterized, both with unidentate and bidentate phosphines.

Tab. 4.2 Structural Parameters for Tin Phosphines and phosphine Oxide Complexes

Compound	CN	Geometry	Sn–P (Å)	Sn–O (Å)
Phosphine Adducts				
$SnI_4(Pr^n_3P)_2$[j]	6	Octahedral	2.69(1)	
$SnCl_4(Et_3P)_2$[m]	6	Octahedral	2.615(5)	
$SnCl_4$(dppe)[o]	6	Octahedral	2.653(2)	
$SnCl_4{\cdot}2$(dppm)[p]	6	Octahedral	2.649(1)	
Phosphine Oxide Adducts				
$SnCl_4O_2$(ddpf)[a]	6	dist. Octahedral		2.111(2)
$Sn_2Br_2(C_7H_7)_2(C_6H_4Cl)_4(C_{26}H_{24}O_2P_2)$[b]	5	Trig. Bipyramidal		2.384(4)
Ph_3SnCl(dppe)[c]	5	Trig. Bipyramidal		2.346(6)
Cis-$SnBr_4(OPPh_3)_2$[d]	6	Octahedral		2.080(8)
$[(SnPh_3Cl)_2(OPPh_2CH_2)_2]$[e]	5	Trig. Bipyramidal		2.357(3)
$Et_2SnCl_2[Me(^iPrO)P(O)]_2CH_2$[f]	6	dist. Octahedral		2.417(7)
Ph_3SnCl(tppo)[g]	5	Trig. Bipyramidal		2.376(6)
$SnBr(C_4H_3S)_3[Ph_3PO]$[h]	5	Trig. Bipyramidal		2.335(4)
$Bu^n_2SnCl_4$(dppoe)[k]	6	Trig. Bipyramidal		2.356(7)
$Bu^n_2SnCl_4$(dppoe)[k]	6	dist. Octahedral		2.640(7)

[a] Yamin, Shawkataly, Hoong-Kun Fun, Sivakamur, *Acta. Cryst., Sect.C*, 1966, **52**, 1996
[b] C.Wei, W.Kong, Das, Jameson, Butcher, *Acta. Cryst., Sect.C*, 2034, **46**, 1990
[c] C.Pelizzi, G.Pelizzi, *Inorg.Nucl.Chem. Lett.*, 451, **16**, 1980
[d] Tudela, Tornero, Monge, Sanchez-Herencia, *Inorg. Chem.*, 3928, **32**, 1993
[e] C.Pelizzi, G.Pelizzi, *J.Organom. Chem*, 411, **202**, 1980
[f] Lorberth, Wocadlo, Massa, Yashina, Grigor'ev, Petrosyan, *J.Organom. Chem*, 163, **408**, 1994
[g] Eppley, Ealy, Yoder, Spencer, Rheingold, *J.Organom. Chem*, 133, **431**, 1992
[h] Allen, Derbyshire, Nowell, Brooks, *J.Organom. Chem*, 263, **260**, 1984
[k] Harrison, Sharpe, Pelizzi, Pelizzi, Tarasconi, J.Chem., *Soc, Dalton Trans.*, 921, 1983
[j] Bricklebank, Godfrey, McAuliffe, Pritchard, *J. Chem. Soc., Chem. Comm.*, 695, 1994.
[m] Mather, McLaughlin, Pidcock, *J. Chem. Soc., Dalton Trans.*, 1823, 1973.
[o] Kunkel, Dahnicke, Goesmann, Fenske, *Z. Naturf., Teil B*, **50**, 848, 1995.
[p] Daktemieks, Hongjian Zhu, Tiekink, *Main Group Metal Chem.*, 519, **17**, 1994.

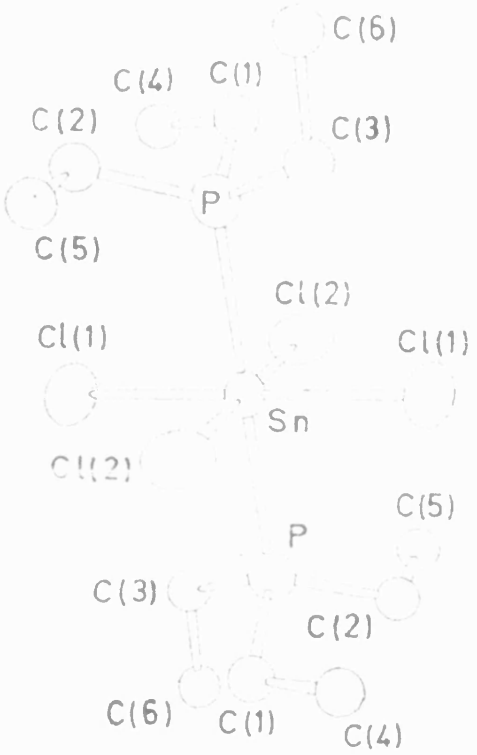

Fig. 4.1 Structure of $SnCl_4{\cdot}2(PEt_3)$ showing the numbering scheme. Selected bonds lengths (Å) and angles (°) for $SnCl_4{\cdot}2(PEt_3)$. Hydrogen atoms have been omitted for clarity. Sn–Cl(1) 2.445(5), Sn–Cl(2) 2.455(5), Sn–P 2.615(5); Cl(1)–Sn–Cl(2) 89.90(18), Cl(1)–Sn–Cl(2') 90.10(18), Cl(1)–Sn–P 91.18(18).

Another structurally authenticated example of a tin complex containing both tertiary phosphine and an iodide ligand was $SnI_4{\cdot}2PPr^n_3$ (Fig.4.2), prepared by reaction between unactivated tin metal powder and $Pr^n_3PI_2$.[131]

$$\mathbf{2Pr^n_3PI_2 + Sn \rightarrow SnI_4{\cdot}2PPr^n_3} \qquad \textbf{(Eq. 4.2)}$$

This is a simple one–step route to tin(IV) complexes containing iodide ligands that have proved difficult to synthesize by conventional methods. This air sensitive compound revealed a *trans* structure in accordance with the previous reported work on $SnCl_4{\cdot}2(Et_3P)$.[129]

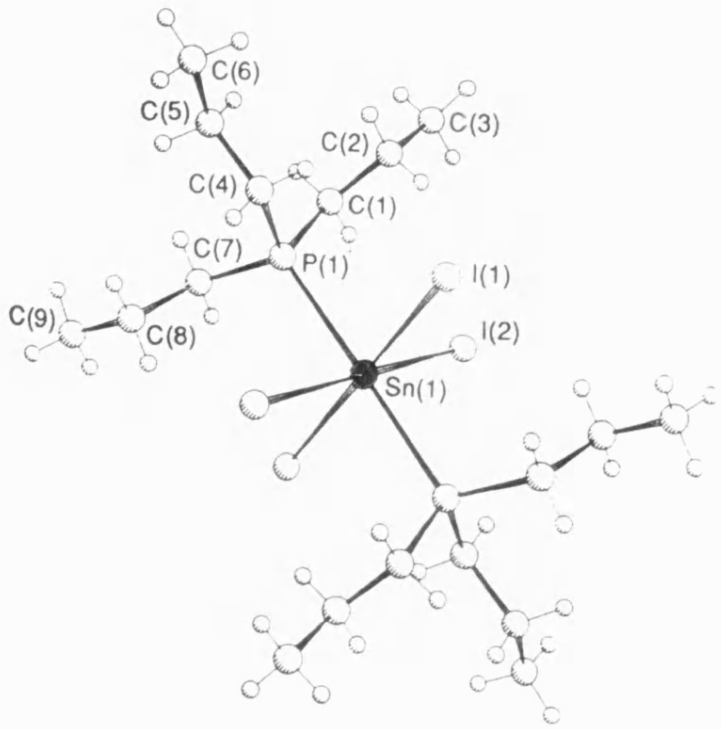

Fig. 4.2 ORTEP plot of $SnI_4{\cdot}2PPr^n_3$. Selected bonds lengths (Å) and angles (°) for $SnI_4{\cdot}2PPr^n_3$: Sn(1)–I(1) 2.872(3), Sn(1)–I(2) 2.863(3), Sn(1)–P(1) 2.69(1); I(1)–Sn(1)–I(1)' 180.00, I(1)–Sn(1)–I(2) 92.2(1), I(1)–Sn(1)–P(1) 88.9(3), I(2)–Sn(1)–P(1) 87.8(2), P(1)–Sn(1)–P(1) 180.00.

Further studies have reported the structures of tin(IV) halides with chelated phosphines. The reaction of tin tetrachloride with dppe has led to a 1:1 complex, *i.e.* $SnCl_4{\cdot}$(dppe), incorporating a bidentate phosphine ligand (Fig. 4.3).[132] This same adduct was previously characterized by XPS (X–ray photoelectron spectroscopy) and Mössbauer spectroscopy together with ^{119}Sn and ^{31}P NMR.[133,134] $SnCl_4$ has also been reacted with another chelating phosphine, dppm, in a 1:1 and 1:2 ratio. Only the complex derived from the 1:2 ratio reaction, *i.e.* $SnCl_4{\cdot}2$(dppm), has been crystallographically characterized (Fig. 4.4). Sn atom has an octahedral coordination (CN = 6) with the potentially chelating ligands acting in a monodentate fashion and occupying *trans* positions (Table 4.2).[134]

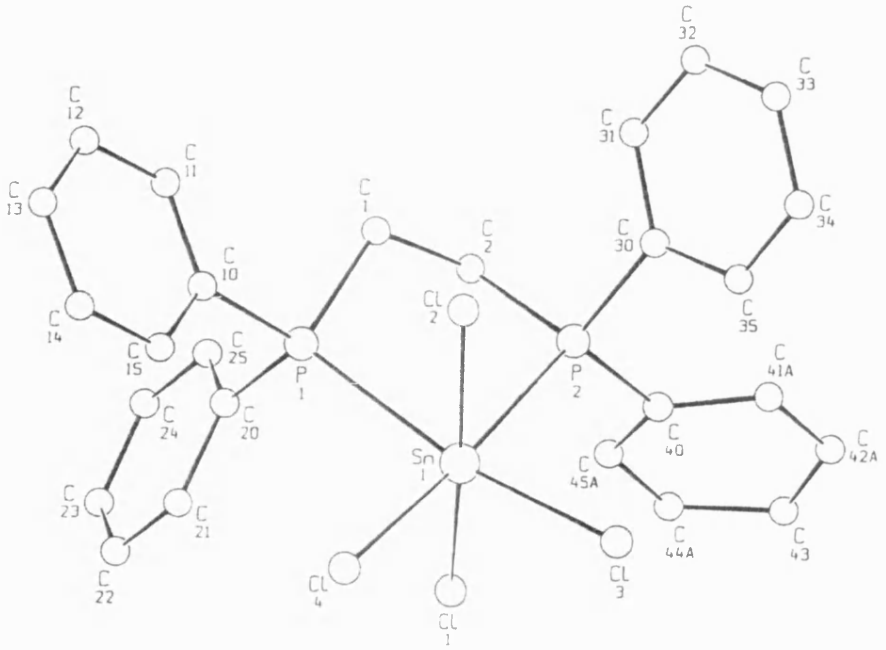

Fig. 4.3 ORTEP plot of $SnCl_4$·(dppe). Selected bonds lengths (Å) and angles (°) for $SnCl_4$·(ddpe): Sn–Cl(1) 2.402(2), Sn–Cl(2) 2.447(2), Sn–Cl(3) 2.408(2), Sn–Cl(4) 2.406(2), Sn–P(1) 2.679(2), Sn–P(2) 2.653(2); P(1)–Sn–P(2) 81.22(5). Cl(3)–Sn–P(1) 170.40(4), Cl(4)–Sn–P(2) 175.64(4). Hydrogen atoms have been omitted for clarity.

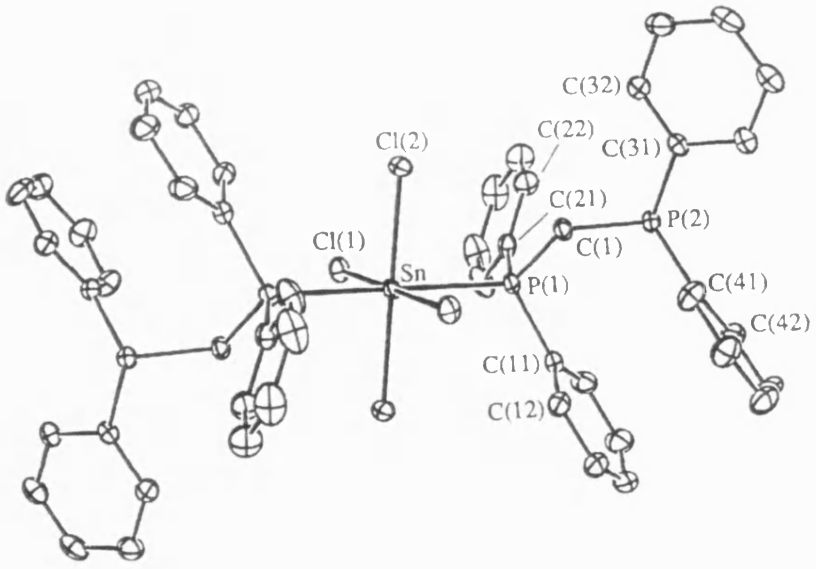

Fig. 4.4 ORTEP plot of $SnCl_4$·2(dppm). Selected bonds lengths (Å) and angles (°) for $SnCl_4$·2(dppm): Sn–Cl(1) 2.450(1), Sn–Cl(2) 2.429(1), Sn–P(1) 2.649(1); Cl(1)–Sn–Cl(2) 90.5(1), Cl(1)–Sn–Cl(2)' 89.5(1), Cl(2)–Sn–P(1) 87.0(1), Cl(2)–Sn–P(1)' 93.0(1), Cl(1)–Sn–P(1) 91.8(1), Cl(1)–Sn–P(1)' 88.2(1). Hydrogen atoms have been omitted for clarity.

It is clear that scientific research in the past has been focused on tin(IV) halides adducts of tertiary phosphines, in the same way that has been seen with germanium(IV) halides of phosphines. The difference with the germanium analogues has been the evident formation of tin(IV) adducts, proved clearly and irrefutably by crystallographic evidence, and no evidence for redox reactions involving tin has been noticed.

While there are only 4 Sn–P adducts there are more adducts of phosphine oxides as seen in Table 4.2, which probably reflects the Sn preference for hard (small) donor atoms and the ease with which phosphines are oxidized to phosphine oxides.

For the purpose of this project, such tin(IV) halide adducts of phosphines may represent a good source of tin and phosphorus for the deposition of tin phosphides using single–source precursors. However, in the light of the research already reported, attention in this thesis has been focused on the syntheses of tin(IV) halide adducts of primary and secondary phosphines, with only a limited focus on tin(II) chemistry. The only known attempt to deposit tin phosphide films has been reported recently using a dual–source approach.[64]

4.2 Results and Discussion

4.2.1 Reaction of $SnCl_2$ and $Et_2P(CH_2)_2PEt_2$ (1:1)

The reaction has been performed using an equimolar ratio of $SnCl_2$ and $Et_2P(CH_2)_2PEt_2$ (depe), in toluene, under an argon atmosphere. The reaction mixture was stirred for 1 hour, during which a white precipitate was formed.

Microanalysis of the white solid is consistent with the formation of a 2:1 adduct, despite the reaction stoichiometry. These experimental values (C = 20.9%, H = 4.1%) are very close to what it is expected for $(SnCl_2)_2$·depe (**10**) (C = 21.9%, H = 4.33%).

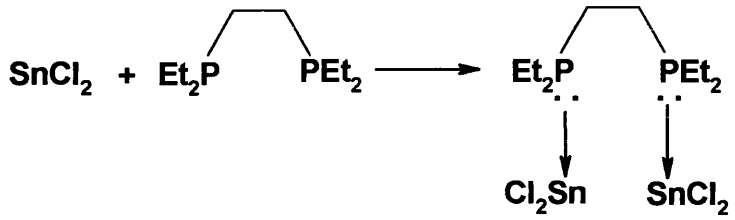

Eq. 4.3

(**10**)

^{31}P NMR on the precipitate, dissolved in dichloromethane, shows two singlets. The main singlet has a chemical shift of -7.3 ppm; it is most likely that this peak belongs to the uncoordinated excess phosphine, which remains as a result of the 2:1 reaction product. Furthermore, a similar chelated phosphine, *i.e.* 1,2 bis(diphenylphosphino)ethane, exhibits a chemical shift of -11.4 ppm. The low–field ^{31}P shift for the other peak implies an involvement of the phosphorus lone pair in bonding, hence the peak at 27.1 ppm has been assigned to **10**.

The Mössbauer analysis (Fig. 4.5) of the precipitate presents a doublet (δ = 3.18 mms^{-1} and ΔE_Q = 1.55 mms^{-1}) which is consistent with a Sn(II) species (δ > 2.5 mms^{-1}). The presence, furthermore, of a positive quadrupole splitting (ΔE_Q) indicates an asymmetry of the special arrangement of the groups around the tin atom and this generates an imbalance in the tin *5p* valence electrons.

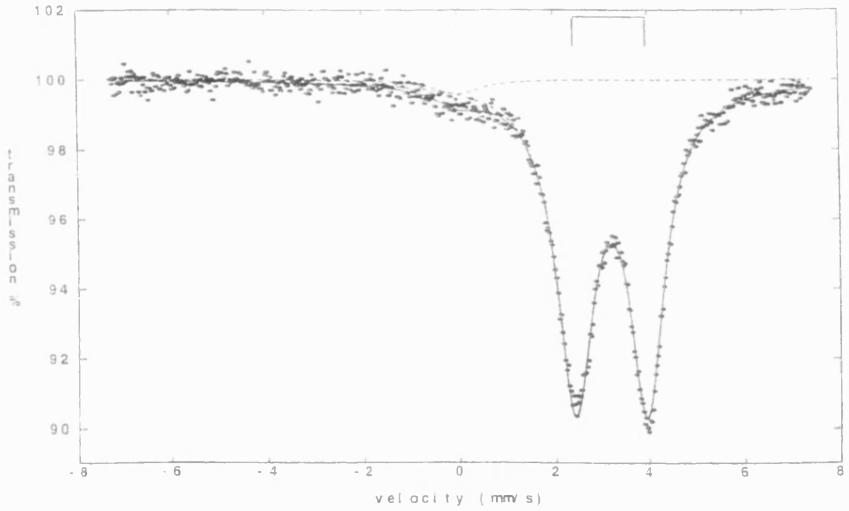

Fig.4.5 Mössbauer Spectrum of $(SnCl_2)_2$·depe (**10**).

$(SnCl_2)_2$·depe, has been studied using TGA in order to have an indication of the temperature at which its decomposition may be expected to begin. The decomposition curve (Fig. 4.6) shows a first step, between 30 and 380°C corresponds to elimination of the organic groups (observed remaining mass 75.4%, theoretical 78.7%). The second step, from 380 to 420°C, corresponds to the loss of four Cl atoms (observed 51.8%, theoretical 51.1%). In the final step, over 430°C, a species with a residual mass corresponding to SnP is formed at 450°C (observed 25.9, theoretical 25.6%).

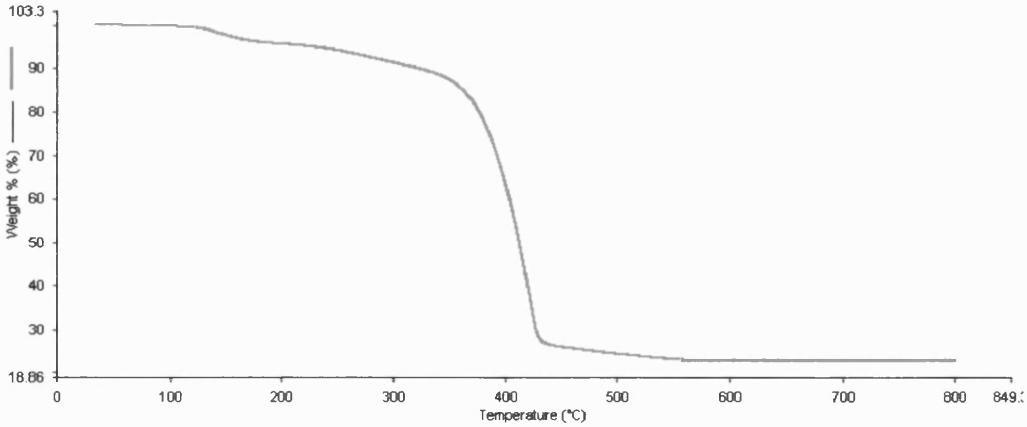

Fig. 4.6 TGA of $(SnCl_2)_2$·depe

4.2.2 Reaction of $SnCl_2$ and $Ph_2P(CH_2)_2PPh_2$ (2:1)

As a consequence of reaction between $SnCl_2$ and depe, a 2:1 reaction of $SnCl_2$ with $Ph_2P(CH_2)_2PPh_2$ (dppe) has been attempted. The reaction was carried out in toluene, under argon, at room temperature. After few minutes a white precipitate appeared at the bottom of the reaction vessel, which was separated by filtration.

Surprisingly, the choice of a 2:1 stoichiometric ratio of the starting materials appears not to have been translated into the reaction product. The theoretical values for a 2:1 adduct, *i.e.* $(SnCl_2)_2$·dppe, (C = 40.1%, H = 3.08%) are not consistent with the experimental ones (C = 52.6%, H = 4.35%). If a 1:1 adduct is considered instead, $SnCl_2$·dppe (**11**), the observed values are consistent with the expected ones (C = 53.0%, H = 4.08%).

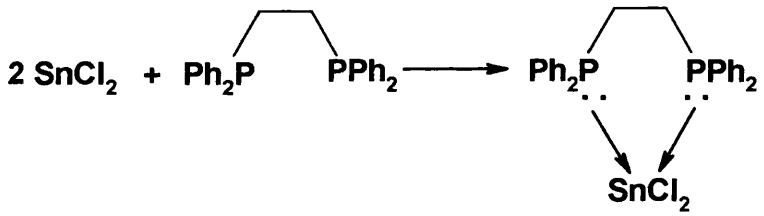

Eq. 4.4

(**11**)

This time, however, the Mössbauer spectrum of the product (Figure 4.7) shows a mixture of both Sn^{II} and Sn^{IV} species. The analysis was carried out on a fresh sample of the precipitated material soon after it has been separated from the solution. From the spectrum, it is clear that there are 3 different species. The singlet (δ = 0.32 and ΔE_Q = 0) could correspond to either $SnCl_4$·dppe or its oxidation product $SnCl_4$·[$Ph_2P(O)CH_2CH_2P(O)Ph_2$] and it is in the Sn(IV) region. Then, there are two species present in the Sn(II) region: a doublet (δ = 3.26 and ΔE_Q = 1.12) which could be $SnCl_2$·dppe or $(SnCl_2)_2$·dppe and it is similar to what it has been seen for $(SnCl_2)_2$·depe (Fig. 4.5), and a singlet that can assigned to $SnCl_2$ (δ = 4.03 and ΔE_Q = 0); literature value δ = 4.05 and ΔE_Q = 0.[135]

It is not easy to see where Sn(IV) comes from in this case. There must also either be a reduction, though it is not easy to see how P(III) is reduced or a disproportionation; *i.e.* $SnCl_2 \rightarrow Sn + SnCl_4$, but there is no evidence for tin metal. The only reasonable explanation is oxidation by adventitious O_2 in the reaction flask.

^{31}P NMR ($CDCl_3$) of the precipitated solid presents three singlets. Considering the position in the low field region, the main peak at δ = 45.1 ppm might belong to either $SnCl_4 \cdot [Ph_2(O)P(CH_2)_2P(O)Ph_2]$, $SnCl_2 \cdot [Ph_2(O)P(CH_2)_2P(O)Ph_2]$, $SnCl_4 \cdot$(dppe) or $SnCl_2 \cdot$(dppe) and it is the most intense of the three. The second peak, δ = -12.2 ppm, belongs to unreacted dppe and is slightly less intense than that at 45.1 ppm. The third very minor singlet, δ = -27.3 ppm, has not been assigned. The ^{31}P NMR was recorded a few hours after the reaction was completed.

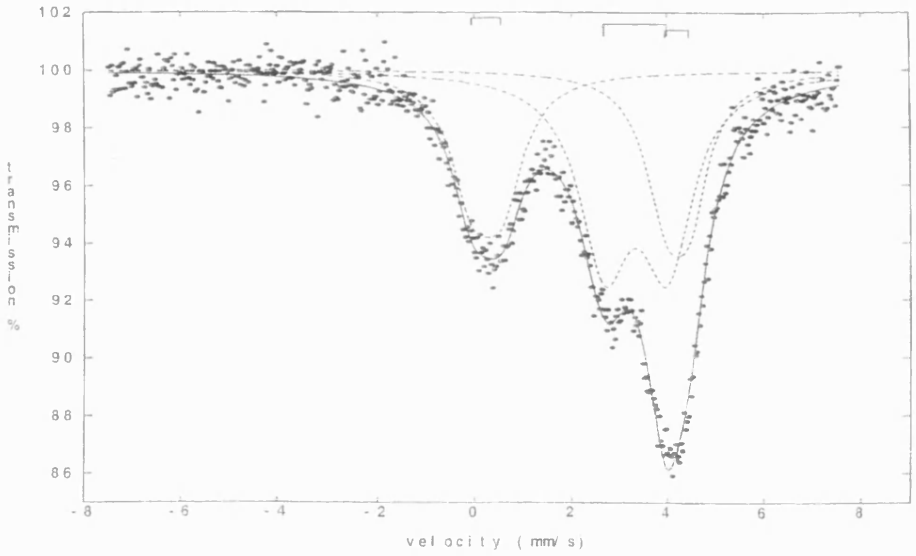

Fig.4.7 Mössbauer Spectrum obtained from the solid product of Eq.4.4

The spectral data thus conflict with the microanalytical data. An X–Ray analysis (Figure 4.8) made on a crystal obtained from the precipitate and grown in

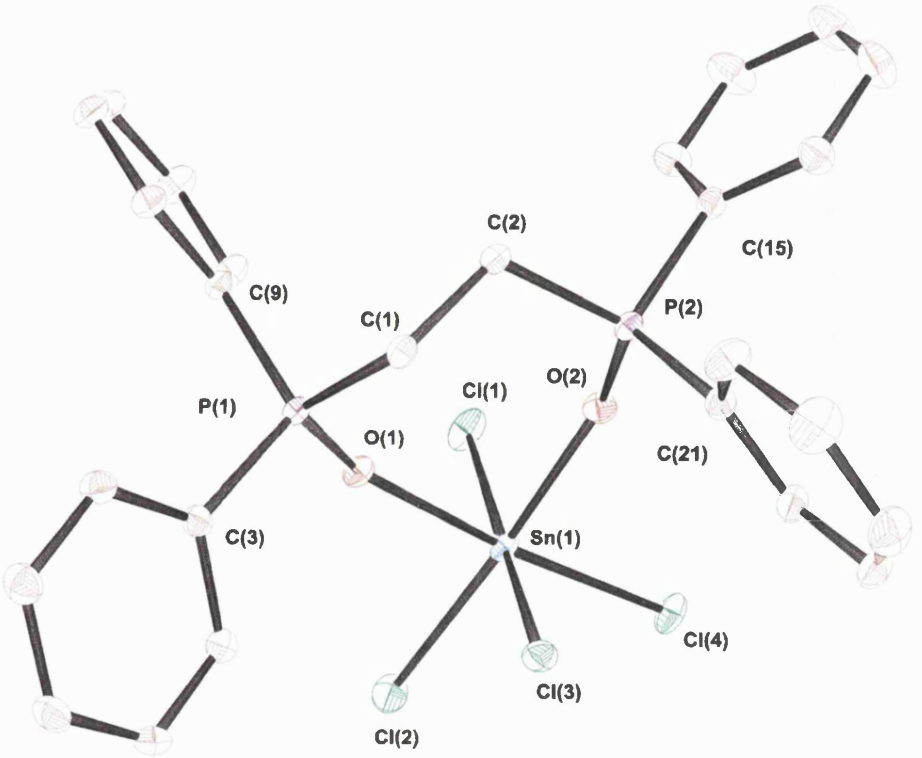

Fig. 4.8 ORTEP plot of $SnCl_4{\cdot}[Ph_2P(O)CH_2CH_2P(O)Ph_2]$ (**12**). Thermal ellipsoids are at the 30% probability level. Selected bonds lengths (Å) and angles (°) for **12**: Sn(1)–Cl(1) 2.3751(6), Sn(1)–Cl(2) 2.3905(7), Sn(1)–Cl(3) 2.3997(6), Sn(1)–Cl(4) 2.3952(6), Sn(1)–O(1) 2.0931(2), Sn(1)–O(2) 2.0868(2); O(1)–Sn(1)–O(2) 87.40(7), Cl(1)–Sn(1)–Cl(3) 172.47(2), O(1)–Sn(1)–Cl(4) 175.10(5), O(1)–Sn(1)–Cl(2) 89.05(5), O(2)–Sn(1)–Cl(4) 87.83(5). Hydrogen atoms have been omitted for clarity.

the NMR tube, shows that one of the reaction products is the oxidation product of the $SnCl_4$ adduct, $SnCl_4{\cdot}[Ph_2(O)P(CH_2)_2P(O)Ph_2]$ (**12**).

The tin is coordinated to four chlorine atoms and two oxygens. The complex contains a chelating phosphine oxide with a distorted octahedral geometry at the tin atom [Sn(1)–O(1) 2.0931(2)Å, Sn(1)–O(2) 2.0868(2) Å, Sn(1)–Cl(1) 2.3751(6) Å, Sn(1)–Cl(2) 2.3905(7) Å, Sn(1)–Cl(3) 2.3997(6) Å, Sn(1)–Cl(4) 2.3952(6) Å; O(2)–Sn(1)–Cl(2) 176.44(5)°, Cl(1)–Sn(1)–Cl(3) 172.47(2)°, O(1)–Sn(1)–Cl(4) 175.10(5)°, O(1)–Sn(1)–O(2) 87.40(7)°] ; the oxygens are bonded in order to give a *cis* configuration. The geometry about both phosphorus atoms is tetrahedral: P(1)–C(1) 1.805(2) Å, P(1)–C(3) 1.798(2) Å, P(1)–C(9) 1.797(2) Å, P(1)–O(1) 1.5151(17) Å; C(1)–P(1)–O(1) 112.52(10)°, C(3)–P(1)–O(1) 109.53(11)°, C(3)–P(1)–C(9) 112.74(11)°, C(9)–P(1)–C(1) 108.00(11)°

The two Sn–O distances are equal [Sn(1)–O(1) 2.0931(2), Sn(1)–O(2) is 2.0868(2) Å]. The Sn–Cl bond lengths, instead, are surprisingly unequal [Sn(1)–Cl(1) 2.3751(6), Sn(1)–Cl(2) 2.3905(7), Sn(1)–Cl(3) 2.3997(6) and Sn(1)–Cl(4) 2.3952(6) Å]. There does not appear to be any systematic effect of the trans ligand (either Cl or O) on the Sn–Cl bond lengths. These values are shorter than those found for dichlorodiethyl{1,2-bis(diphenylphosphoril)ethylene}tin(IV), $Et_2SnCl_2{\cdot}(dppeo_2)$ where the range for Sn–Cl bond distance is 2.532 – 2.561 Å. These Sn–Cl can also be compared and are shorter than those obtained for $SnCl_4{\cdot}$(dppe) (Fig. 4.3) where the Sn–Cl distances are 2.402(2), 2.447(2), 2.408(2), 2.406(2) Å. The O(1)–Sn(1)–O(2) angle is 87.40(7)° which is more open than that found in the Et_2SnCl_2 adduct, *i.e.* 76.7(4)°.[136]

The solid material precipitated has been also investigated by TGA in order to ascertain the decomposition pathway and product. The curve for the compound (Fig. 4.9) presents a first step, between 40 and 300°C, which corresponds to elimination of the CH_2 groups (observed residue 95.3%, theoretical 95.2%). The second step, from 300 to 450°C, shows the loss of four phenyl groups (observed

residue 40.3%, theoretical 37.6%). From 430 to 630°C, the elimination of two Cl atoms takes place; over 630°C, a species with mass corresponding to SnP is formed at 650°C (observed 25.5, theoretical 23.4%).

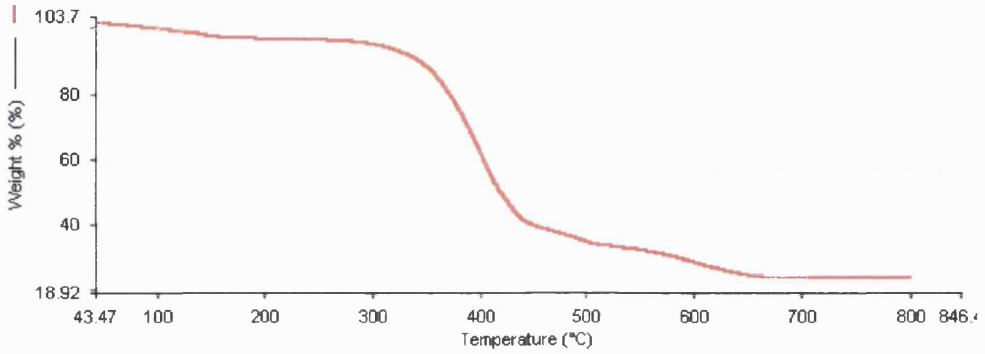

Fig. 4.9 TGA of **11**

4.2.3 Reaction of $SnCl_4$ and $CyPH_2$ (1:1)

The reaction of $SnCl_4$ with $CyPH_2$ in a 1:1 ratio has been investigated. The reaction was carried out in toluene and under an argon atmosphere. Once the addition of the reagents was over, a white precipitate had formed and the reaction mixture was left to stir for 30 minutes. The white precipitate was then separated from the solution and analyzed.

^{31}P NMR carried out on the white solid redissolved in THF shows two peaks: an intense singlet at δ = -68.3 ppm, which has been assigned to $(CyP)_4$ as literature reports a singlet at δ = -68.9,[137] and a less intense triplet at δ = 24.4 ppm. The peak at 24.4 ppm can possibly arise from $SnCl_4$←:$PCyH_2$ or $SnCl_2$←:$PCyH_2$ (**13**) by analogy with the ^{31}P NMR of the germanium compounds **3** and **5**.

The Mössbauer spectrum (Figure 4.10) shows two peaks, a major singlet belonging to a Sn^{II} species (δ = 4.05 and ΔE_Q = 0) and is believed to be $SnCl_2$ by comparison with literature data (δ = 4.04 and ΔE_Q = 0).[135] The second, a sharper peak, belongs to a Sn^{IV} species (δ = 0.45 and ΔE_Q = 0). In this latter case, the peak could belong to either $SnCl_4(CyPH_2)$, $SnCl_4[CyP(O)H_2]$ or the corresponding 1:2 adducts.

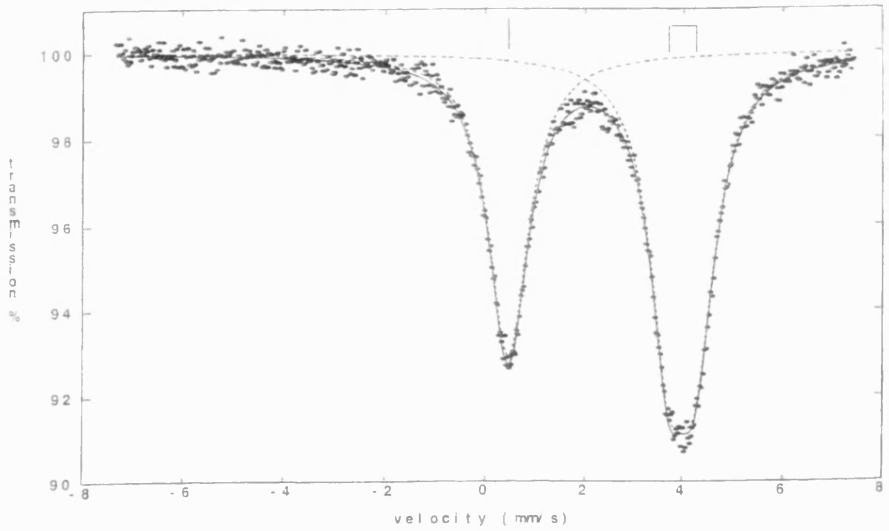

Fig. 4.10 Mössbauer spectrum of the precipitate obtained on reacting $SnCl_4$ and $CyPH_2$

Microanalysis of the solid is not consistent with the formation of the expected adduct, *i.e.* $SnCl_4{\cdot}P(H_2)Cy$ [Found (calc.) C = 24.7 (19.0)%, H = 4.38 (3.45)%].

The impossibility to purify and obtain a single species from the precipitate makes this solid material unsuitable as a precursor for CVD.

4.2.4 Reaction of $SnCl_4$ and $CyPH_2$ (4:1)

Tin(IV) chloride and cyclohexylphosphine have been made to react in a 4:1 ratio in toluene. The mixture, left to stir of 30 minutes under an argon atmosphere,

produced a white precipitate soon after the $SnCl_4$ was added to the phosphine. The precipitate was separated from the solution by cannula filtration.

^{31}P NMR of the white solid redissolved in THF shows one peak, a singlet, at δ = -68.3 ppm which has been previously attributed to $(CyP)_4$.[137] No other peak is present in the spectrum. ^{31}P NMR of the filtrate does not show any peak that indicates all of the $CyPH_2$ has reacted.

4.2.5 Reaction of $SnCl_4$ and Ph_2PH (1:1)

The reaction has been attempted by adding an equimolar amount of diphenylphosphine to a solution of tin(IV) chloride in toluene. As soon as the first drops of phosphine was added, a white precipitate appeared in the reaction flask. The mixture was left stirring for 30 minutes under an argon pressure. The precipitate was then separated from the solution by cannula filtration and dried under vacuum.

^{31}P NMR analysis performed on the solid precipitate redissolved in THF shows a doublet at δ = 27.2 ppm (J = 538.1 Hz). These data can be possibly associated with either the species $SnCl_4 \leftarrow :Ph_2PH$ or $SnCl_2 \leftarrow :Ph_2PH$ (**14**) in the same way as seen for compounds **3**, **5** and **13** when the doublets (**5**) and triplets (**3** and **13**) were found in the ^{31}P low field area. ^{31}P NMR on the filtrate shows a doublet at δ = 30.7 ppm (J = 537.2 Hz) which is probably more of the same species.

The Mössbauer spectrum (Figure 4.11) shows two peaks: one bigger and wider that probably belongs to $SnCl_2$ (δ = 4.06 and ΔE_Q = 0), the second is a sharper peak belonging to a Sn^{IV} species (δ = 0.45 and ΔE_Q = 0).

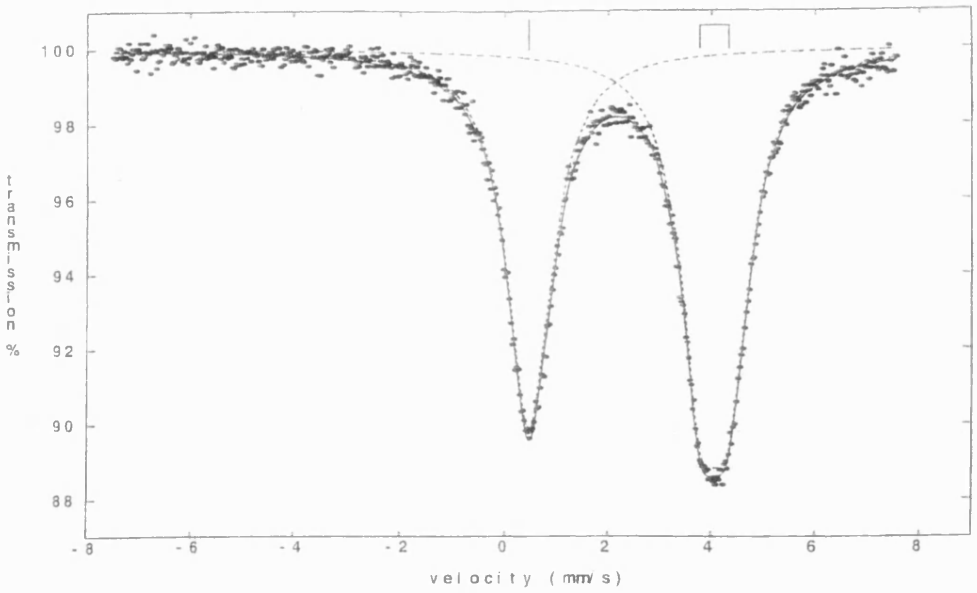

Fig. 4.11 Mössbauer spectrum of the precipitate obtained on reaction $SnCl_4$ and Ph_2PH

It is evident and clear from the Mössbauer spectroscopy that the precipitate is a mixture of Sn(II) and Sn(IV) species.

Crystals grown in the NMR tube from the reaction filtrate solution have been isolated and analyzed by X–ray diffraction (Fig. 4.12). The crystals are the oxidation product of the 1:2 adduct of $SnCl_4$ with Ph_2PH, *i.e* $SnCl_4{\cdot}[PH(O)Ph_2]_2$ (**15**). The geometry about the tin is a slightly distorted octahedron with the two oxygen atoms bonded to give a *cis* configuration [O(1)–Sn–O(2) 83.56(14)°]. The geometry around the P atoms is tetrahedral: O(1)–P(1)–C(19) 111.5(2)°, C(13)–P(1)–C(19) 109.6(2)°, O(1)–P(1)–C(13) 110.5(2)°; P(1)–O(1) 1.497(4) Å, P(1)–C(13) 1.822(5) Å, P(1)–C(19) 1.767(5) Å.

The four Sn–Cl bond distances are not equal [Sn(1)–Cl(1) 2.3794(1), Sn(1)–Cl(2) 2.4195(1), Sn(1)–Cl(3) 2.3644(1), Sn(1)–Cl(4) 2.3879(1) Å].

Structure **15** is very similar to that reported for **12**. The average Sn–O bond distance is 2.092(3) Å and the average Sn–Cl bond distance is 2.3876(1) Å, very close for what has been found for **12**: Sn–O 2.090(2) Å, Sn–Cl 2.3901(6) Å. It has to be noticed that in both **15** and **12** there seems to be either one short and three long Sn–Cl or one long and three short Sn–Cl, but the unique Sn–Cl, be it short or long, is always *trans* to Cl. The angles are 88.23(9)° for Cl(1)–Sn(1)–O(1) and 171.69(10)° for Cl(1)–Sn(1)–Cl(2) in **15**, while in **12** are 89.05(5)° for Cl(2)–Sn(1)–O(1) and 172.47(2)° for Cl(1)–Sn(1)–Cl(3).

Structures very similar to that presented by **15** have been reported by others.[138,139] Reaction of $SnCl_4$ with dppf in acetonitrile yielded yellow crystal of formula $SnCl_4{\cdot}[C_{34}H_{28}FeO_2P_2]$ (**16**) (Fig. 4.13). The Sn atom has octahedral coordination with O(1) *cis* with respect to the O(2), while the geometry about both P atoms is tetrahedral. Reaction of $SnBr_4$ with Ph_3PO produced a mixture of crystals of the *cis* and *trans* isomers, *i.e.* $SnBr_4(OPPh_3)_2$ (**17**) (Fig. 4.14). In this latter case, the Sn–O bond distances [2.080(8) Å] are close and similar to those found in **15** [2.092(3) Å] and **12** [2.090(2) Å].

Both structures of **12** and **15** can be compared and indeed are very similar to those obtained reacting $SnBr_4$ with PCy_3. This reaction did not produce any adduct, but the precipitate obtained, dissolved in THF, gave rise to crystals of formula $[H_2O{\cdot}SnBr_4(O)PCy_3]{\cdot}2THF$ (see paragraph 4.2.10).

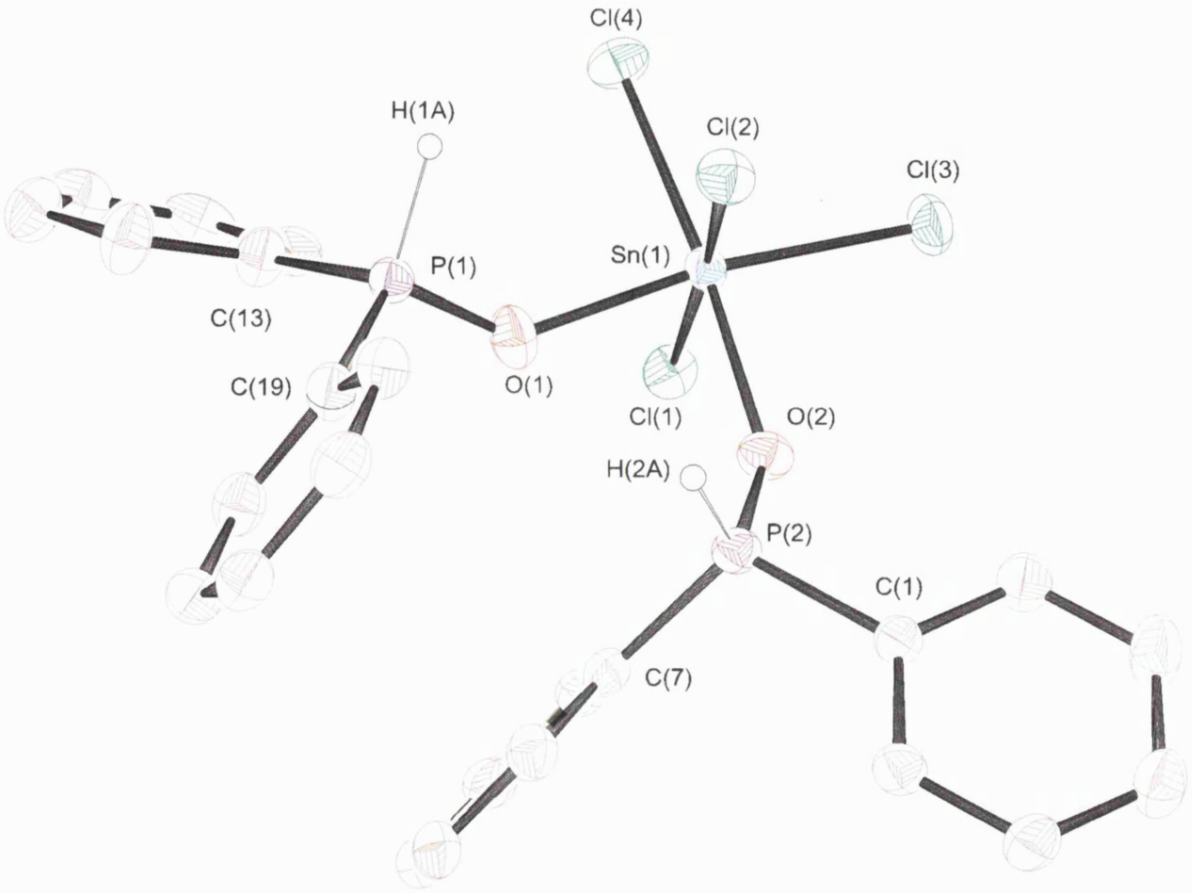

Fig. 4.12 ORTEP plot of $SnCl_4{\cdot}[PH(O)Ph_2]_2$ (**15**). Thermal ellipsoids are at the 30% probability level. Selected bonds lengths (Å) and angles (°) for **15**: Sn(1)–O(1) 2.097(3), Sn(1)–O(2) 2.087(3), Sn(1)–Cl(1) 2.3794(1), Sn(1)–Cl(2) 2.4195(1), Sn(1)–Cl(3) 2.3644(1), Sn(1)–Cl(4) 2.3879(1); Cl(1)–Sn(1)–Cl(2) 171.69(10), Cl(3)–Sn(1)–O(1) 171.46(11), Cl(4)–Sn(1)–O(2) 173.61(1), Cl(1)–Sn(1)–O(1) 88.23(9), O(2)–Sn(1)–O(1) 85.56(1). Hydrogen atoms on the phenyl groups have been omitted for clarity.

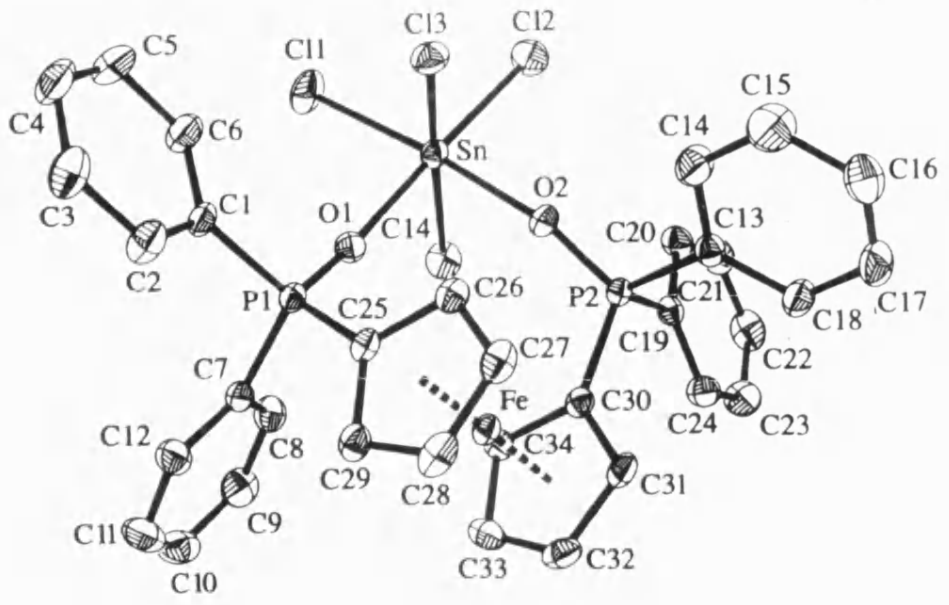

Fig. 4.13 ORTEP plot of $SnCl_4{\cdot}[C_{34}H_{28}FeO_2P_2]$ (**16**). Thermal ellipsoids are at the 30% probability level. Selected bonds lengths (Å) and angles (°) for **16**:Sn–Cl(1) 2.3894(9), Sn–Cl(2) 2.3828(10), Sn–Cl(4) 2.3710(11), Sn–Cl(3) 2.3779(10), Sn–O(1) 2.127(2), Sn–O(2) 2.111(2); Cl(4)–Sn–Cl(3) 168.38(3), O(1)–Sn–O(2) 85.31(8). Hydrogen atoms have been omitted for clarity.

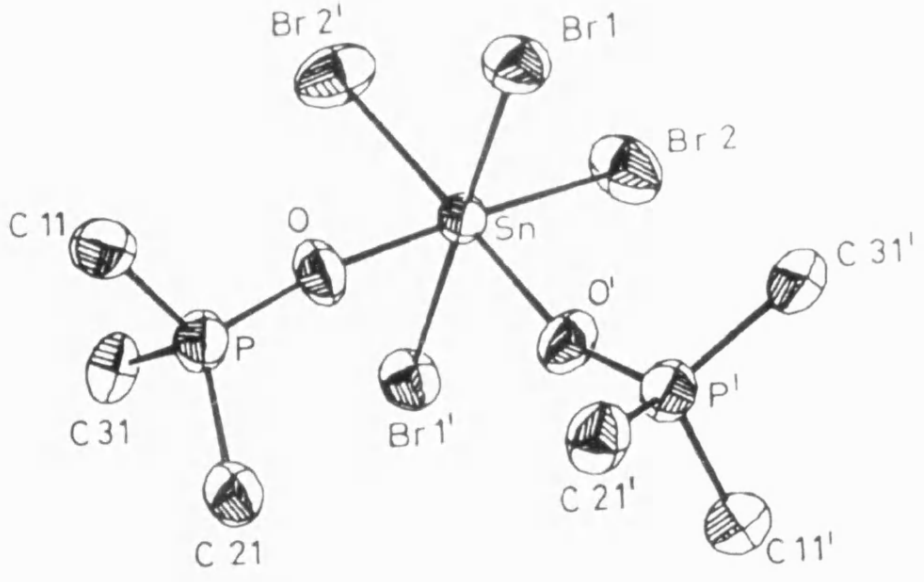

Fig. 4.14 ORTEP plot of *cis* - $SnBr_4(OPPh_3)_3$ (**17**). The phenyl rings have been omitted for clarity.Selected bonds lengths (Å) and angles (°) for **17**: Sn–Br(1) 2.537(1), Sn–Br(2) 2.557(2), Sn–O 2.080(8); Br(1)–Sn–Br(1)' 170.92(7), O–Sn–O' 85.2(3), Br(1)–Sn–O 86.1(2).

4.2.6 Reaction of SnI_4 and $CyPH_2$ (1:1)

Adduct formation using $CyPH_2$ has been also attempted with SnI_4 as Lewis acid. As soon as the phosphine had been injected dropwise into a solution of tin(IV) iodide in CH_2Cl_2, a yellow precipitate formed. The mixture was left to stir under an atmosphere of argon for 30 minutes and then the precipitate separated from the solution by cannula filtration.

Microanalysis of the precipitate is not consistent with the expected adduct product. In fact production of the adduct $SnI_4 \cdot (CyPH_2)$ implies C = 9.7% and H = 1.8. The value found for C is 19.8% and 2.6% for H.

The yellow solid was analyzed by ^{31}P and ^{119}Sn NMR ($CDCl_3$). The ^{31}P NMR shows two signals: a peak at δ = -111.2 ppm and one at 36.2 ppm. The peak at δ = -111.2 belongs most likely to the uncoordinated phosphine (δ = -111.5 ppm). ^{119}Sn NMR shows a singlet at -1610 ppm which is not SnI_4 for which the ^{119}Sn NMR is at δ = -1720 ppm. ^{31}P NMR on the filtrate presents a peak at δ = -10.7; ^{119}Sn NMR of the filtrate shows the same signal seen before for the precipitate, at δ = -1610 ppm.

Yellow crystals have been obtained in the NMR tube containing a solution of the above yellow precipitate. X–ray diffraction studies show that the crystals are the result of a redox reaction that produces $[SnI_4]^{2-}[CyPH_3]^{+}_2$ (**18**) and represented in Figure 4.15. In this system, the inorganic portion is represented by tin iodide octahedral units connected into layers through corner–sharing. The organic portion, in this case a phosphonium cation, balances the negative charge from the inorganic layer.

The structure is part of a family of layered perovskites that can be derived by terminating the three dimensional cubic perovskite structure along different crystal faces. These have formulae $(cat)_{n+1}Sn_nI_{3n+1}$ where n relates to the number of layers within the structure. All the known cations are based on quaternary ammonium salts.

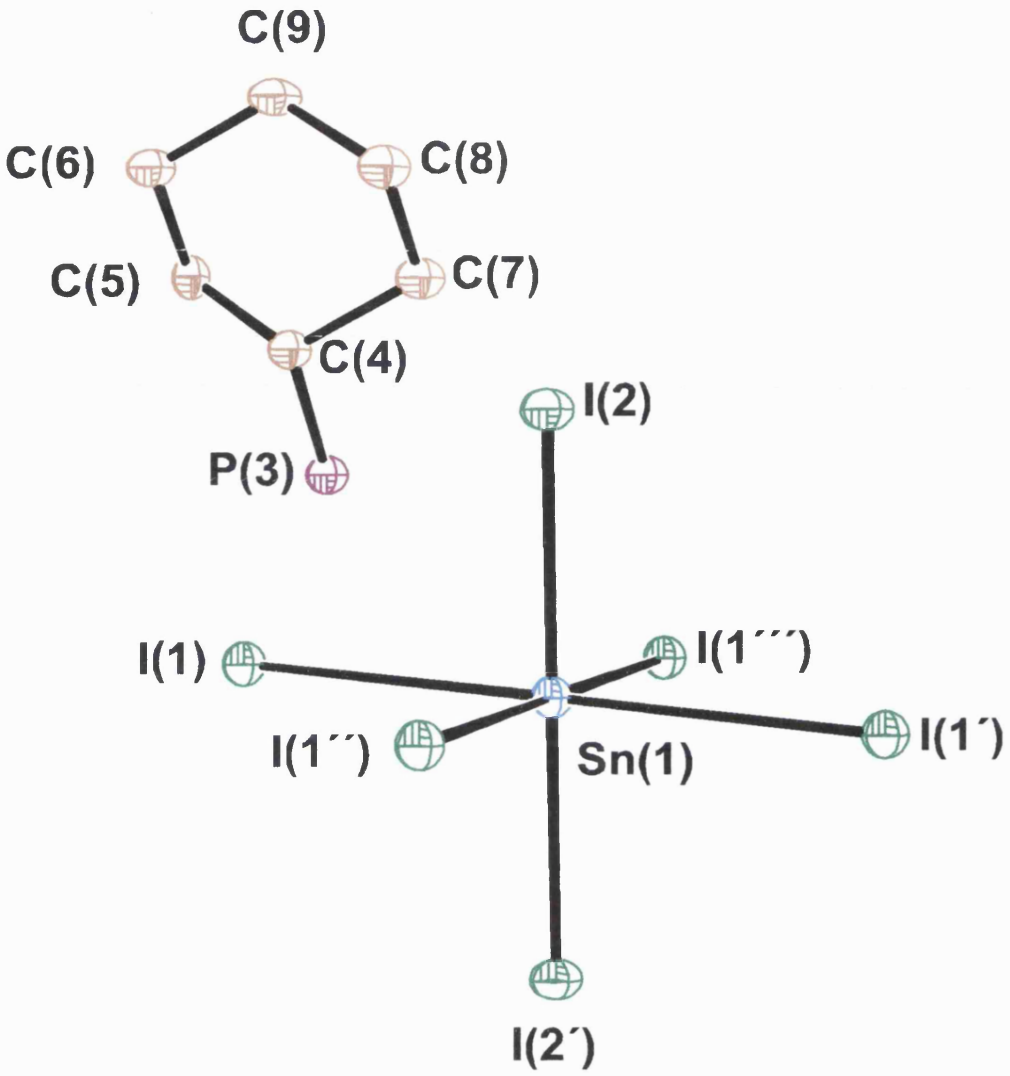

Fig. 4.15 ORTEP plot of $[SnI_4]^{2-}[CyPH_3]^{+}_2$ (**18**). Thermal ellipsoids are at the 30% probability level. Selected bonds lengths (Å) and angles (º) for **18**. Hydrogen atoms are omitted for clarity. Sn(1)–I(1) 3.1186(4), Sn(1)–I(1') 3.1186(4), Sn(1)–I(1'') 3.1812(4), Sn(1)–I(1''') 3.1812(4), Sn(1)–I(2) 3.2011(4), Sn(1)–I(2') 3.2011(4); I(2)–Sn–I(2') 180.0, I(2)–Sn–I(2') 89.56(1), I(1)–Sn–I(2) 86.11(1), Sn(4)–I(1)–Sn(1) 160.95(1).

The tin atoms, which lie on an inversion center, show a geometry that is slightly distorted from the ideal octahedral coordination: Sn(1)–I(1) 3.1186 Å, Sn(1)–I(1') 3.1186 Å, Sn(1)–I(1'') 3.1812 Å, Sn(1)–I(1''') 3.1812 Å, Sn(1)–I(2) 3.2011(4) Å, Sn(1)–I(2') 3.2011(4) Å; I(1)–Sn–I(1') 180.0°, I(1'')–Sn–I(1''') 180.0°, I(2)–Sn–I(2') 180.0°, I(1)–Sn–I(2) and I(1')–Sn–I(2') 86.11(1)°, I(1')–Sn–I(1'') and I(1)–Sn–I(1''') 90.439(1)°, I(1)–Sn–I(1'') and I(1')–Sn–I(1''') 89.56(1)°, I(1')–Sn–I(2) and I(1)–Sn–I(2') 93.889(1)°, I(1'')–Sn–I(2) and I(1''')–Sn–I(2') 92.21(3)°, I(1''')–Sn–I(2) and I(1'')–Sn–I(2') 87.79(3)°. Tin is in the +2 oxidation state and therefore has a pair of non–bonding electrons in its outer electronic configuration. It is believed, as reported previously,[140] that this nonbonding pair of electrons are responsible for the distorted octahedral coordination, with two long and two short Sn–I(1) bonds [3.1186 Å vs. 3.1812 Å] in the plane of the sheets, and two Sn–I(2) apical bonds [3.2011(4) Å] perpendicular to the sheets. However, these values for the Sn–I bond distances are all significantly longer than those observed for SnI_4 where the same bonds present a value of 2.63 Å.[141] Bond angles deviate moderately from 90° with I–Sn–I, ranging from 86.11(1)° to 93.889(1)°. These values are similar to those reported for $[SnI_4]^{2-}[C_4H_9NH_3]^{+}_2$.[140]

The angle Sn–I–Sn shows a value of 160.94(1)° and in Figure 4.16 and 4.17 is possible to see the non linear nature of this moiety. This value is higher than usually observed in single–layered perovskites systems such as $[SnI_4]^{2-}[C_6F_5C_2H_4NH_3]^{+}_2{\cdot}(C_6H_6)$ [151.23(6)°], $[SnI_4]^{2-}[C_6H_5C_2H_4NH_3]^{+}_2{\cdot}(C_6H_6)$ [152.73(3)°],[142] $[SnI_4]^{2-}[C_4H_9NH_3]^{+}_2$ [159.61(5)°],[140] $[SnI_4]^{2-}[2–ClC_6H_4C_2H_4HN_3]^{+}_2$ [154.5(6)°] and $[SnI_4]^{2-}[2–BrC_6H_4C_2H_4HN_3]^{+}_2$ [148.71(1)°] (Fig. 4.18 and 4.20).[142,143] In contrast, there are only a few papers which report the synthesis of an organic–inorganic perovskite where fairly large bond angles are observed for the bridging Sn–I–Sn units, e.g. 171.5(4)° for $[(CH_3)_3NCH_2CH_2NH_3]SnI_4$[144] and 172.8(2)° for $(C_4H_9NH_3)_2(CH_3NH_3)_2Sn_3I_{10}$.[145] The SnI_6 octahedra in $[SnI_4]^{2-}[CyPH_3]^{+}_2$ share corners to form SnI_4 sheets. As indicated by the value of 160.94(1)° for the Sn(4)–I(2)–Sn(1) bond angle, the octahedra alternately tilt along the axis, producing a slight corrugation to the sheets as it is evident looking at Figure 4.16 and 4.17

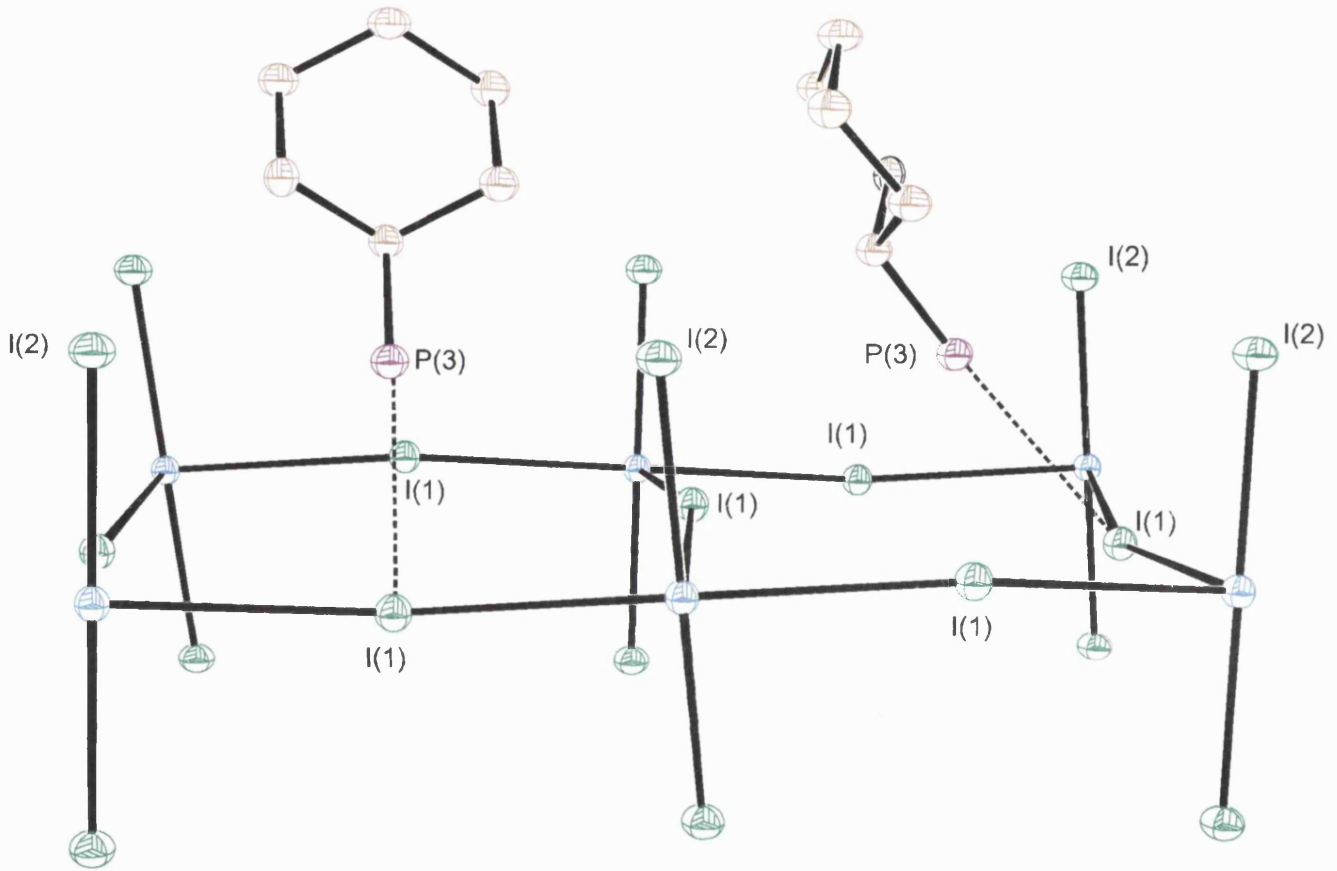

Fig. 4.16 ORTEP representation of $[SnI_4]^{2-}$ layer. Thermal ellipsoids are at the 30% probability level. The angle Sn–I–Sn is 160.95(1)°. The dotted lines represent the interactions between P and I believed to occur through the hydrogen atoms bonded to the phosphorus.

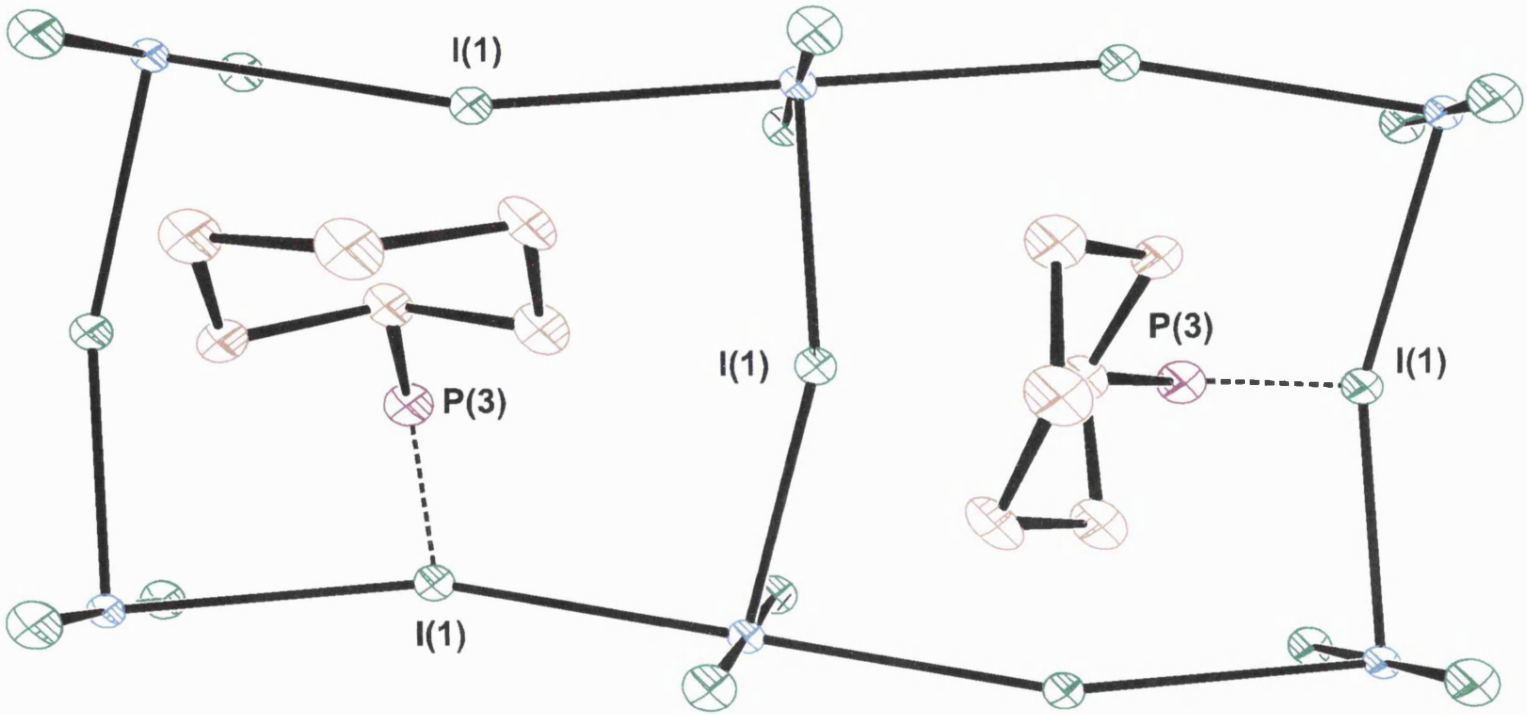

Fig. 4.17 ORTEP representation of $[SnI_4]^{2-}$ layer.

The orthorhombic structure for **18**, which adopts a *Pbac* space group, consists of single MI_4^{2-} infinite sheets, perovskite–like slab of anionic network, of corner–shared MI_6 octahedra, separated by layers of $CyPH_3^+$ cations.[140] It is the only example found in literature where the cation balancing the negative charge of the sheet is not an organic ammonium cation.[140,142-147] Literature has reported several works done to prepare these organic–inorganic hybrid materials that bring attractive features of organic and inorganic systems within a single materials and show interesting magnetic, optical and electrical properties.

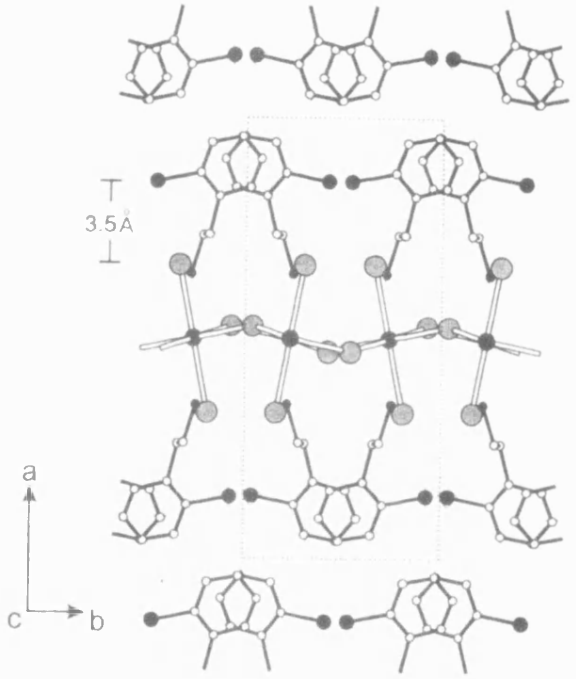

Fig. 4.18 Crystal structure of $(SnI_4)^{2-}(2\text{–}BrC_6H_4C_2N_4NH_3)^+_2$ viewed along the *c* axis. Open bonds are used for the tin(II) iodide and filled bonds for organic cations. Sn: large black sphere. I: gray sphere. C: small open sphere. N: small black phere. Br: medium black sphere. The number (3.5 Å) refers to the distance between the plane of the bromide atoms and that of the apical iodine atoms. Typical Sn–I–Sn angle is 148.71°.

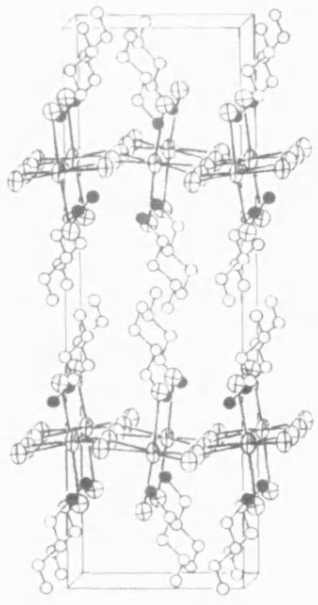

Fig. 4.19 Unit cell of $SnI_4^{2-}(C_4H_9NH_3)^+_2$ highlighting the slight corrugation of the SnI_4 sheets.

4.2.7 Reaction of SnI_4 and Ph_2PH (1:1)

SnI_4 has been reacted with Ph_2PH in DCM. The solution, left stirring for 3 hours under argon, produced a yellow precipitate soon after the phosphine has been added. The yellow solid and the light orange solution were separated by filtration.

Both the solid and the solution have been analyzed by ^{31}P and ^{119}Sn NMR ($CDCl_3$) and both produced the same identical results. There are two peaks in the ^{31}P: a singlet at δ = 40.6 ppm and a second singlet at δ = -35.4 ppm, neither of which can correspond to Ph_2PH.

Both orange and yellow crystals grew on standing in the NMR tube of the filtrate and have each been studied by X–ray diffraction. The orange crystals are the salt $[Sn_3I_{12}]^{6-}[Ph_2PH_2]^+_6$ (**19**) (Fig. 4.20) coming from a redox reaction that reduces

the Sn atom from +4 to +2 and oxidizes the P atom from +3 to +5. The yellow crystals

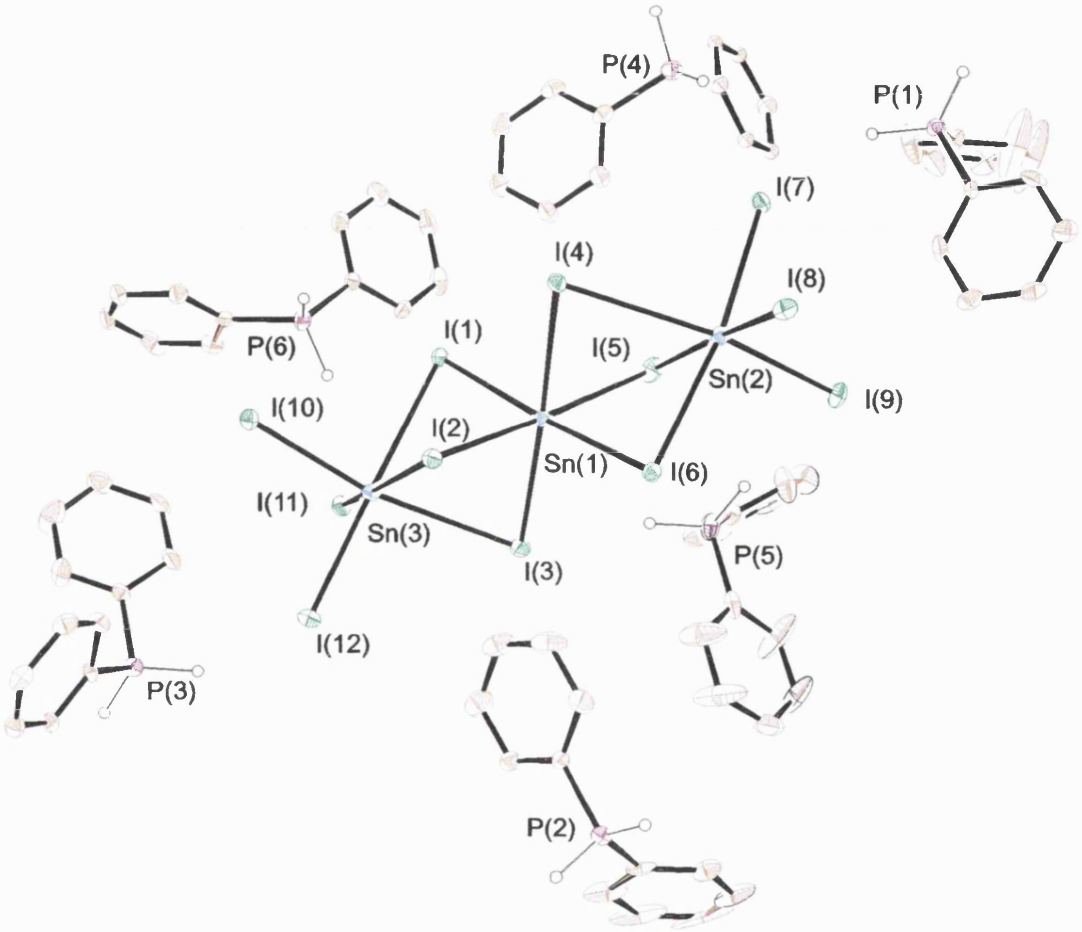

Fig. 4.20 ORTEP plot of $[Sn_3I_{12}]^{6-}[Ph_2PH_2]_6^+$ (**19**). Thermal ellipsoids are at the 30% probability level. Hydrogen atoms attached to the phenyl groups are omitted. Selected bonds lengths (Å) and angles (º) for **19**. Sn(1)–I(1) 3.1756(7), Sn(1)–I(3) 3.3489(7), Sn(1)–I(4) 3.1336(7), Sn(1)–I(2) 3.1443(7), Sn(1)–I(5) 3.1838(8), Sn(1)–I(6) 3.1259(7), P(6)–C(67) 1.791(8), P(6)–C(61) 1.791(8); I(1)–Sn(1)–I(6) 176.18(2), I(1)–Sn(1)–I(4) 87.883(2), I(6)–Sn(1)–I(4) 88.75(2), C(67)–P(6)–C(61) 112.3(4).

are shown to be the salt $[SnI_6]^{2-}[Ph_2PH_2]^{+}_2$ (**20**) (Fig. 4.21 and 4.22). This time it is less obvious where the reduction occurred because while the phosphorus passes from +3 to +5, Sn remains +4.

Compound **19** shows a distorted octahedral geometry about the tin atoms (CN = 6) [I(1)–Sn(1)–I(6) 176.18(2)°, I(1)–Sn(1)–I(4) 87.883(2)°, I(6)–Sn(1)–I(4) 88.75(2)°, I(2)–Sn(1)–I(5) 175.08(2)°, I(4)–Sn(1)–I(3) 174.34(2)° , I(2)–Sn(1)–I(6) 92.71(2)°, I(4)–Sn(1)–I(2) 91.402(2)°, I(2)–Sn(1)–I(1) 89.17(2)°]. The configuration at the P atom is tetrahedral, e.g. C(67)–P(6)–C(61) 112.3(4)°. The terminal Sn–I bonds, ranging from 2.923(7) – 3.1868(8) Å, are geometrically shorter than the bridging ones, ranging from 3.1259(7) – 3.5756(7) Å. The Sn–I–Sn angles present values from 74.93(2) to 82.34(2)° those are much narrower that those found for **19** where the angle is 160.95(1)°. The hydrogen atoms bonded to the phosphorus atoms are in calculated positions; it is assumed that each of the 6 phosphorus atoms is P(V) and brings a positive charge to counterbalance the 6 negative charges brought by the anion.

It is possible to observe that, differently from compound **18** where SnI_4^{2-} formed sheets of corner–sharing SnI_6 octahedra, this system does not form layers of SnI_4^{2-}. Similar compounds, $[NH_2C(I)=NH_2]_2(CH_3HN_3)_2Sn_2I_8$ and $(C_4H_9NH_3)_2(CH_3HN_3)_2Sn_3I_{10}$ do present a perovskite–like structure.[145,147] While $[Sn_3I_{10}]^{4-}$ forms a perovskite structure, $[Sn_3I_{12}]^{6-}$ in **19** does not fit the general formula $(cat)_{n+1}Sn_nI_{3n+1}$. This is the first example of the $[Sn_3I_{12}]^{6-}$ anion.

The crystal structure of **20** is illustrated in Figure 4.21. The tin(IV) atom, which is on an inversion center, adopts a nearly perfect octahedral geometry [I(1A)–Sn–I(1) 180.0°, I(2A)–Sn–I(2) 180.0°, I(3A)–Sn–I(3) 180.0°, I(2A)–Sn–I(1A) 90.526(1)°, I(2)–Sn–I(1A) 89.474(1)°, I(2A)–Sn–I(3) 89.131(1)°, I(2)–Sn–I(3) 90.869(1)°, I(3)–Sn–I(1A) 89.926(1)°, I(3)–Sn–I(1) 90.074(1)°]. The Sn–I bonds vary from 2.8442(5) to 2.8706(5) Å. The phosphorus atom shows a distorted tetrahedral geometry, C(1)–P–C(7) 113.1(4)°.

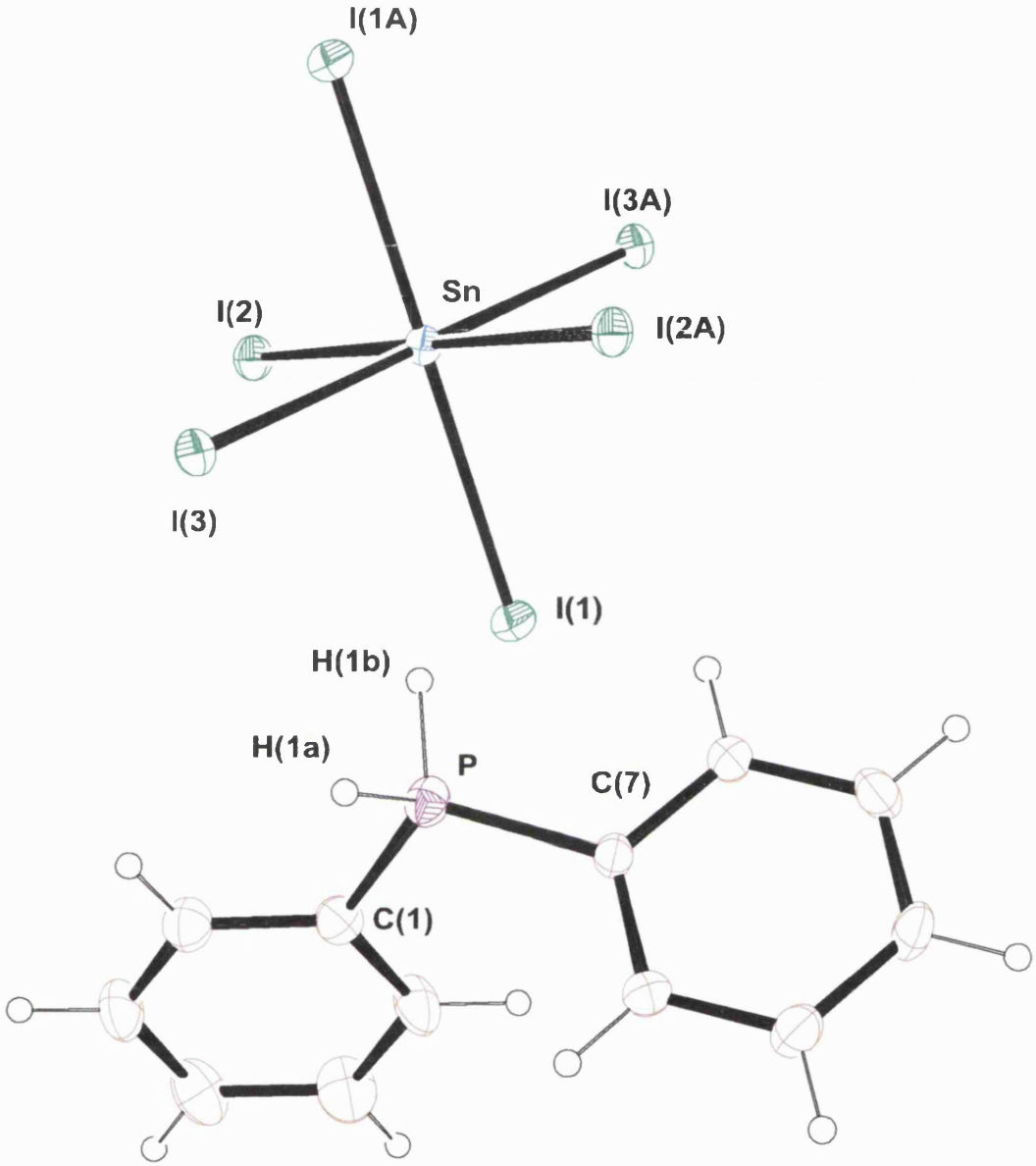

Fig. 4.21 ORTEP plot of $[SnI_6]^{2-}[Ph_2PH_2]_2^+$ (**20**) . Thermal ellipsoids are at the 30% probability level. Selected bonds lengths (Å) and angles (º) for **20**. Sn–I(1) 2.8599(5), Sn–I(2) 2.8442(5), Sn–I(3) 2.8706(5), P–C(1) 1.765(7), P–C(7) 1.787(8); I(1A)–Sn–I(1) 180.0, I(1A)–Sn–I(2A) 90.53(1), C(1)–P–C(7) 113.1(4).

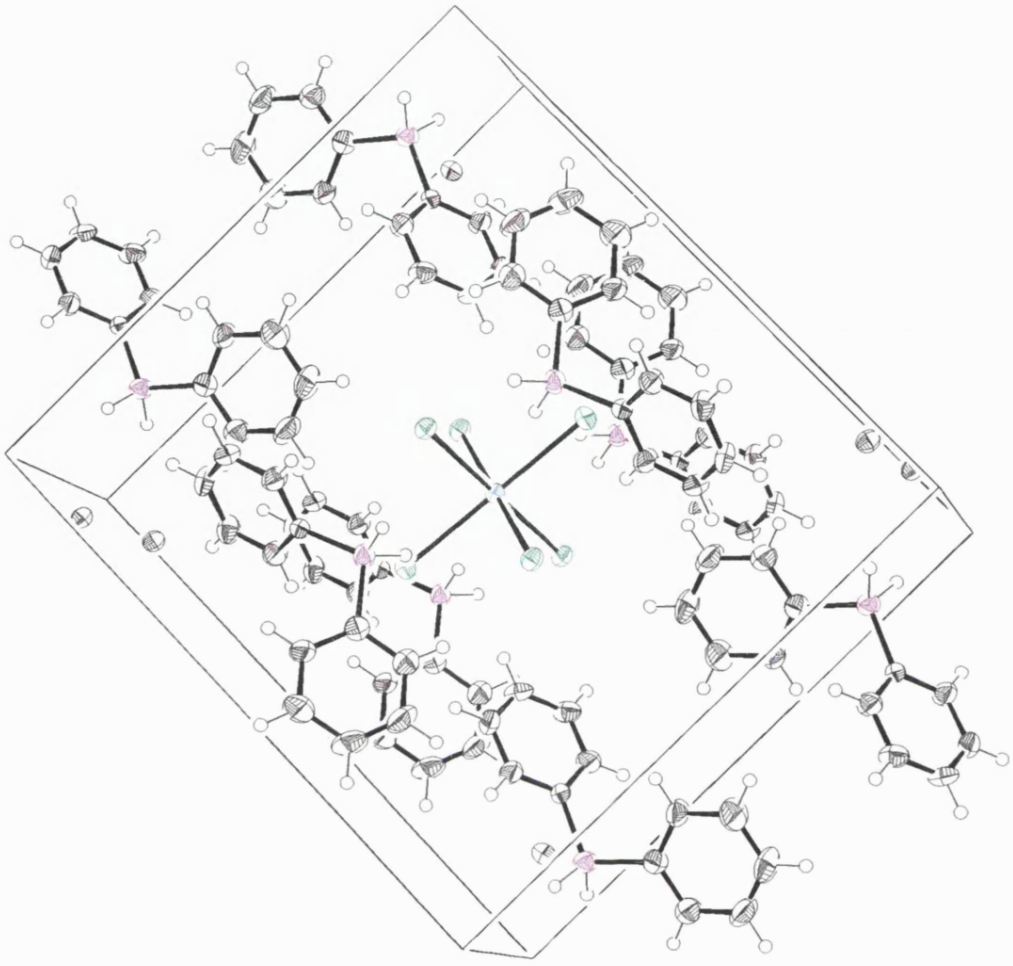

Fig. 4.22 Unit cell content of $[SnI_6]^{2-}[Ph_2PH_2]_2^+$ (**20**) .

The same results were obtained when the reaction was attempted using Sn metal, Ph_2PH and I_2, a methodology used to achieve the adduct $SnI_4{\cdot}2PPr^n_3$.[131] The reaction was carried out in toluene and under an argon atmosphere and is independent of the order in which the reagents were added; the result was a

mixture of a yellow precipitate and light orange solution from which **19** and **20** were again isolated.

The fact that the yellow solid precipitated from the reaction contains two different species and neither contains the Sn–P bond crucial for the deposition of tin phosphide, makes this material unsuitable as precursor for the CVD.

4.2.8 Reaction of SnI_4 and Cy_3P (1:1)

Reactions of tin(IV) halides with primary and secondary phosphine have demonstrated the difficulty of producing any phosphine adducts required for the deposition of thin films of tin phosphide.

Attempts to produce phosphine adducts have been made, however, reacting tin(IV) iodide with a tertiary phosphine. SnI_4 was dissolved in DCM to give a clear yellow solution and then added dropwise into a Schlenk tube containing Cy_3P. The reaction was left to stir for 2 hours producing a clear red solution.

^{31}P NMR, carried out on a sample of the reaction mixture, shows one singlet at δ = 72.9 ppm and a singlet at δ = 25.6 ppm. These peaks do not belong to Cy_3P (singlet, δ = 10.6 ppm). Crystals were grown in the NMR tube and X–ray study reveals formation of the salt $[SnI_3]^-[Cy_3PI]^+$ (**21**) (Fig. 4.23).

The solvent was then removed from the main reaction mixture under reduced pressure leaving a black solid. The black solid was dissolved in THF and studied by NMR spectroscopy. ^{31}P NMR provides one single peak, a singlet at δ = 72.9 ppm. X–ray studies done on the crystals grown in the NMR tube show they actually are the salt $[SnI_5]^-[Cy_3PI]^+$ (**22**) (Fig. 4.24). Microanalysis of the crystals is perfectly

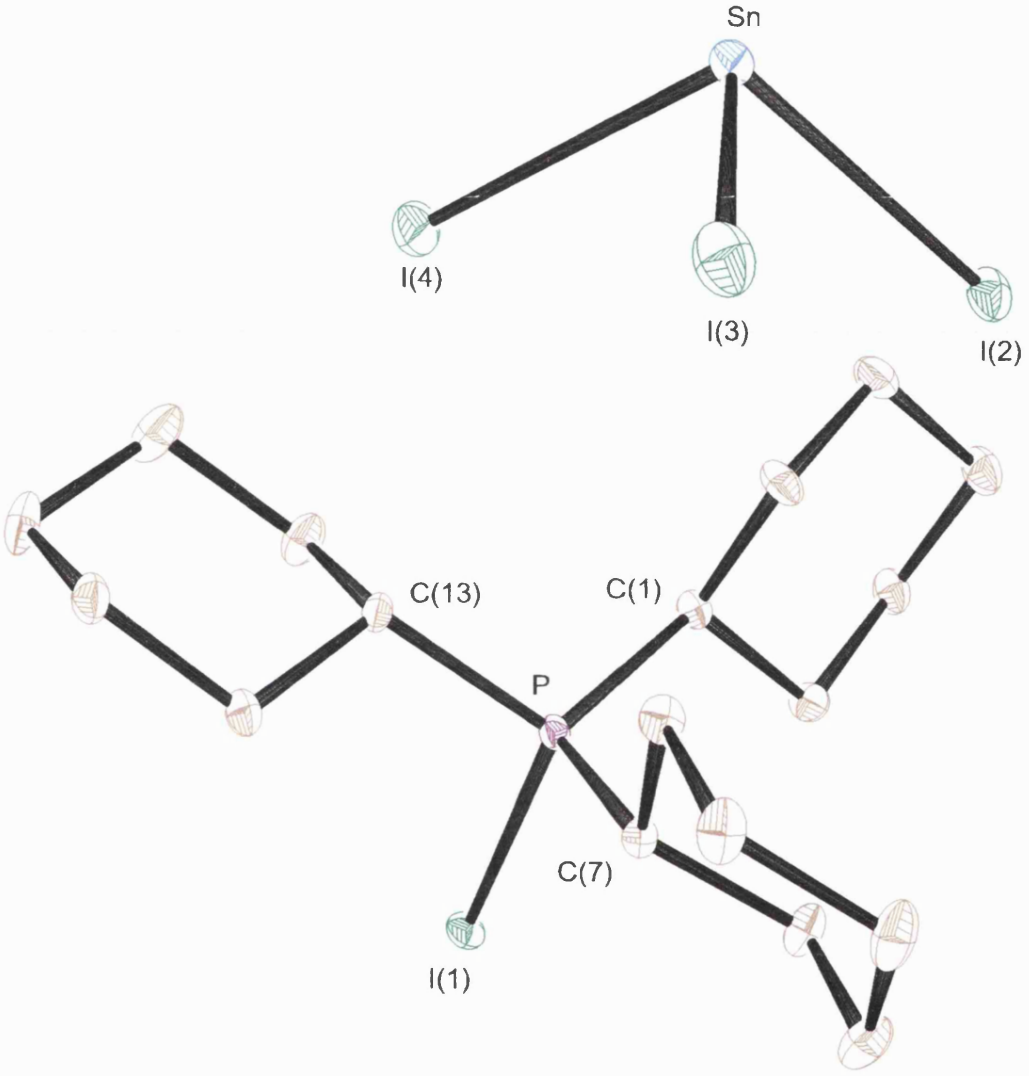

Fig. 4.23 ORTEP plot of $[SnI_3]^-[Cy_3PI]^+$ (**21**). Thermal ellipsoids are at the 30% probability level. Selected bonds lengths (Å) and angles (°) for **21**. Sn–I(2) 2.862(1), Sn–I(3) 2.8457(1), Sn–I(4) 2.8577(9), P–C(1) 1.84(4), P–C(7) 1.823(4), P–C(13) 1.819(4), P–I(1) 2.401(1) ; I(4)–Sn–I(2) 97.44(2), I(4)–Sn–I(3) 97.472(2), I(2)–Sn–I(3) 97.352(2), C(7)–P–C(1) 115.97(2), C(1)–P–C(13) 109.2(2), C(7)–P(1)–I(1) 107.32(2). Hydrogen atoms have been omitted for clarity.

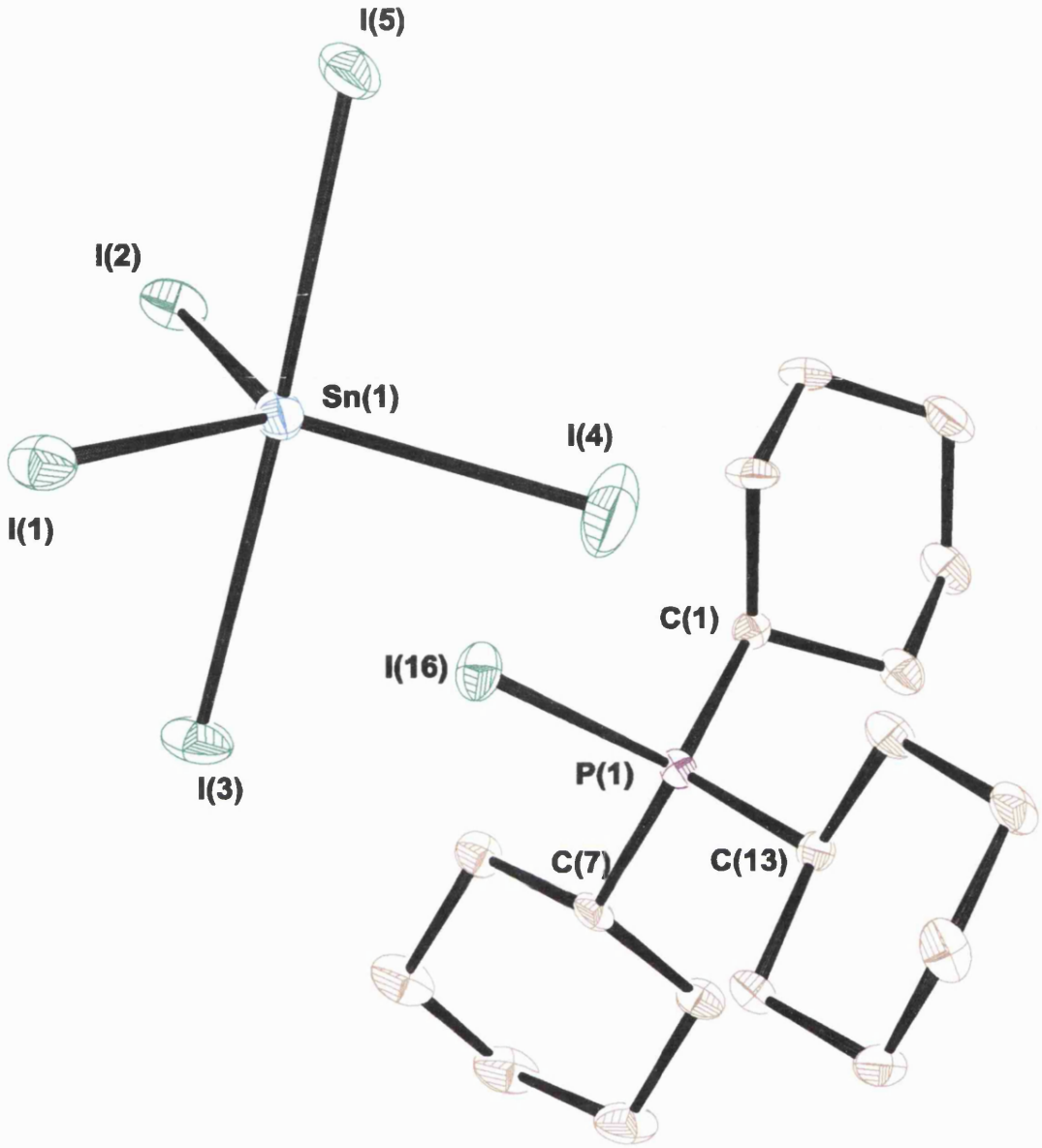

Fig. 4.24 ORTEP plot of $[SnI_5]^-[Cy_3PI]^+$ (**22**). Thermal ellipsoids are at the 30% probability level. Selected bonds lengths (Å) and angles (°) for **22**. Sn(1)–I(1) 2.7339(8), Sn(1)–I(2) 2.7428(8), Sn(1)–I(3) 2.8742(7), Sn(1)–I(4) 2.7265(9), Sn(1)–I(5) 2.8272(7), P(1)–C(1) 1.834(7), P(1)–C(7) 1.833(7), P(1)–I(16) 2.3919(19); I(3)–Sn(1)–I(5) 177.43(3) I(4)–Sn(1)–I(1) 118.00(3), I(4)–Sn(1)–I(2) 121.05(3), I(2)–Sn(1)–I(1) 120.83(3), I(4)–Sn(1)–I(5) 91.70(3), I(5)–Sn(1)–I(1) 91.83(2), I(2)–Sn(1)–I(5) 89.98(3), C(7)–P(1)–C(1) 114.4(4), C(1)–P(1)–I(16) 111.5(3), C(7)–P(1)–I(16) 104.7(3). Hydrogen atoms have been omitted for clarity.

consistent with the formulation of $[SnI_5][Cy_3PI]^+$ (**22**) [Found (calc) C = 18.4 (18.6)%, H = 2.95 (2.84)%].

From this evidence, it is most likely that the peak found in the ^{31}P NMR at 72.9 ppm belongs to the halophosphonium ion, $[Cy_3PI]^+$, while the peak at 25.6 ppm may possibly be assigned to the adduct $SnI_4 \cdot PCy_3$.

21 is obviously the result of a redox reaction. This result is perhaps not surprising considering that similar result have been reported when Ge(IV) halides react with tertiary phosphines. In addition, at the beginning of this chapter, formation of $SnI_4 \cdot 2PPr^n_3$ was reported to be prepared by reaction between unactivated tin metal powder and $Pr^n_3PI_2$.[131] This confirms the difficulty in the synthesis of adducts using conventional techniques.[148]

Tin, now in its +2 state, shows a coordination number of three (trigonal pyramid) with the I–Sn–I bond angles ranging from 97.44(2) to 97.352(2)°. The range for the Sn–I distance is 2.8457(1) to 2.862(1) Å. The geometry about the phosphorus atom is tetrahedral [C(7)–P–C(1) 115.97(2)°, C(1)–P–C(13) 109.2(2)°, C(7)–P–I(1) 107.32(2)°, C(7)–P–C(13) 109.7(2)°, C(13)–P–C(1) 109.2(2)°] and while the 3 P–C bonds range from 1.819(4) to 1.84(4) Å, the P–I distance is 2.401(1) Å.

In Table 4.3, the P–I bond distance are reported for several compounds. While for a similar cation, $[Ph_3PI]^+$, the P–I bond length is shorter [2.38(1) Å] than that found for **21**, compounds $Ph_3P \cdot I_2$ and $^tBu_3PI_2$, which can be considered as intermolecular in the formation of the iodophosphonium cation, show higher values, respectively 2.481(4) and 2.461(2) Å.

Tab. 4.3 P – I bond distances (Å) for various compounds

Compounds	P–I (Å)
21	2.401(1)
22	2.392(2)
$[Ph_3PI][Co(PPh_3)I_3]\cdot OEt_2$ [a]	2.38(1)
$Pr^i_3PI_4$ [b]	2.383(1)
$Ph_3P\cdot I_2$ [c]	2.481(4)
$^tBu_3PI_2$ [d]	2.461(2)

[a] S.M. Godfrey *et al.*, J. Chem. Soc. Dalton Trans., 1993, 1599.
[b] W.I. Cross *et al.*, J. Chem. Soc. Dalton Trans., 1999, 2795.
[c] S.M. Godfrey *et al.*, J. Chem. Soc. Dalton Trans., 1991, 1163.
[d] W.-W. du Mont *et al.* Angew.Chem.Int.Ed.Engl., 26, 1987,912.

The P atom changes its oxidation state from +3 to +5, the tin atom has its oxidation state unchanged from the value of +4. The Sn atom present a coordination number of five and its geometry is close to a perfect trigonal bipyramid. The equatorial angles are I(4)–Sn(1)–I(1) 118.00(3)°, I(4)–Sn(1)–I(2) 121.05(3)°, I(2)–Sn(1)–I(1) 120.83(3)°. The axial Sn–I bonds [Sn(1)–I(3) 2.8742(7), Sn(1)–I(5) 2.8272(7)] are longer than the equatorial ones [Sn(1)–I(1) 2.7339(8), Sn(1)–I(2) 2.7428(8), Sn(1)–I(4) 2.7265(9)], as expected. The geometry about the phosphorus atom is tetrahedral, [C(7)–P(1)–C(1) 114.4(4)°, C(1)–P(1)–I(16) 111.5(3)°, C(7)–P(1)–I(16) 104.7(3)°, C(7)–P(1)–C(13) 108.7(3)°, C(13)–P(1)–C(1) 113.8(4)°] and while the 3 P–C bonds range from 1.808(8) to 1.834(7) Å, the P–I distance is 2.392(2) Å, shorter than the one found in **21**, *i.e.* 2.401(1) Å.

In the literature, only two compounds with the SnI_5 units have been reported.[149,150] These compounds, $[SnI_5]^{3-}[NH_2C(I)=NH_2]_3$ and $[SnI_5]^{3-}$

$[NH_2C(I)=NH_2]_2(NH_2CH=NH_2)$, are related to the layered organic–inorganic perovskite $[NH_2C(I)=NH_2]_2(CH_3NH_3)_mSn_mI_{3m+2}$, which consists of *m* oriented $CH_3NH_3SnI_3$ perovskite sheets, separated by a layer of cations. In both these examples, the tin atoms present an oxidation state of +2, while **22** has +4 as oxidation state. In Figure 4.25, $[SnI_5]^{3-}[NH_2C(I)=NH_2]_3$ is shown. In this structure, each tin atom is connected to six iodine atoms at distances ranging from 2.957 to 3.484 Å forming a distorted octahedron. It is thought the lone pair electrons presumably cause the distortion. The octahedra share opposite corners forming a one–dimensional SnI_5 chain (Fig 4.26). The same kind of behaviour is shown by $[SnI_5]^{3-}[NH_2C(I)=NH_2]_2(NH_2CH=NH_2)$, where each tin(II) adopts a slightly distorted octahedral coordination of six iodine atoms with the bond lengths ranging from 3.140 to 3.210 Å. The tin(II) iodide octahedral share opposite corners to form a one–dimensional chains, with the I(1)–Sn–I(1) bond angle [179.4º] indicating that the chains are almost linear (Fig. 4.27). It is clear that compound **22**, although incorporating the SnI_5 unit, does not form chains of corner–shared octahedral in the typical perovskite–like slab and it shows a trigonal bypiramid geometry about the tin atom. It is thought that **22** is the only example of an isolated $[SnI_5]^-$ anion.

It is thought that the reaction of SnI_4 and Cy_3P produces the adduct $SnI_4{\cdot}PCy_3$ which in solution is equilibrium with $[SnI_3]^-[Cy_3PI]^+$ (**21**). When the solvent is removed from the reaction mixture and the black solid formed redissolved in THF, $[SnI_3]^-[Cy_3PI]^+$ reacts with some unreacted SnI_4 to form $[SnI_5]^-[Cy_3PI]^+$ (**22**) and SnI_2.

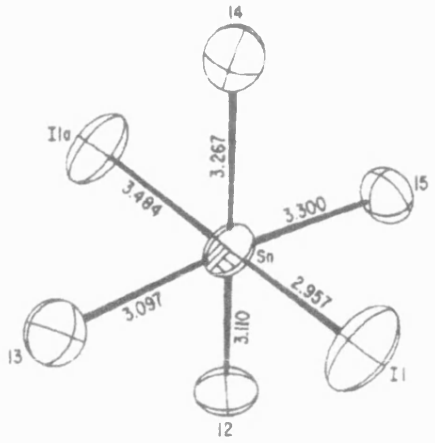

Fig. 4.25 The ORTEP drawing of SnI_6 octahedra showing the distortion indicated by the Sn–I bond distances.

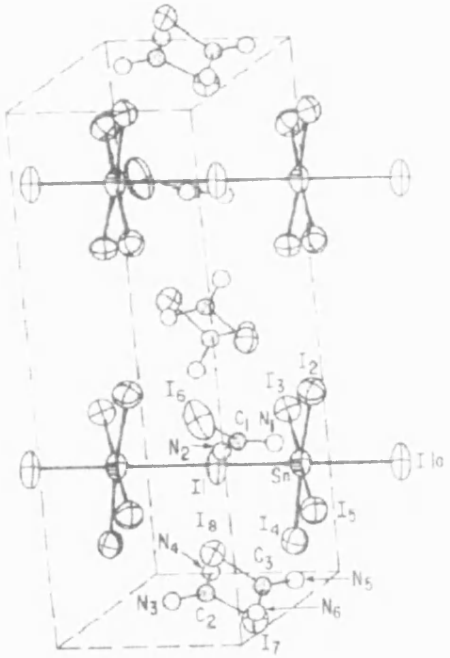

Fig. 4.26 A half unit cell of $[NH_2C(I)=NH_2]_3SnI_5$ showing the detailed structure and the SnI_5 chains along the axis.

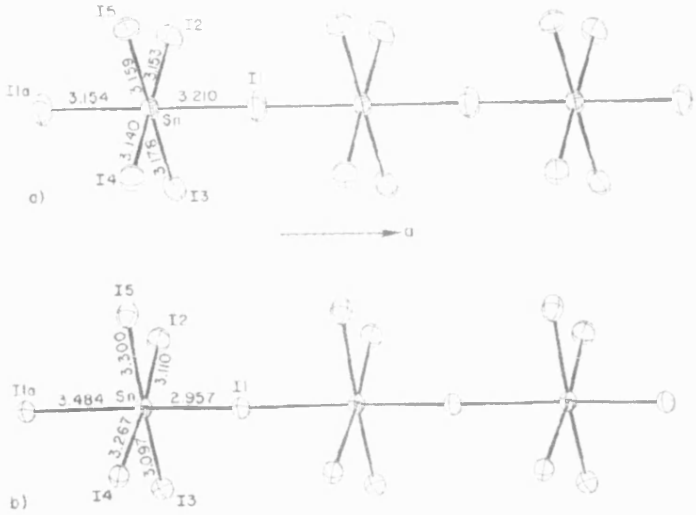

Fig. 4.27 The ORTEP drawings of the inorganic chains formed by the edge–sharing SnI_6 octahedra in $[NH_2C(I)=NH_2]_2As_nI_5$, where A is a) $NH_2CH=HN_2^+$ and b) $NH_2C(I)=HN_2^+$. The figure shows atom labeling and bond lengths.

4.2.9 Reaction of $SnCl_4$ and Cy_3P (1:1)

Reaction of $SnCl_4$ with Cy_3P has been performed in *n*–hexane under an argon atmosphere. The tertiary phosphine was first dissolved in hexane and then tin(IV) chloride has been added dropwise to this solution. As soon as the tin compound had been injected, a white precipitate formed. The reaction mixture was left to stir for 30 minutes and after that the solid has been separated from the solution by cannula filtration and then dried under a reduced pressure.

Microanalysis of the white solid is consistent with the formation of the adduct, *i.e.* $SnCl_4 \cdot PCy_3$ (**23**) [Found (calc): C = 39.6 (39.9)%, H = 6.08 (6.1)%].[124]

The solid has been submitted for Mössbauer analysis, which presents a broad singlet (δ = 0.82 and ΔE_Q = 0). This result is similar but not identical with the value reported in literature for $SnCl_4 \cdot PCy_3$ that shows a doublet (δ = 0.49 and ΔE_Q = 0.36).[124] The presence of a broad singlet could mean that the peak could possibly

be a very narrow doublet. If it was a real singlet, which implies a spherical symmetry around the tin atom, the $SnCl_4$ would have been surrounded by two phosphines in *trans* positions to each other and the actual adduct would have been $SnCl_4 \cdot (Cy_3P)_2$. Nevertheless, the value reported in literature indicates the doublet is actually a narrow one. In addition, the authors also reported the impossibility to synthesize the 1:2 adduct.

^{31}P NMR of the white precipitate redissolved in THF soon after the solid was separated from the solution shows a doublet at δ = 24.8 ppm (J = 477.6 Hz), while ^{119}Sn NMR presents a singlet at -611.1 ppm. The same results are obtained when the solid is dissolved in DCM.

Crystals were isolated from the above NMR sample. X–ray diffraction reveals formation of the salt $[SnCl_5 \cdot THF]^-[Cy_3PH]^+$(**24**) (Fig. 4.28). There has probably been some hydrolysis of $SnCl_4$ producing HCl which has added to the adduct, together with THF forming **24**.

As it was seen previously, Sn remains with an oxidation state of +4, while the oxidation of the P atoms is evident in its change of oxidation number to +5. It is also clear, now, that the doublet observed in the ^{31}P NMR belongs to the phosphonium cation $[Cy_3PH]^+$.

The tin atom presents a distorted octahedral geometry (CN = 6), O(1)–Sn(1)–Cl(3) 178.14(5)°, Cl(1)–Sn(1)–Cl(4) 171.64°, Cl(2)–Sn(1)–Cl(5) 171.20(2)°. The Sn(1)–O(1) bond distance is 2.235(1) Å and the Sn–Cl bond length varies from 2.3906(7) to 2.4035(6) Å. Clearly, the phosphorus atom adopts a tetrahedral geometry (CN = 4), though this is distorted [C(5)–P(1)–C(11) 110.58(12)°, C(5)–P(1)–C(17) 115.10(13)°, C(11)–P(1)–C(17) 112.27(12)°] and the P–C bond distances ranging from 1.815(3) to 1.826(3) Å, values similar to those encountered for **22**. In the literature the formations of a THF adduct of $SnCl_4$ has been reported.[151] $SnCl_4 \cdot 2THF$ exhibits a *trans* configuration and an extremely regular

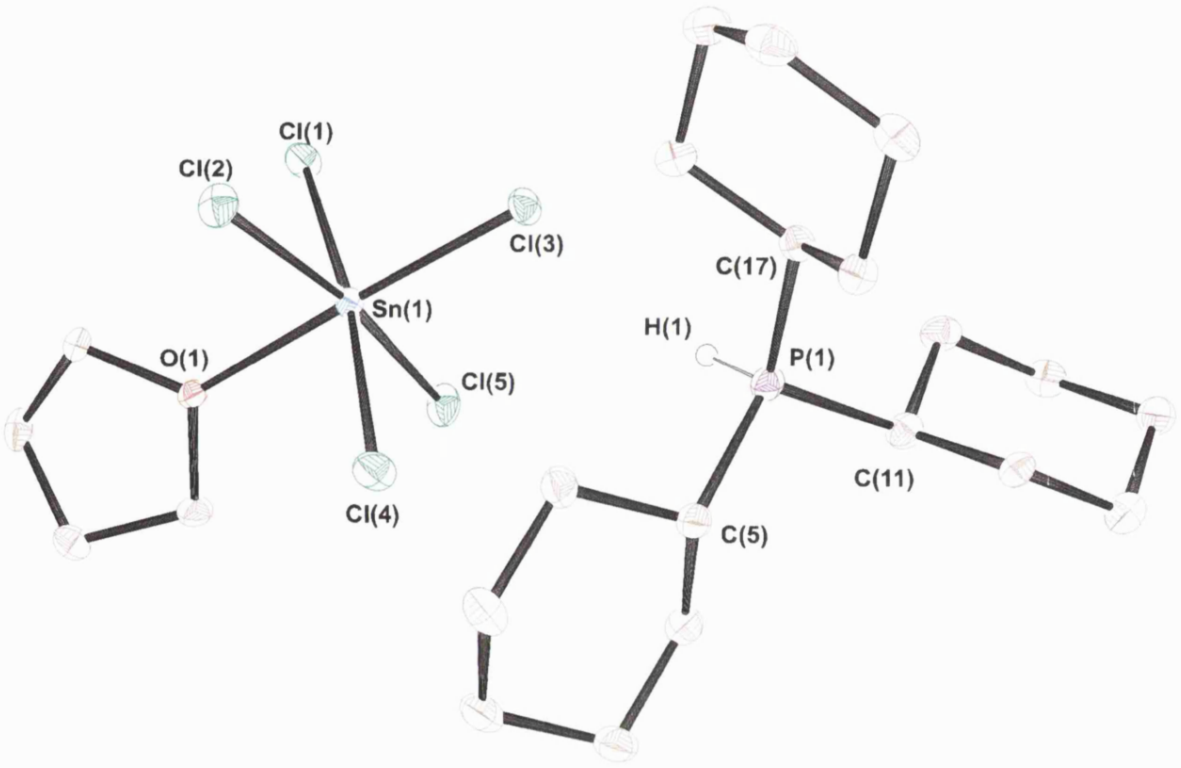

Fig. 4.28 ORTEP plot of $[Cy_3PH]^+[SnCl_5{\cdot}THF]^-$ (**24**). Thermal ellipsoids are at the 30% probability level. Selected bonds lengths (Å) and angles (°) for **24**. Sn(1)–O(1) 2.235(1), Sn(1)–Cl(2) 2.3906(7), Sn(1)–Cl(3) 2.4006(6), P(1)–C(5) 1.815(3), P(1)–C(11) 1.818(3); O(1)–Sn(1)–Cl(3) 178, 14(5), O(1)–Sn(1)–Cl(1) 86.02(4), Cl(1)–Sn(1)–Cl(4) 171.64, Cl(1)–Sn(1)–Cl(3) 95.42(2), C(5)–P(1)–C(11) 110.58(12), C(5)–P(1)–C(17) 115.10(13), C(11)–P(1)–C(17) 112.27(12). Hydrogen atoms on the cyclohexyl groups have been omitted for clarity

octahedral geometry with an 180° O–Sn–O angle. The inter–ligand angles around the tin are close to the ideal, *e.g.* Cl–Sn–Cl 89.90(3) – 90.10(3)°, O–Sn–Cl 89.33(7) – 90.67(7)°. The Sn–O bond distance is 2.166(2) Å. A comparison of the bonds and angles values reported for **24** shows that the Sn–O bond is longer in $[SnCl_5 \cdot THF]^-$ [2.235(1) vs. 2.166(2) Å] and that the geometry at the tin atom is less regular. The Sn–Cl bond distances are also longer in **24** [2.3906(7) – 2.4035(6) Å vs 2.3735(9) – 2.3828(8) Å].

In Figure 4.29 the thermal decomposition of **23** is shown. TGA analysis shows decomposition of the product starts at approximately 180°C and it is effectively over by 500°C. Weight loss observed at 600°C corresponds to SnP (found residual mass 25.8%, theoretical 27.7%).

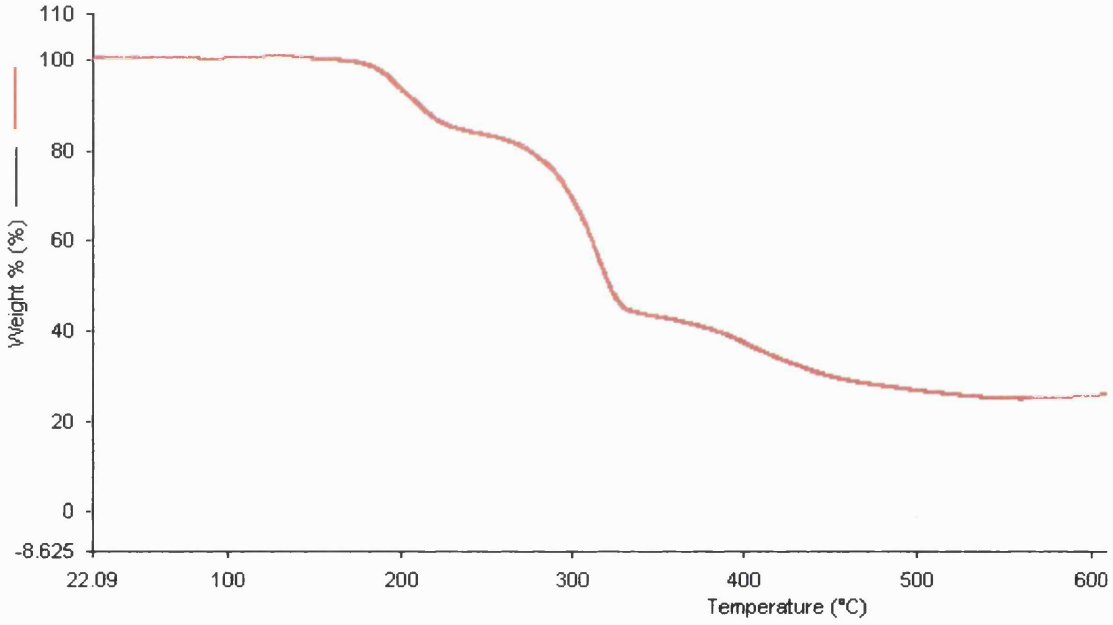

Fig. 4.29 TGA of $SnCl_4 \cdot PCy_3$

4.2.10 Reaction of $SnBr_4$ and Cy_3P (1:1)

Reaction of $SnBr_4$ and Cy_3P was attempted adding a solution of Cy_3P in DCM to a solution of $SnBr_4$ and DCM. The light yellow mixture was left to stir

under argon for three hours and then the solvent was removed under reduced pressure to give a yellow solid.

^{31}P NMR of the solid redissolved in THF shows a main peak, a singlet, at δ = 68.4 ppm, region of the spectrum typical of the coordinated phosphine. There are also two smaller peaks, a doublet at δ = 24.5 ppm and a singlet at 101.8 ppm.

Crystals grown in the NMR tube were studied by X–ray diffraction and were found to be $[H_2O{\cdot}SnBr_4(O)PCy_3]{\cdot}2THF$ (**25**) (Fig. 4.30). The tin adopts a distorted octahedral configuration [O(1)–Sn–O(2) 84.66(9), Br(1)–Sn–O(2) 172.70(7), Br(3)–Sn–Br(4) 169.43(2), Br(2)–Sn–Br(3) 94.726(15)] with the Sn–Br bond lengths varying from 2.5357(4) to 2.5677(4) Å. The Sn–Br(1) bond *trans* to Sn–O(2) is 2.5677(4) Å and is longer than any other Sn–Br bonds in the molecule. This bond is also longer than that reported for **17** where the Sn–Br bond *trans* to the Sn–O one is 2.557(2) Å. Sn–Br(3) and Sn–Br(4) have similar distances, 2.5557(4) and 2.553(4) Å respectively. Sn–Br(2), *trans* to O(1) is the shortest of the Sn–Br bonds [2.5357(4) Å] and it is *trans* to Sn–O(1) [2.137(2) Å]. The Sn–O(2) bond [2.067(2) Å] is shorter than the Sn–O(1) one and is also shorter that the Sn–O bond found for **17** [2.080(8)]. Phosphorus shows a distorted tetrahedral configuration [O(2)–P–C(1) 107.8(2), C(1)–P–C(13) 114.22(17), C(1)–P–C(7) 108.08(2), O(2)–P–C(7) 108.55(15)°] with the distance P–O(2) showing a value of 1.514(3) Å and the three P–C bonds ranging from 1.806(3) to 1.815(3) Å.

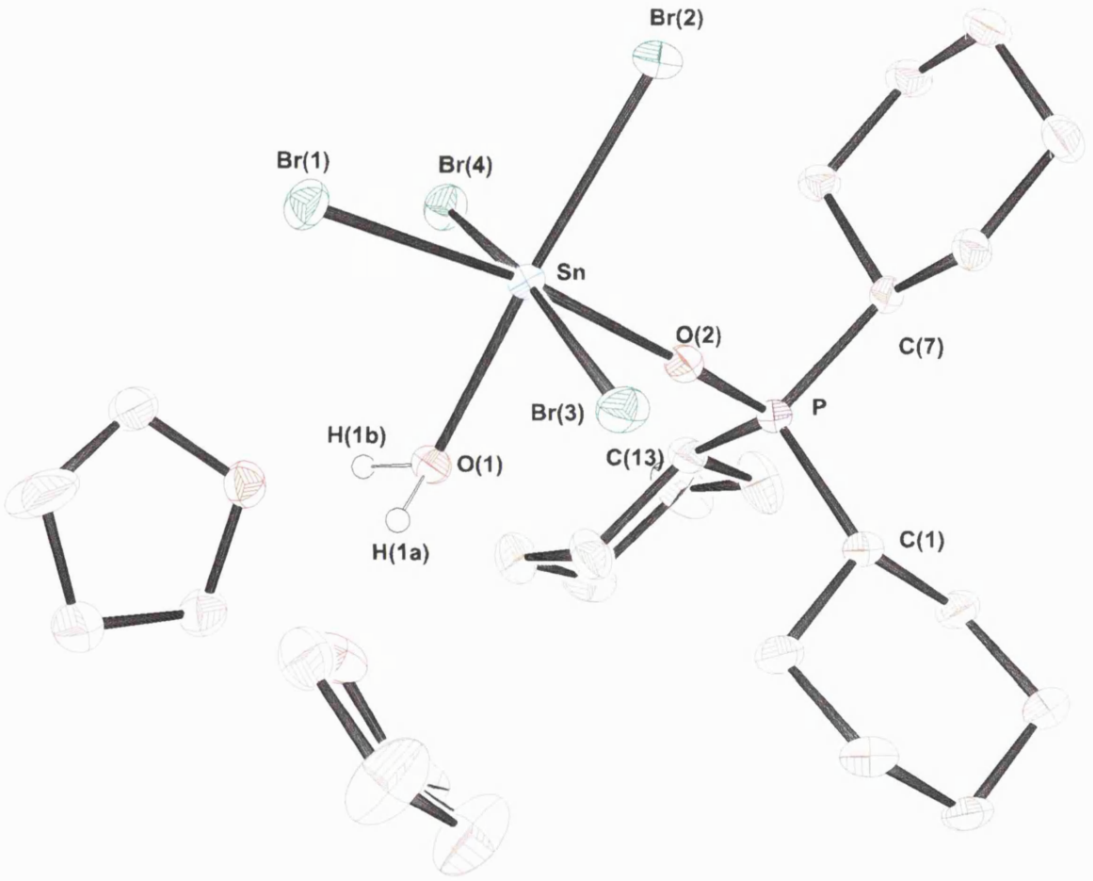

Fig. 4.30 ORTEP plot of $[H_2O{\cdot}SnBr_4(O)PCy_3]{\cdot}2THF$ (**25**). Thermal ellipsoids are at the 30% probability level. Selected bonds lengths (Å) and angles (°) for **25**. Sn–O(1) 2.137(2), Sn–O(2) 2.067(2), Sn–Br(1) 2.5677(2), Sn–Br(2) 2.5357(2), Sn–Br(3) 2.5557(4), Sn–Br(4) 2.553(4), P–O(2) 1.514(2); O(1)–Sn–O(2) 84.66(9), Br(1)–Sn–O(2) 172.70(7). Hydrogen atoms attached to the carbon atoms have been omitted for clarity.

4.2.11 CVD studies of $SnCl_4$·PCy_3

$SnCl_4$·PCy_3 has been evaluated as a potential CVD precursor for its suitability to produce tin phosphide films under CVD condition (see Appendix Two for the apparatus details).

The white solid **23**, approximately 0.47g, has been used to produce a thin film by AACVD at 600°C. The film produced has a gold color with refringence patterns. The film has been investigated by scanning electron microscopy (SEM) and presented in Figure 4.30. The picture shows two different type of spots, one perfectly spherical with a diameter of *ca.* 1μm and the other one, bigger, presents an irregular shape. Both of them are qualitatively identical by EDAX.

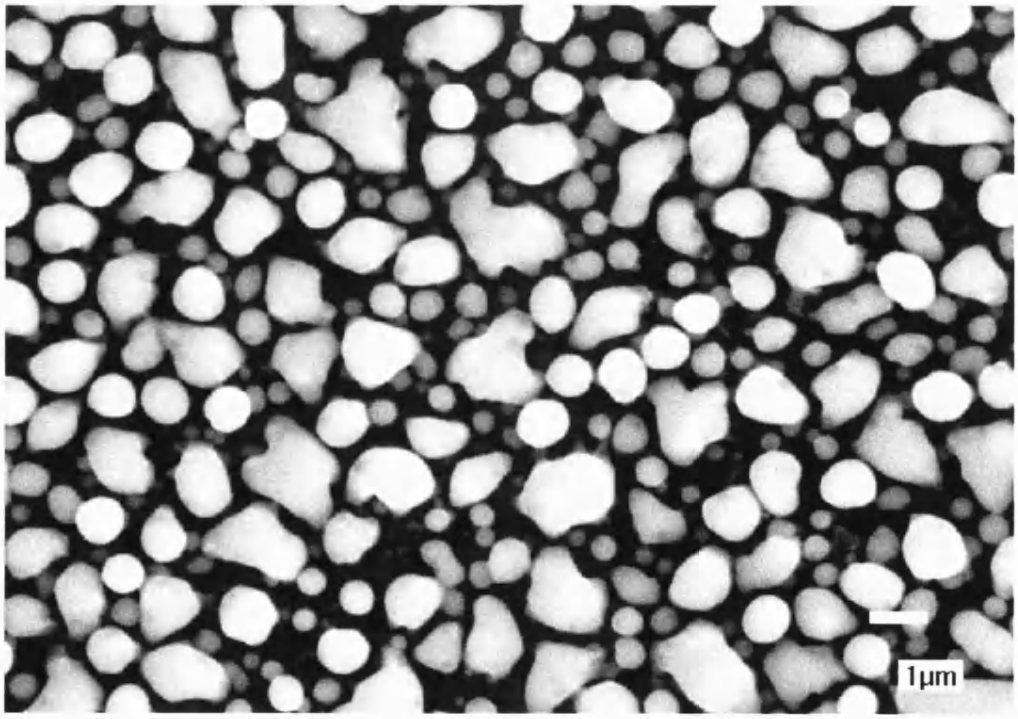

Fig. 4.30 SEM (15 kV) of film grown by AACVD from $SnCl_4$·PCy_3 (**23**) at 600°C

SEM picture of this film is similar to those reported in literature for the preparation of tin phosphide coatings by dual–source APCVD using $SnCl_4$ and R_xPH_{3-x} (R = Cy or Ph). In this latter case, SnP films were obtained and found they were all electrical insulators.[64]

EDAX of the film demonstrates that both tin and phosphorus are present in the film (Fig. 4.31). However, as the picture also shows, at 4 KV there is still the presence of silicon from the glass substrate indicating that the film produced very thin. In fact any attempt to get quantitative information about the film has failed due to the thickness of the film itself.

Fig. 4.31 EDAX (4 KV) of film grown by AACVD from $SnCl_4$·PCy_3 (**23**) at 600°C

4.3 Conclusions

Considering the reported successful synthesis of tin(IV) halides adducts with chelating phosphines, $SnCl_2$ has been reacted with depe, first, and then with dppe.

Reaction with depe successfully produced the adduct $(SnCl_2)_2$·depe, while reaction with dppe generated 3 different species, including both Sn(II) and Sn(IV), and from which $SnCl_4$·$[Ph_2P(O)CH_2CH_2P(O)Ph_2]$ was ultimately isolated and crystallographically studied.

The reaction of SnI_4 with Cy_3P did not lead to formation of the phosphine adduct but to $[SnI_3]^-[Cy_3PI]^+$ and $[SnI_5]^-[Cy_3PI]^+$. $[SnI_5]^-$ occurs as isolated anions, in contrast to the known $[SnI_5]^{3-}$ which forms a linear array of SnI_6 octahedra.

When Cy_3P reacts with $SnCl_4$, instead, the resulting product is the phosphines adduct $SnCl_4$·PCy_3 that has been used as single–source precursor for the growth of SnP film. However, when $SnCl_4$·PCy_3 is dissolved in THF, and crystallized over an extended period, $[SnCl_5$·$THF]^-[Cy_3PH]^+$ is produced resulting from partial hydrolysis (liberation of HCl).

Reaction of tin(IV) halide with primary and secondary phosphines does not lead to the production of phosphine adducts as hoped, but mixtures of compounds, where tin shows both +2 and +4 oxidation states. It is believed that the mechanism behind this result is similar to that reported for the analogous germanium reactions.

In the case of $SnCl_4$, the formation of the adduct is followed by its partial decomposition into $SnCl_2$ and $(CyP)_4$ probably through formation of $Cl_3SnP(H)Cy$. In the case of the reaction with Ph_2PH, formation of the oxidized form of the adduct $SnCl_4$·$(PH_2PH)_2$ has been crystallographically ascertained.

The interesting result of the reaction between SnI_4 and $CyPH_2$ is the formation of $[SnI_4]^{2-}[CyPH_3]_2^+$, whose perovskite–like sheets structure is formed by corner–shared MI_6 octahedra, separated by layers of $CyPH_3^+$ cations. The reaction product is the result of a redox process, whose mechanism is thought to be identical to that observed for related germanium chemistry (Scheme 1, page 38), involving $CyPH_2$, SnI_2 and HI. It is also the first example of

perovskite–like compound to have a counterion different than the ammonium cations. When SnI_4 is reacted with Ph_2PH, the result is the formation of two different kind of salts, $[Sn_3I_{12}]^{6-}[Ph_2PH_2]_6^+$ and $[SnI_6]^{2-}[Ph_2PH_2]_2^+$. $[Sn_3I_{12}]^{6-}$ $[Ph_2PH_2]_6^+$ exists as single independent unit, rather than as part of an extended structure. The products indicated that both reduction to Sn(II) and liberation of HI are components of the reaction mechanism.

From these results, it can be seen how the tin tends to form products where it assumes both the oxidation states +2 and +4. This behaviour is expected, considering the Group 14 trend and is more marked than in the case of germanium.

4.4 Experimental Section

4.4.1 *Reaction of $SnCl_2$ and $Et_2P(CH_2)_2PEt_2$ (1:1)*

1,2 bis(diethylphosphino)ethane (0.49 ml, 2.1 mmol) was added to a solution of anhydrous $SnCl_2$ (0.41 g, 2.1 mmol) in toluene (40 ml), in an argon-filled Schlenk tube. A white precipitate formed immediately, though stirring was continued for 1 hour. The white solid was then isolated by filtration and dried under vacuum.

Microanalysis:

Found (calc.) for $C_{10}H_{24}P_2Cl_4Sn_2$ (**10**) : C 21.9(20.9)%; H 4.1(4.33)%

^{31}P NMR [δ (ppm), $CDCl_3$]:

-7.3 ppm [s, depe]; 27.1 ppm [s, $(SnCl_2)_2$·depe]

Mössbauer:

doublet, $(SnCl_2)_2$·depe, (δ = 3.18 mms^{-1} and ΔE_Q = 1.55 mms^{-1}).

4.4.2 Reaction of $SnCl_2$ and $Ph_2P(CH_2)_2PPh_2$ (2:1)

Anhydrous tin dichloride (0.4 g, 2.1 mmol) was dissolved in toluene (30 ml), in an argon filled round bottom flask. To the resulting solution, 1,2 bis(diphenylphosphino)ethane (0.42 g, 1.05 mmol) was added and stirring continued for one hour. After few minutes a white precipitate appeared. The precipitate was then separated from the solution and dried under vacuum.

Microanalysis:

Found (calc.) for $C_{26}H_{24}P_2Cl_2Sn$ (**11**): C 52.6(53.0)%; H 4.35(4.08)%

^{31}P NMR [δ (ppm), $CDCl_3$]:

45.1 ppm [s, unassigned]; -12.2 ppm [s, dppe]; -27.3 ppm [s, unassigned].

Mössbauer:

doublet, Sn^{II}, (δ = 3.26 and ΔE_Q = 1.12), singlet, $SnCl_2$ (δ = 4.03 and ΔE_Q = 0); singlet, Sn^{IV}, (δ = 0.32 and ΔE_Q = 0).

4.4.3 Reaction of $SnCl_4$ and $CyPH_2$ (1:1)

A round bottom flask, connected to the Schlenk line, was charged under an argon atmosphere with toluene (40 ml) and then tin tetrachloride (0.88 ml, 7.52 mmol) added. Cyclohexylphosphine (1.0 ml, 7.52 mmol) was added dropwise to the resulting solution, which was then stirred for 30 minutes. After few minutes a white precipitate appeared. The precipitate was separated from the solution by cannula filtration and dried.

Microanalysis:

Found (calc.) for $C_6H_{13}PCl_4Sn$ (**13**): C 24.7 (19.0)%; H 4.33(3.45)%

^{31}P NMR [δ (ppm), $CDCl_3$]:

24.4 ppm (t, assigned to $SnCl_4$←:$PCyH_2$ or $SnCl_2$←:$PCyH_2$); -68.3 ppm [s, $(CyP)_4$].

Mössbauer:

singlet, $SnCl_2$ (δ = 4.05 and ΔE_Q = 0); singlet, Sn^{IV} (δ = 0.45 and ΔE_Q = 0).

4.4.4 Reaction of $SnCl_4$ and $CyPH_2$ (4:1)

Cyclohexylphosphine (0.54 ml, 4.1 mmol) was added to toluene (20 ml) under argon. Tin tetrachloride (3 ml, 12.2 mmol) was added dropwise forming a white precipitate immediately. The reaction mixture was left stirring for 30 minutes and after that the solution and the precipitate were separated by cannula filtration and the solid material dried in vacuo.

^{31}P NMR [δ (ppm), $CDCl_3$]:

precipitate: -68.3 ppm [s, $(CyP)_4$].

4.4.5 Reaction of $SnCl_4$ and Ph_2PH (1:1)

Diphenylphosphine (0.5 ml, 2.8 mmol) was added dropwise by syringe into a solution of tin tetrachloride (0.336 ml, 2.8 mmol) in toluene (40 ml) under an argon atmosphere. Soon after the first drop of phosphine had been added, a white precipitate formed. The mixture was left to stir for 30 minutes before the solid was separated from the solution and dried under vacuum.

^{31}P NMR [δ (ppm), $CDCl_3$]:

precipitate: 27.2 ppm, [d, $SnCl_4$←:Ph_2PH or $SnCl_2$←:Ph_2PH (**14**)] J_{P-H} = 538.1 Hz;

supernatant: 30.7 ppm [d, $SnCl_4$←:Ph_2PH or $SnCl_2$←:Ph_2PH (**14**)] J_{P-H} = 537.2 Hz.

Mössbauer:

singlet, $SnCl_2$ (δ = 4.06 and ΔE_Q = 0); singlet, Sn^{IV}, (δ = 0.45 and ΔE_Q = 0).

4.4.6 Reaction of SnI_4 and $CyPH_2$ (1:1)

$CyPH_2$ (0.1 ml, 0.75 mmol) was syringed dropwise into a solution of DCM (10 ml) and SnI_4 (0.47g, 0.75 mmol) under an argon atmosphere, with stirring. As soon as the first drops of phosphine had been added, a yellow precipitate formed. The mixture was left stirring for 30 minutes. The solid was then separated from the solution by filtration and left to dry under vacuum.

Microanalysis:

Found (calc.) for $C_6H_{13}PCl_4Sn$: C 19.8 (9.7)%; H 2.6 (1.8)%

^{31}P NMR [δ (ppm), $CDCl_3$]:

precipitate: -111.2 ppm [$CyPH_2$], 36.2 ppm [unassigned];
supernatant: -10.7 ppm [unassigned].

^{119}Sn NMR [δ (ppm), $CDCl_3$]:

precipitate: -1610 ppm [s];
supernatant: -1610 ppm [s].

4.4.7 Reaction of SnI_4 and Ph_2PH (1:1)

A clear yellow solution was made by adding SnI_4 (041 g, 0.65 mmol) to DCM (20 ml). Ph_2PH (0.11 ml, 0.65 mmol) was syringed into the mixture, kept under constant argon flow and with stirring, producing a yellow precipitate and a

light orange solution. The mixture was left to stir for 3 hours. The yellow solid and the light orange solution were separated by filtration.

^{31}P NMR [δ (ppm), $CDCl_3$]:
precipitate: 40.6 ppm [s], -35.4 ppm [s];
supernatant: 40.6 ppm [s], -35.4 ppm [s].

4.4.8 Reaction of SnI_4 and Cy_3P (1:1)

A Schlenk tube, filled with argon, was charged with DCM (20 ml) and SnI_4 (0.89 g, 1.4 mmol). The mixture produced a clear yellow solution. This solution was added dropwise to Cy_3P (0.4 g, 1.4 mmol) to give a clear red solution. The mixture was kept under argon and left stirring for two hours. Solvent was then removed under reduced pressure to yield a black solid. The solid was then redissolved in THF from which deep red crystals formed .

Microanalysis:
Found (calc.) for $C_{18}H_{33}PI_6Sn$ (**22**) : C = 18.4 (18.6)%, H = 2.95 (2.84)%.

^{31}P NMR [δ (ppm), $CDCl_3$]:
reaction mixture: 72.9 ppm [s, Cy_3PI^+], 25.6 ppm [s, $SnI_4 \cdot PCy_3$].
redissolved precipitate: 72.9 ppm [s, Cy_3PI^+].

4.4.9 Reaction of $SnCl_4$ and Cy_3P (1:1)

A clear and colorless solution containing *n*–hexane (20 ml) and Cy_3P (0.57 g, 2.03 mmol) was prepared under an argon atmosphere. To this solution, $SnCl_4$ (0.24 ml, 2.03 mmol) was added dropwise forming a white precipitate. The mixture was left to stir of 30 minutes and the solid separated from the solution by cannula filtration and dried under a reduce pressure.

Microanalysis:

Found (calc.) for $C_{18}H_{33}PCl_4Sn$ (**23**): C = 39.6 (39.9)%, H = 6.08 (6.1)%

^{31}P NMR [δ (ppm), $CDCl_3$]:

24.8 ppm [d, $(Cy_3PH)^+$] J_{P-H} = 477.6 Hz.

^{119}Sn NMR [δ (ppm), $CDCl_3$]:

-611.1 ppm (s).

Mössbauer:

broad singlet (δ = 0.82 and ΔE_Q = 0).

4.4.10 Reaction of $SnBr_4$ and Cy_3P (1:1)

To a solution of $SnBr_4$ (0.43 g, 1 mmol) in DCM (10 ml), Cy_3P dissolved in DCM (10 ml) was added dropwise originating a light yellow solution. The mixture has been left to stir for three hours under an argon atmosphere. The solvent was then removed under reduce pressure and left dry under vacuum. Crystals of (**25**) were isolated from the NMR tube.

^{31}P NMR [δ (ppm), $CDCl_3$]:

68.4 ppm [s, unassigned], 24.5 ppm [d, unassigned], 101.8 ppm [s, unassigned].

4.4.11 AACVD of $SnCl_4$·PCy_3

Films were grown using aerosol-assisted chemical vapor deposition (AACVD) on standard borosilicate glass slides under a N_2 atmosphere at 1 bar pressure, using a horizontal cold wall reactor; details of the reactor assembly

have been given in Appendix Two. Glass substrates were cleaned prior to use by washing with water and soap, then acetone and subsequently dried in air. Approximately 0.47g of the compound were dissolved in 30 ml of toluene and swept into the reactor using N_2 as the carrier gas. The precursor was consumed over a period of 20 mins. The reactor temperature was 600°C.

CHAPTER FIVE

Organotin Phosphides

5.1 Introduction

The first two authentic examples of compounds containing the tin–phosphorus bonds were the tris(trimethylstannyl)phosphine[152] and diphenyl(triethylstannyl)phosphine.[153] Apart from their physical properties, the only mentioned was a sensitivity to air and moisture. The first work concerning the preparation of organotin phosphide was carried out few years later by Campbell and co workers.[154] They ascertained the air and moisture sensitivity of the compounds, observing formation of the phosphinic esters, and the difficulty of forming compounds containing more than one Sn–P link. They also noted that the same bond was quite strong and suggested the reason as the overlapping of the phosphorus lone pair (p_π) with a vacant *d* orbital of tin.[155]

The interactions between organotin(IV) halide compounds, R_nSnX_{4-n} (n = 1–3), with phosphines has been well documented and the general reactions lead to one simple adduct with an increase of the coordination number about the tin atom.[156-160] Mössbauer studies as well as ^{119}Sn and ^{31}P NMR data have been reported and interpreted. In a few cases, crystal structures of the organotin phosphides have also been reported and given in details either for diorganotin phosphides (Fig. 5.1–5.4)[159,161-163] and for triorganotin phosphides (Fig. 5.5–5.7).[164,165] It has also been noticed how the use of secondary and primary phosphines leads to further reactions, beyond the simple organotin phosphide. It was found that these secondary reactions were dependent on the Lewis acidity of the initial organotin(IV) halide used.[112]

However, in the majority of the cases observed, the reaction between the organotin halides and the phosphine needs the presence of a base to promote reaction and help formation of the metal–phosphorus bond.[116,118,119,166-169] NMR data of an equimolar mixture of R_3MCl (M = Sn) and HPR'_2 (R = Ph, Me, Et, Bu; R' = Ph, c-C_6H_{11}) consist only of a single resonance at the chemical shift of uncoordinated phosphine. Only when the reaction takes place in presence of a

base, *e.g.* dbu, does the ^{31}P NMR of the mixture reveals a singlet with tin satellites, while the ^{119}Sn NMR consists of a doublet with a coupling constant the same as that derived from the corresponding ^{31}P spectrum. [157]

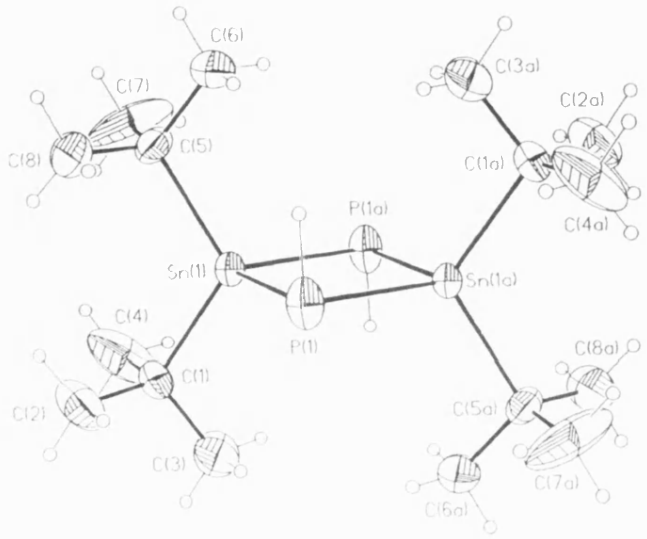

Fig. 5.1 ORTEP plot of $^{t}Bu_4Sn_2(PH)_2$. Thermal ellipsoids are at the 30% probability level. Selected bonds lengths (Å) and angles (°) for $^{t}Bu4Sn_2(PH)_2$. Sn(1)–P(1) 2.541(1), Sn(1)–C(5) 2.204(4); C(1)–Sn(1)–C(5) 114.1(2), Sn(1)–P(1)–Sn(1a) 82.0(1), P(1)–Sn(1)–P(1a) 98.0(1).

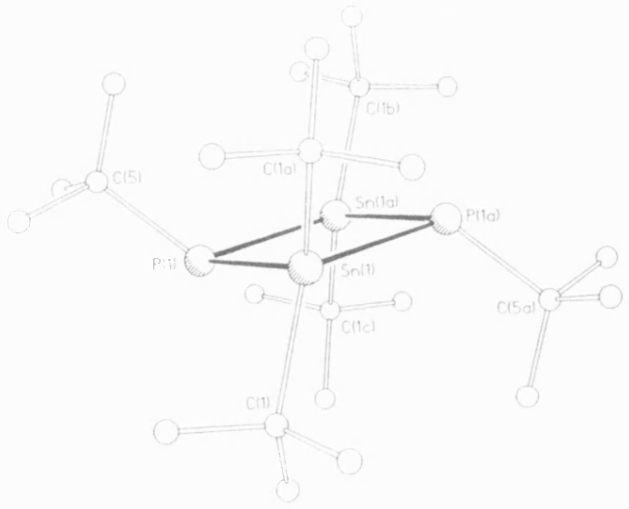

Fig. 5.2 Molecule of $(^{t}Bu_2SnP\text{-}^{t}Bu)_2$. Selected bonds lengths (Å) and angles (°) for $(^{t}Bu_2SnP\text{-}^{t}Bu)_2$. Sn–P 2.556(1), Sn–C 2.232(5), P–C 1.895(9); Sn–P–Sn 88.1(1), P–Sn–P 91.9(1), C–Sn–C 111.7(3).

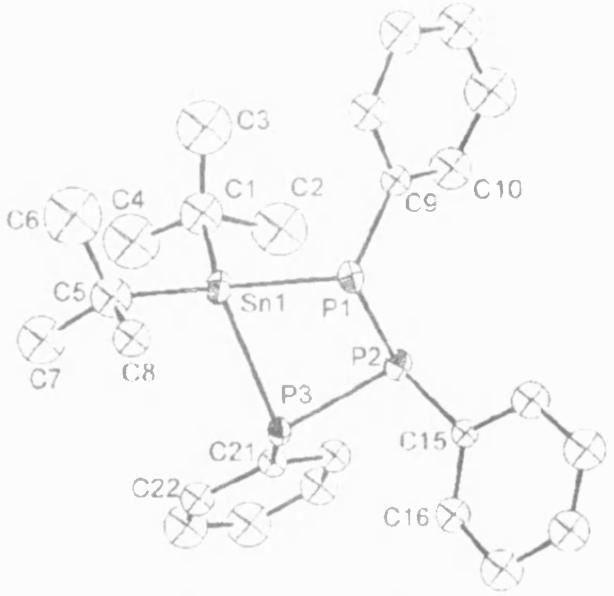

Fig. 5.3 ORTEP drawing of $(^tBu)_2Sn(PPh)_3$. Thermal ellipsoids are at the 30% probability level. Selected bonds lengths (Å) and angles (°) for $(^tBu)_2Sn(PPh)_3$. Sn(1)–P(1) 2.538(8), Sn(1)–P(1) 2.538(8), Sn(1)–P(1)–P(2) 88.3(3), Sn(1)–P(3)–P(2) 83.1(3), P(3)–P(2)–P(1) 92.2(4).

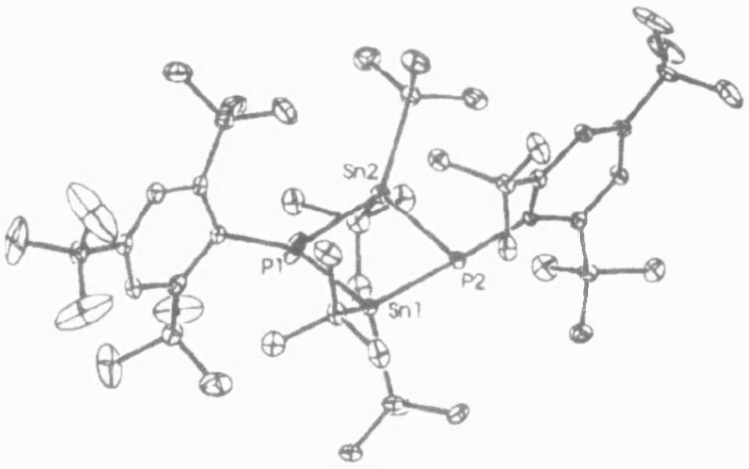

Fig. 5.4 ORTEP drawing of $(^tBu_2SnPR)_2$. Thermal ellipsoids are at the 30% probability level. Selected bonds lengths (Å) and angles (°) for $(^tBu_2SnPR)_2$. Sn(1)–P(1) 2.523(3), Sn(1)–P(2) 2.614(2), Sn(2)–P(1) 2.556(3), Sn(2)–P(2) 2.557(2), P(1)–Sn(1)–P(2) 87.30(9), P(1)–Sn(2)–P(2) 87.87(9), Sn(1)–P(1)–Sn(2) 93.0(1), Sn(1)–P(2)–Sn(2) 90.92(7).

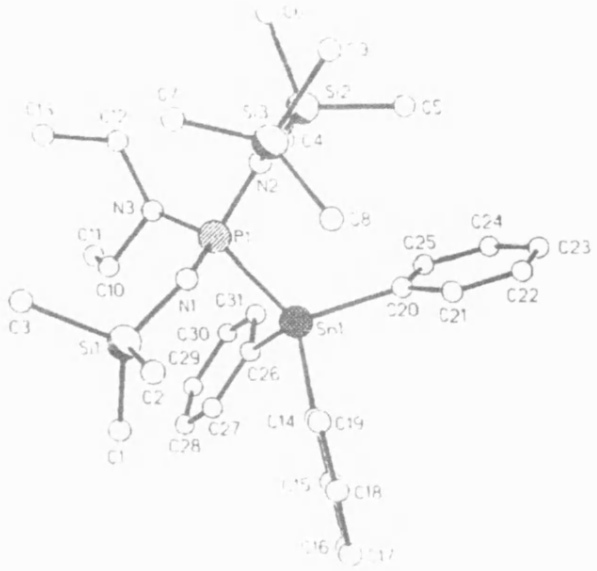

Fig. 5.5 ORTEP plot of $Ph_3Sn(Et_2N)P(=NPh)NPh_2$. Selected bonds lengths (Å) and angles (°) for $Ph_3Sn(Et_2N)P(=NPh)NPh_2$. P(1)–Sn(1) 2.569(1); N(1)–P(1)–Sn(1) 107.0(1), N(2)–P(1)–Sn(1) 107.0(1) 109.8(1), N(2)–P(1)–Sn(1) 106.4(1).

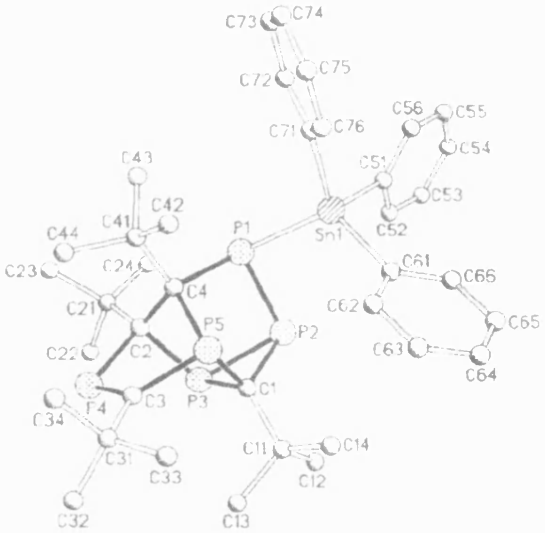

Fig. 5.6 Molecule structure of $C_4{}^tBu_4P_5SnPh_3$. Selected distances in Å. Sn(1)–P(1) 2.522(9), P(1)–P(2) 2.155(1), P(3)–P(2) 2.209(1).

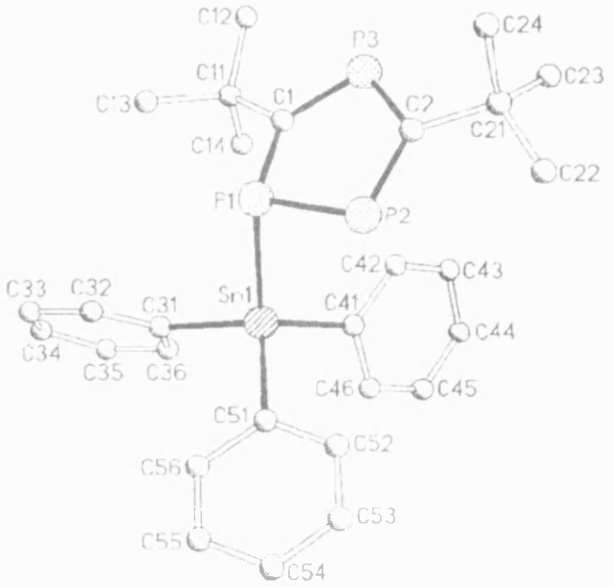

Fig. 5.7 Molecule structure of $C_2{}^tBu_2P_3SnPh_3$. Selected distances (Å) and angles (°). Sn(1)–P(1) 2.521(2), P(1)–P(2) 2.131(2); P(2)–P(1)–Sn(1) 96.28(7), C(1)–P(1)–Sn(1) 112.7(2), C(2)–P(2)–P(1) 97.0(2).

Tiorganotin phosphides have also been prepared by reaction of triorgantin lithium or sodium and several halophosphines in a range of ratios. The reactions, as Schumann and co–workers reported, produced the expected organotin phosphide and the correspondent metal chloride.[168,169] The works ascertained that covalent tin–phosphorus compounds are sensitive to oxygen and that the degree of sensitivity depends considerably on the nature of the shielding organic radicals. Thus alkyl derivatives are, in general, less stable than the phenyl analogues. NMR data for these reaction products show the tin–119 resonance moves to lower frequency when the halide is replaced by a PR'_2 group and it is consistent with the tin remaining four–coordinated. The coupling constants $^1J(Sn, P)$ for the triphenyltin derivates are larger than those for the trialkyltin derivates, probably because the electronegative phenyl groups on tin maximize the s–content of the Sn–P bond (Table 5.1).

As pointed out previously in the Introduction, growing SnP films from single–source precursor by CVD was a major task of this project. The main requirement is finding suitable precursors which deliver to the substrate the bonded components required for the growth of thin films of tin phosphide. Organotin phosphides, in this sense, become a target material and as seen above, there are different routes that can be taken into consideration for the synthesis of these compounds.

Tab 5.1 ^{31}P and ^{119}Sn NMR for known Triorganyltin Complexes in CH_2Cl_2 Solution[a]

Complex	$\delta(^{31}P)$ (ppm)	$\delta(^{119}Sn)$ (ppm)	J (Sn, P) (Hz)	Temp (° C)
Ph_3SnPPh_2	- 56.7	-125 (d)	702	+ 30
Me_3SnPPh_2	- 61.2	+ 6 (d)	569	- 100
Et_3SnPPh_2	- 62.4	+ 7 (d)	635	- 110
Bu_3SnPPh_2	- 59.2	- 8 (d)	625	- 50
$Ph_3SnP(c\text{-}C_6H_{11})_2$	- 24.1	- 109 (d)	784	- 90
$Me_3SnP(c\text{-}C_6H_{11})_2$	- 43.4	- 19 (d)	644	- 100
$Et_3SnP(c\text{-}C_6H_{11})_2$	- 42.8	- 13 (d)	705	- 110
$Bu_3SnP(c\text{-}C_6H_{11})_2$	- 41.0	- 28 (d)	706	- 80

[a] D. Daktemieks, B.F. Hoskins and C.L. Rolls, *Aust. J. Chem.*, 1221, **39**, 1986.

5.2 Results and Discussion

5.2.1 Reaction of Ph_3SnCl and $KPPh_2$ (1:1)

Ph_3SnCl has been reacted with $K^+(PPh_2)^-$ in a 1:1 stoichiometric ratio, in order to form the known compound Ph_3SnPPh_2 (**26**).

$$Ph_3SnCl + K^+(PPh_2)^- \rightarrow Ph_3SnPPh_2 + KCl \qquad \textbf{(Eq. 5.1)}$$

(26)

The reaction was carried out in THF at room temperature and under nitrogen. The reaction, left going for an hour, presented a light yellow color. After the solvent was removed, a yellow solid appeared at the bottom of the reaction vessel. This was redissolved in toluene and filtered to remove any insoluble impurities. Concentration of the toluene solution gave a white solid. The melting point of the white solid was 103°C, as reported in literature for **26**.[154]

The Mössbauer spectrum (Figure 5.8) shows a singlet (plus a shoulder arising from an impurity), with an Isomer Shift δ of 1.33 mm s^{-1}, also close to that reported in literature.[170] However a doublet might be anticipated due to the molecular asymmetry, raising doubt about the literature data.

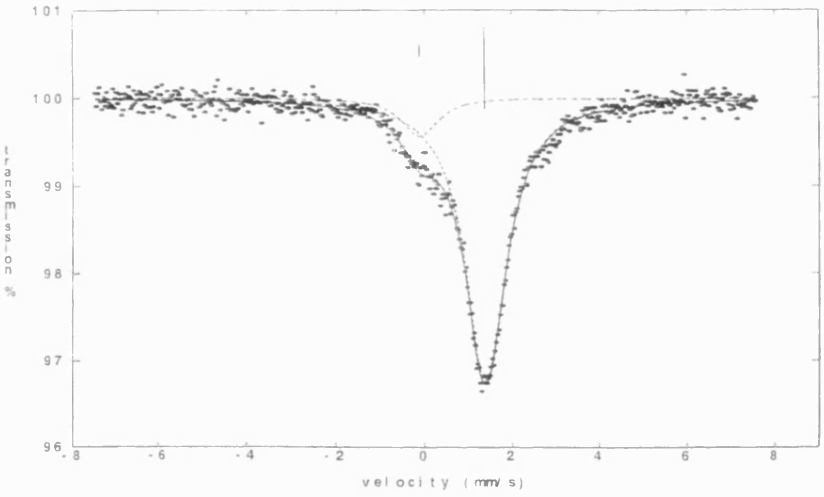

Fig. 5.8 Mössbauer Spectrum of Ph_3SnPPh_2 (**26**)

In the NMR tube a few crystals appeared after two weeks. X–Ray analysis of these crystals has shown how the material contains tin. Unfortunately, the crystal composition is the oxidation version of (**26**), *i.e.* $Ph_3SnOP(O)PPh_2$ (**27**), whose hexameric structure is shown in Figures 5.9 and 5.10.

It would appear that while Sn–P bond no longer exists; the product is formally the oxidation product of the target Ph_3SnPPh_2. The structure of the compound is

hexagonal, almost flat and the values for the angles O(1A)–P(1C)'–O(2C)' and O(1A)–Sn1–O(2A) are respectively 116.41(1) and 176.98(8). The distances are 2.192(2) for Sn1–O(2A), 2.188(2) for Sn1–O(1A), 1.500(2) for O(1A)–P(1C)', 1.490(2) for P(1C)'–O(2C)'. The Sn–Sn and P–P internuclear separations across the hexagon are, respectively, 12.33 – 12.69 Å and 14.23 – 14.8 Å. The coordination geometry about the tin is close to a perfect trigonal bypyramid with

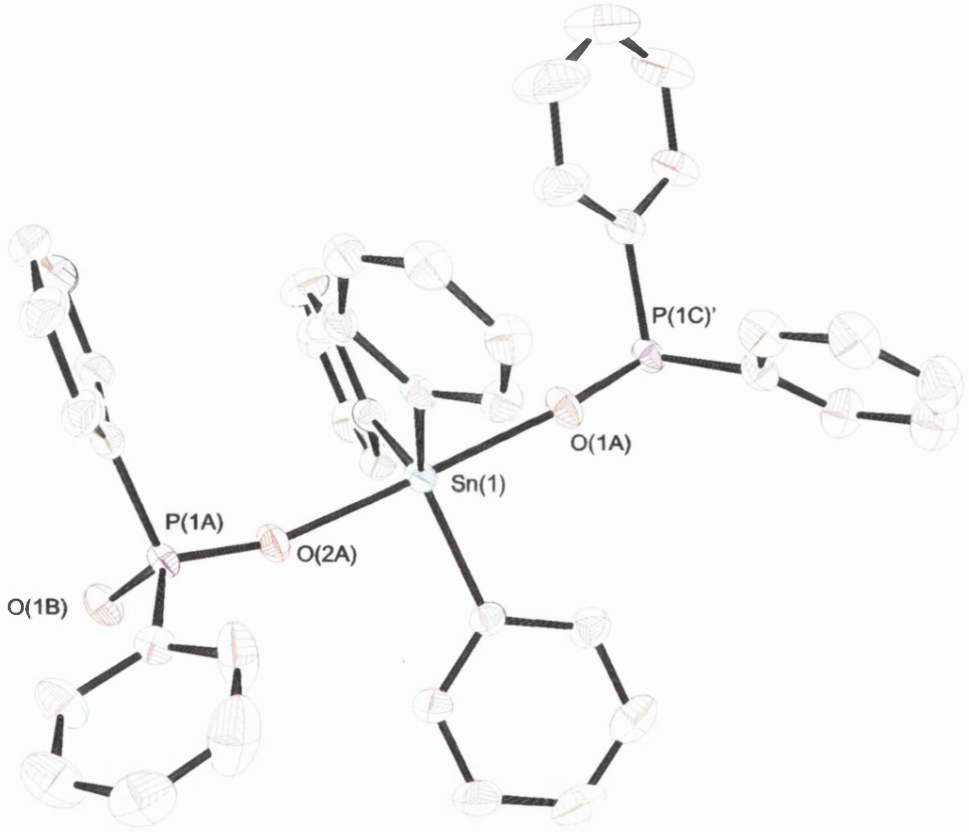

Fig. 5.9 Coordination geometry at the tin and phosphorus atoms for (**27**) shown with the atomic numbering.

average C–Sn–C angles of 119.9(1)° and an axial O–Sn–O angle of 176.98(8)°. The geometry about the phosphorus atom is that of a distorted tetrahedron with bonds angles ranging from 108.43(1)° for O–P–C to 116.14(1) for O–P–O.

However, this is not the first and only hexamer of this type to be reported.[171,172] Previously, two other hexamers, *i.e.* $Ph_3SnO_2P(OPh)_2$ (**28**) and $Ph_3SnOP(O)(OCH_3)(CH_3)$ (**29**), have been crystallographically characterized. The geometrical characteristics for the three hexamers are shown in Table 5.2, from where it is evident these compounds have similar bond lengths and angles.

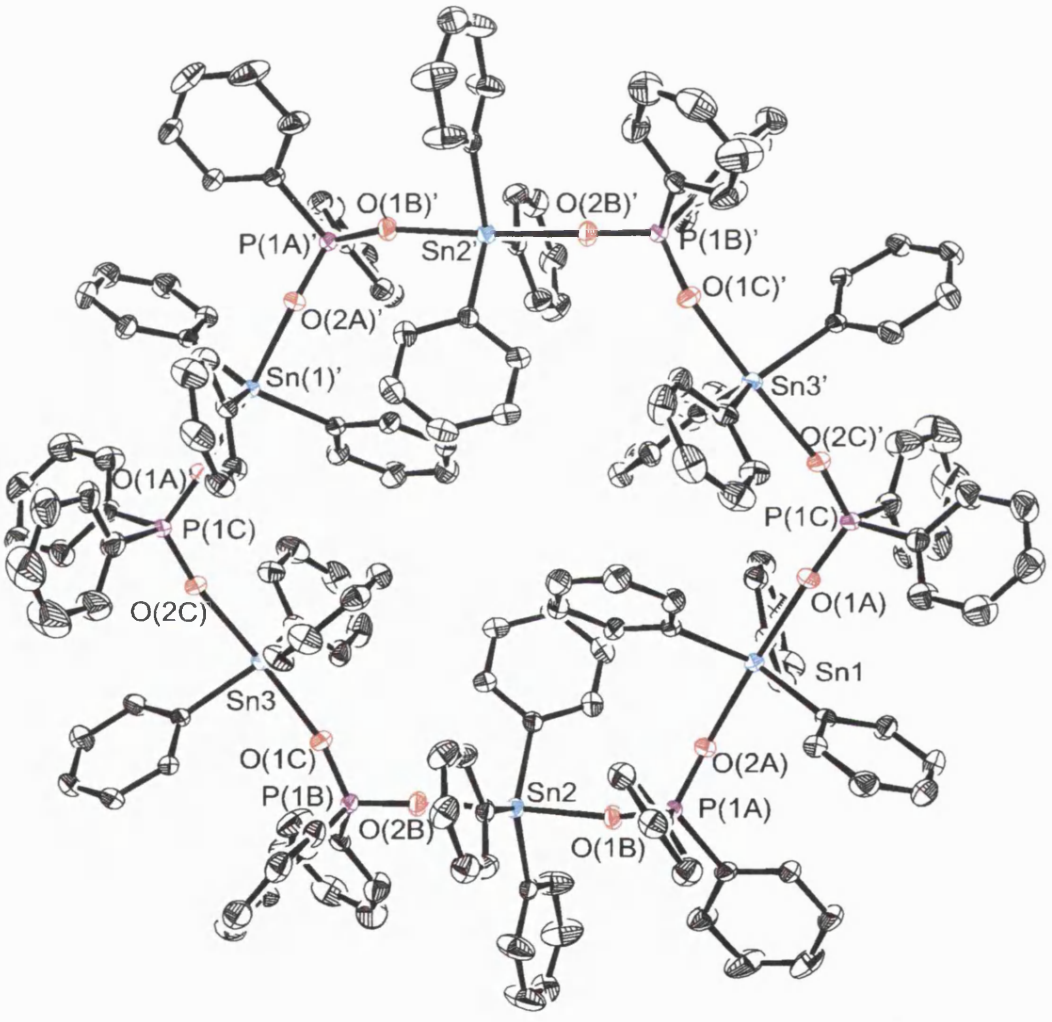

Fig. 5.10 ORTEP plot of $Ph_3SnOP(O)PPh_2$ (**27**). Thermal ellipsoids are at the 30% probability level. Selected bonds lengths (Å) and angles (°) for $Ph_3SnOP(O)PPh_2$. Sn1–O(2A) 2.192(2), Sn1–O(1A) 2.188(2), O(1A)–P(1C)' 1.500(2), P(1C)'–O(2C)' 1.490(2); O(1A)–P(1C)'–O(2C)' 116, 41(1), O(1A)–Sn1–O(2A) 176.98(8), P(1A)–O(2A)–Sn(1) 163.90(1). Hydrogen atoms are omitted for clarity.

Tab. 5.2 Geometrical features of various [O–Sn–O–P–O] compounds

Compound	Sn–O (Å)	P–O (Å)	O–Sn–O (°)	O–P–O (°)	Sn····Sn (Å)	P····P (Å)
27	2.194(2)	1.502(2)	176.96(8)	116.41(1)	12.51	14.51
28	2.241(8)	1.486(8)	177.0(3)	118.5(5)	12.394	13.931
29	2.01(3)	1.489(3)	177.1(2)	117.1(2)	12.40	14.278

Because the tin atoms have to accommodate at least 1 phenyl group each, within the ring (the phenyl group on the phosphorus atoms point out from the ring and do not influence its formation) the hexameric structure is the smallest geometrical arrangement that compound **27** can assume. This conformation can be compared with the tetrameric structure shown by $[Me_3SnOPPh_2]_4$ (**30**) where the methyl groups produce less steric hindrance inside the ring compared to that produced by the phenyl groups (Fig. 5.11).[173]

The Sn–O bond distance for **30** is, 2.244(5) Å and it is longer than that presented by **27**, *i.e.* 2.182(2) Å. The P–O bond length is 1.494(6) Å and is close to that shown by **27**, *i.e.* 1.490(2). The angle values are also similar: O–Sn–O 176.2(3) and O–P–O 117.2(4) for the tetramer, while O–Sn–O 176.96(8) and O–P–O 116.41(1) for the hexamer. The Sn····Sn and P····P internuclear separations across the rings are 12.33 – 12.69 Å and 14.23 – 14.8 Å for hexameric **27** and 7.568 – 7.827 and 10.001 Å for tetrameric **30**.

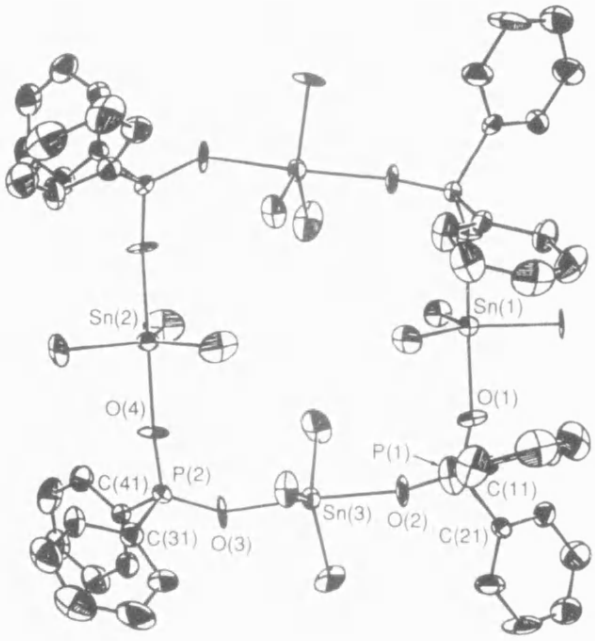

Fig. 5.11 ORTEP plot of tetrameric $[Me_3SnOPPh_2]_4$ (**30**). Hydrogen atoms are omitted for clarity. Selected bonds lengths (Å) and angles (°) for **30**. Sn(3)–O(3) 2.243(5), P(1)–O(1) 1.509(6); O(3)–Sn(3)–O(2) 176.2(3), O(3)–P(2)–O(4) 117.2(4). The Sn···Sn and P···P internuclear separations across the tetramer are, respectively, 7.827 and 10.001 Å.

A Mössbauer spectrum of the toluene–soluble material deliberately exposed to the air for a day comprised a doublet (ΔE_Q = 3.33 mms^{-1} and δ = 1.2 mms^{-1}) consistent with the oxidized product $Ph_3SnO_2PPh_2$ and a singlet (ΔE_Q = 0 mms^{-1} and δ = 1.34 mms^{-1}) evident in the spectrum of the material. Despite the fact that the Mössbauer data for Ph_3SnPPh_2 is reported to be a singlet, the only other crystalline material we have isolated from the reaction is $Ph_3SnSnPh_3$, which also exhibits a singlet in the Mössbauer spectrum.

The reaction reported above for the synthesis of Ph_3SnPPh_2 appears to have been unsuccessful, even though isolation of the oxidized compound signifies that the species has been formed. It is likely that the oxidation didn't occur to the bulk of the product, but only restricted to the sample used for the NMR analysis. This is something expected according to the former literature, where the tin phosphides are reported to be sensitive to atmospheric oxygen.[154] At room temperature dry air

cleaves the Sn–P bond and simultaneously converts phosphorus into the pentavalent state.

5.2.2 Reaction of Ph_3SnCl and Ph_2PH in presence of dbu (1:1)

When Ph_3SnCl is made to react with Ph_2PH, it has been noticed that no reaction occurs over a period of 24 hours, as it is evidenced by no change in the ^{31}P and ^{119}Sn NMR. The employment of a base, however, facilitated the reaction.

$$\mathbf{Ph_3SnCl + Ph_2PH + dbu \rightarrow Ph_3SnPPh_2 + dbuH^+Cl^-} \qquad \textbf{(Eq. 5.2)}$$

(26)

30 minutes after the addition was completed, a sample of the colorless mixture was submitted for ^{31}P and ^{119}Sn NMR. ^{31}P NMR shows a singlet with satellites at δ = -55.4 ppm (J = 705) Hz and no evidence for the unreacted phosphine (Fig. 5.12), while ^{119}Sn NMR shows a doublet at δ = -125 ppm (J = 702 Hz) and again no evidence for the unreacted Ph_3SnCl.

A few hours later the same sample has been resubmitted for ^{31}P and ^{119}Sn NMR. While the ^{119}Sn NMR does not exhibit any change, ^{31}P NMR shows several peaks in the low field region of the spectrum with the main peak at δ = 14.5 ppm belonging to Ph_2PPPh_2 (δ = 15.1).[175] Presence of Ph_2PH as well as Ph_3SnPPh_2 is also shown. It is evident that the compound has been subject to decomposition on standing.

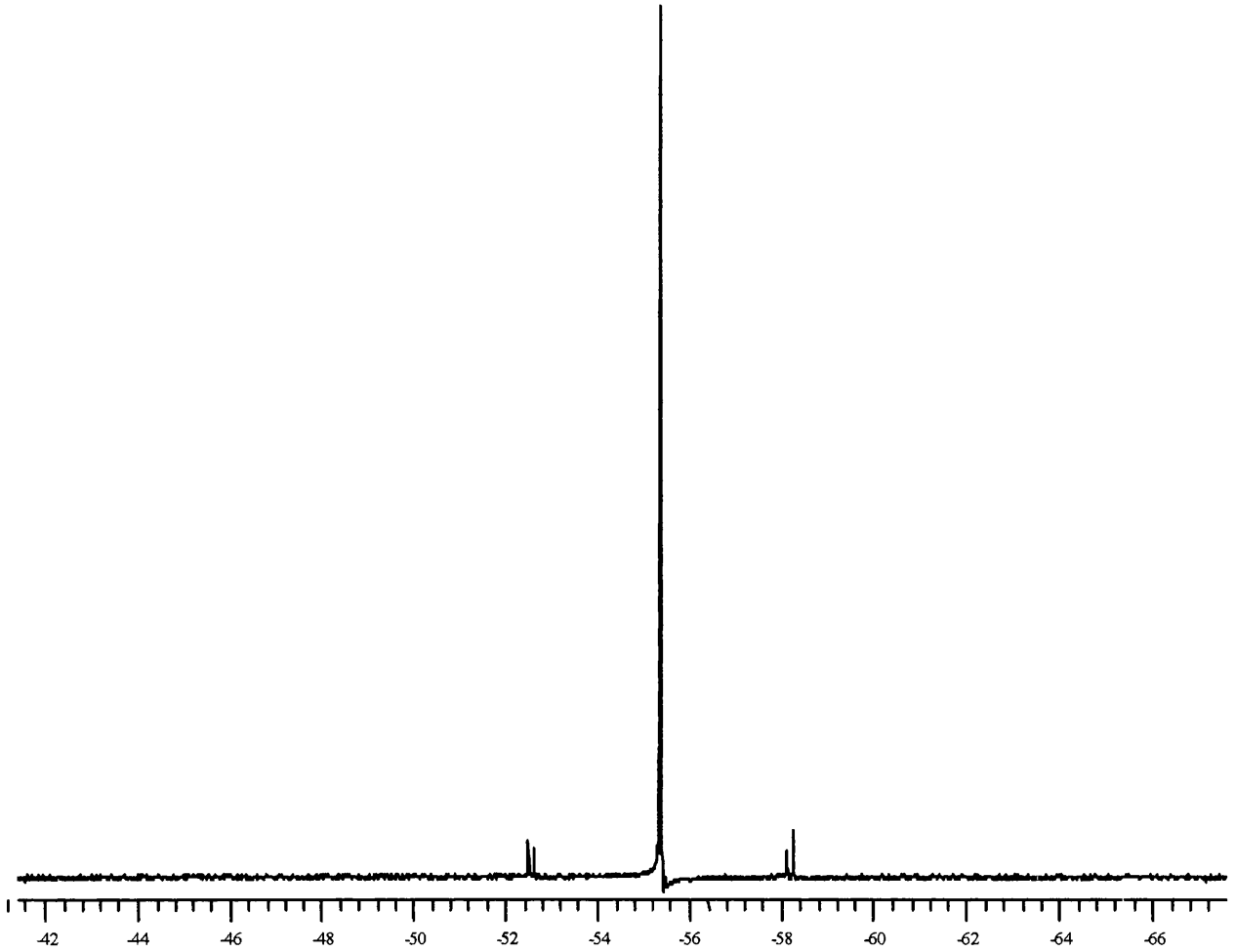

Fig.5.12 ^{31}P NMR of Ph_3SnPPh_2 (**26**).

Mössbauer spectroscopy, carried out on a sample of the solid **26**, reveals a singlet with an isomer shift of 1.34 mms^{-1} and no quadrupole splitting. Although literature data reports a singlet,[170] consistent with the values reported in this Chapter, a doublet might have been expected considering the asymmetry at the tin atom.

Any effort to separate the product from the dbu salts has failed. The product, although it contains the desired Sn–P required to deposit and grow thin films of tin phosphide, cannot be used for the purpose due the difficulty in purifying the precursor.

5.2.3 Reaction of Ph_3SnCl and Ph_2PSiMe_3 (1:1)

The synthesis of Ph_3SnPPh_2 has been then attempted in a different way, using diphenyl(trimethylsilyl)phosphine as phosphorus source. It is known that reaction of several dialkyl or diphenyl(trimethylsilyl)phosphines with triphenyltin chloride has been proven to give rise to triphenyltin phosphides.[175,176] The route, reported to be efficient and productive, also produces Me_3SiCl which can be removed under reduced pressure.

$$\mathbf{Ph_3SnCl + Ph_2PSiMe_3 \rightarrow Ph_3SnPPh_2 + Me_3SiCl} \qquad \textbf{(Eq. 5.3)}$$

(26)

The reaction, performed in toluene and left stirring for half an hour under an argon atmosphere, produced a colorless solution. Solvent and Me_3SiCl were removed under reduce pressure and the solid white material left has been analyzed by NMR. ^{31}P NMR consists only of a singlet at δ = -55.4 ppm with satellites (J= 701 Hz), while the ^{119}Sn magnetic resonance presents a doublet at -125 ppm (J = 702 Hz) proving formation of our product. Few hours later, the same sample has been resubmitted for NMR analysis. The results show still the presence of the Ph_3SnPPh_2 but also a doublet for Ph_2PH. Therefore, it has

been concluded that the presence of Ph_2PH in the phosphorus NMR of the sample can only mean that the produced material has started to decompose.

Mössbauer spectroscopy, carried out on the reaction product, shows a singlet with an isomer shift of 1.34 mms^{-1} and no quadrupole splitting consistent with the literature[170] and reaction 5.1.

5.2.4 Reaction of Bu_3SnCl and Ph_2PH in presence of dbu (1:1)

Reaction of Bu_3SnCl with Ph_2PH in presence of an equimolar quantity of dbu has been attempted to synthesize a suitable precursor, *i.e.* Bu_3SnPPh_2 (**31**) to grow thin film of tin phosphide. The reaction, carried out in DCM and under an argon atmosphere, was stirred for half an hour and remained colorless throughout all this time. The reaction mixture, then, has been set under vacuum to remove the solvent and a white compound appeared in the reaction flask.

$$\mathbf{Bu_3SnCl + Ph_2PH + dbu \rightarrow Bu_3SnPPh_2 + dbuH^+Cl^-} \qquad \textbf{(Eq. 5.5)}$$

(31)

A sample of the white material has been taken to investigate whether or not the expected product has been formed. ^{31}P NMR ($CDCl_3$) shows a singlet with satellites at δ = -57.0 ppm (J = 655 Hz) consistent with what has been reported in literature,[119] plus several minor peaks. Amongst these, only Ph_2PPPh_2 has been identified at δ = +14.5 ppm. ^{119}Sn NMR shows a doublet at δ = -8 ppm (J = 653 Hz).[119]

As it is possible to see from the ^{31}P NMR, the material contains not only the expected product but also several other species yet to be identified. Any attempts to purify the phosphide to get a pure precursor to be utilized to grow thin film have failed, making the compound produced impossible to use for the purpose.

5.2.5 CVD studies of Ph_3SnPPh_2

Ph_3SnPPh_2 has been tested as a potential CVD precursor for its suitability to produce tin phosphide films under CVD conditions (see Appendix Two). The material, once produced and purified (see section 5.2.3), has been used immediately for CVD.

Films from the solid (**26**), approximately 0.35 g, have been produced by AACVD. Deposition was made, at 550°C, producing transparent films with a slight haze. The film, examined by scanning electron microscopy (SEM), is presented in Figure 5.13 and it shows two types of spots: one smaller and spherical with a diameter of *ca.* 0.5 μm and the other one bigger with an irregular feature. The film has the same appearance as the film deposited from **23**.

The film has been proven to contain both Sn and P as it is shown by the EDAX analysis (Fig. 5.14), but as picture clearly shows, even at 4kV peak belonging to the silicon is still the biggest. Any quantitative analysis of the film to show the elements ratio was precluded by the thinness of the film.

SEM picture of this film is similar to those reported in literature for the preparation of SnP coatings by APCVD using a dual–source approach of $SnCl_4$ and R_xPH_{3-x} (R = Cy or Ph).[64]

CVD of the unreacted reagents, *i.e.* Ph_3SnCl and Ph_2PH in the absence of dbu, resulted in a film containing only phosphorus. This proves that the conditions necessary to obtain the SnP film are the formation, *a priori*, of the precursor already containing the Sn–P bond.

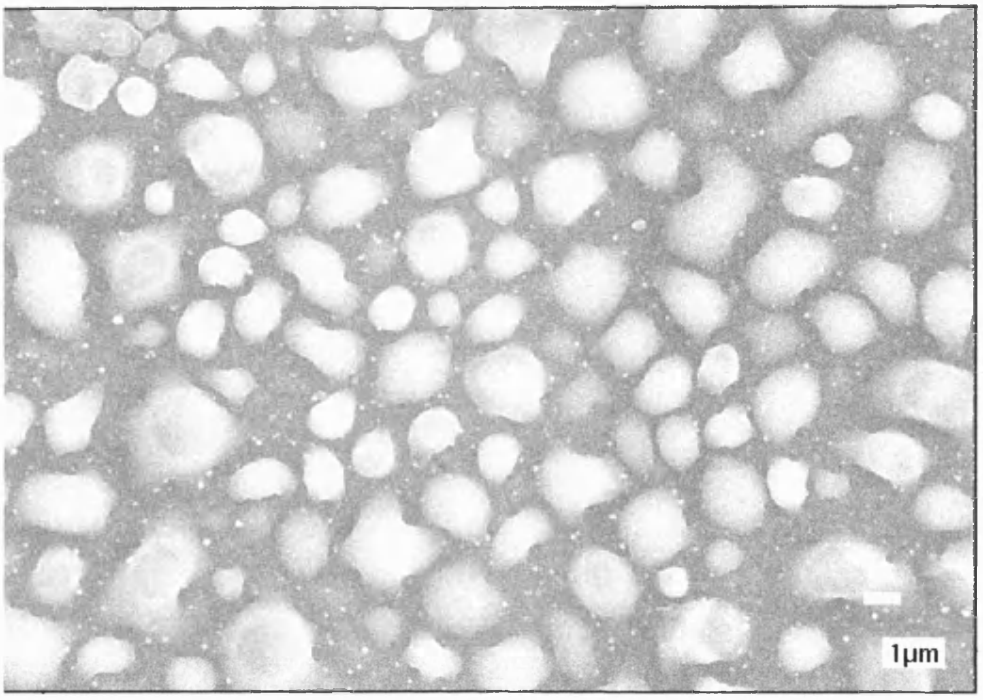

Fig. 5.13 SEM (15 kV) of film grown by AACVD from Ph_3SnPPh_2 (**26**) at 550°C

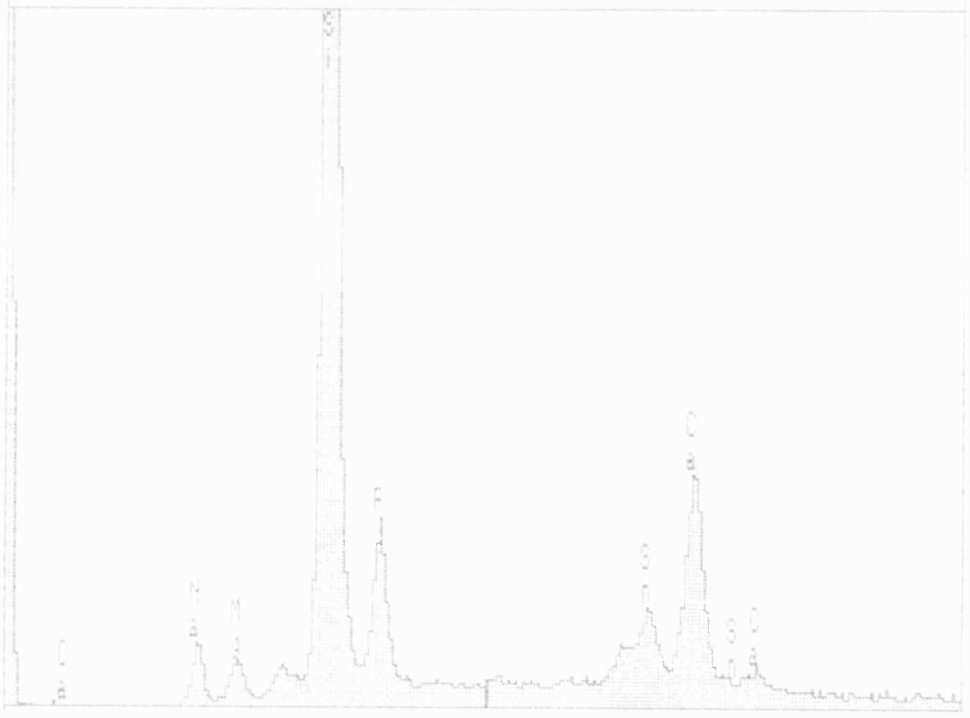

Fig. 5.14 EDAX (4 kV) of film grown by AACVD from Ph_3SnPPh_2 (**26**) at 550°C

5.3 Conclusions

Several syntheses to prepare Ph_3SnPPh_2 (**26**) have been attempted and all of these have led to formation of the expected product. Only in the case where **26** have been isolated pure has it been used as a CVD single–source precursor. Crystal structure of the oxidized Ph_3SnPPh_2, *i.e.* $Ph_3SnOP(O)PPh_2$ (**27**), has been obtained and studied by X–ray diffraction. Production of Bu_3SnPPh_2 (**31**) has also been successful, but any effort to have it pure has failed.

5.4 Experimental Section

5.4.1 *Reaction of Ph_3SnCl and $KPPh_2$ (1:1)*

A round bottom flask, connected to the Schlenk line, was charged with triphenyltin chloride (1.93 g, 5.38 mmol) and then tetrahydrofuran (50 ml) added. Further, potassium diphenylphosphide (1.29 ml, 5.38 mmol) was added to the resulting solution, which was stirred for one hour. After a few minutes a white precipitate appeared. The solution and the precipitate have been separated by filtration; m.p of the white precipitate (**26**), 103–105°C (103–105°C).[170]

Mössbauer:

singlet (δ = 1.33 mm s^{-1}, ΔE_Q = 0).

5.4.2 Reaction of Ph_3SnCl and Ph_2 PH in presence of dbu (1:1)

To a solution of triphenyltin chloride (0.3 g, 0.8 mmol) and DCM, in an argon-filled Schlenk tube, diphenylphosphine (0.14 ml, 0.8 mmol) was added by

syringe, followed by dbu (0.12 ml, 0.8 mmol). Stirring was continued for 30 minutes giving a colorless reaction mixture.

^{31}P NMR [δ (ppm), $CDCl_3$]:

-55.4 ppm [s with satellites, Ph_3SnPPh_2], $^1J_{P—Sn}$= 705 Hz.

^{119}Sn NMR [δ (ppm), $CDCl_3$]:

-125 ppm [d, Ph_3SnPPh_2], $^1J_{Sn—P}$= 702 Hz.

Mössbauer:

singlet (δ = 1.33 mm s^{-1}, ΔE_Q = 0).

5.4.3 Reaction of Ph_3SnCl and Ph_2PSiMe_3 (1:1)

Ph_3SnCl (0.25 g, 0.7 mmol) was added to a solution of Ph_2PSiMe_3 (0.18 ml, 0.7 mmol) in toluene (10 ml), prepared in argon filled Schlenk tube. The colorless and clear reaction mixture was left stirring for 30 minutes.

^{31}P NMR [δ (ppm), $CDCl_3$]:

-55.4 ppm [s with satellites, Ph_3SnPPh_2], $^1J_{P—Sn}$ = 701 Hz.

^{119}Sn NMR [δ (ppm), $CDCl_3$]:

-125 ppm [d, Ph_3SnPPh_2], $^1J_{Sn—P}$= 702 Hz.

Mössbauer:

singlet (δ = 1.33 mm s^{-1}, ΔE_Q = 0)

5.4.4 Reaction of $^{t}Bu_3SnCl$ and Ph_2PH in presence of dbu (1:1)

A solution of DCM (10 ml) and Bu_3SnCl (0.2 ml, 0.74 mmol) has been prepared under an atmosphere of argon and then Ph_2PH (0.13 ml, 0.74 mmol) added to it. To this mixture, dbu (0.11 ml, 0.74 mmol) was added with stirring. The reaction was left stirring for 30 minutes.

^{31}P NMR [δ (ppm), $CDCl_3$]:

-57.0 ppm [s with satellites, Bu_3SnPPh_2], $^{1}J_{P—Sn}$ = 655 Hz.

^{119}Sn NMR [δ (ppm), $CDCl_3$]:

-8.0 ppm [d, $^{t}Bu_3SnPPh_2$], $^{1}J_{Sn-P}$ = 653 Hz.

5.4.5 AACVD of of Ph_3Sn PPh_2

Films were grown using aerosol-assisted chemical vapor deposition (AACVD) on standard borosilicate glass slides under a N_2 atmosphere at 1 bar pressure, using a horizontal cold wall reactor; details of the reactor assembly have been given in Appendix Two. Glass substrates were cleaned prior to use by washing with water and soap, then acetone and subsequently dried in air. The precursor (0.35 g) was delivered in the gas phase as an aerosol of the compound dissolved in 30 ml of toluene and swept into the reactor using N_2 as the carrier gas. The precursor was consumed over a period of 20 mins. The reactor temperature was 550°C.

CHAPTER SIX

Conclusions and Future Work

The target of this research project was to prepare single–source precursors for the chemical vapor deposition of Main Group metal phosphides, avoiding the use of PH_3 as phosphorus source. The choice of germanium and tin, as Main Group metals, lay in the fact that little research had been done on the synthesis of single–source precursors for thin films deposition, except for the Group 13 metals (*i.e.* GaP and InP). In addition, as reported in the Introduction to this thesis, formation of germanium and tin phosphide films have been achieved only by dual–source technique.

Formation of adducts through reaction of Ge(IV) and Sn(IV) halides with primary, secondary and tertiary phosphines have proven to be extremely difficult. It has been found that the driving force for the process is a redox reaction which facilitates formation of salts that have been crystalographically characterized.

In the case of $GeCl_4$ with primary and secondary phosphines ($CyPH_2$, $PhPH_2$ and Ph_2PH), reactions proceed through formation of an adduct, which then decomposes to give $Cl_3GeP(H)_{2-n}R_n$ (n = 1, 2) and HCl, which plays a very important role in these reactions. In fact, in solution, $Cl_3GeP(H)_{2-n}R_n$ forms an equilibrium with $ClP(H)_{2-n}R_n$ and $GeCl_2$, which then reacts with some unreacted phosphine to produce $R_nH_{3-n}P{:}\rightarrow GeCl_2$. This Ge(II) adduct reacts with HCl previously formed to give the crystallographically characterized $[GeCl_3]^-[R_nPH_{4-n}]^+$ with n = 1,2. Only when an excess of $GeCl_4$ is used and all the phosphine reacted, $R_nH_{3-n}P{:}\rightarrow GeCl_2$ cannot be formed and the only product observed is $Cl_3GeP(H)_{2-n}R_n$. In particular, $Cl_3GeP(H)Cy$ (**2**) and $Cl_3GeP(H)Ph$ (**4**) have been synthesized, fully characterized, proven to be air stable for short periods and also tested for CVD. EDAX on the films obtained from AACDV of **2** shows a ratio of Ge:P of 2:1 while from LPCVD the Ge:P ratio is virtually 1:1. EDAX obtained on films produced by LPCVD of **4** shows a Ge:P ratio of 1:1.4. Large amounts of oxygen are also observed, and its presence in the films does not depend by the particular CVD technique used (AACVD or LPCVD) or by the oxidation of the precursors, which are stable over a period of several minutes, but from a post–reaction that converts part of the germanium phosphide into

phosphate. The films are amorphous and show a band gap of 1.1 eV typical of GeP.

Although it was not possible to isolate any $Cl_3SnP(H)_{2-n}R_n$ (n = 1, 2), reactions of SnI_4 and $SnCl_4$ with the same phosphines show a similar mechanism to $GeCl_4$. In particular, reaction of SnI_4 with $CyPH_2$ produces as a consequence of a redox process the salt $[SnI_4]^{2-}[CyPH_3]^{+}_2$ which consists of single SnI_4^{2-} which generates an anionic network of corner–shared MI_6 octahedra, separated by layers of $[CyPH_3]^+$ cations. In a similar way, when Sn(IV) iodide is reacted with Ph_2PH the result is the formation of the salts $[Sn_3I_{12}]^{6-}[Ph_2PH_2]^{+}_6$ and $[SnI_6]^{2-}[Ph_2PH_2]^{+}_2$. In this case, while $[Sn_3I_{12}]^{6-}$ $[Ph_2PH_2]^{+}_6$ is the result of a redox reaction and $[Sn_3I_{12}]^{6-}$ is the first example of this anion, in $[SnI_6]^{2-}[Ph_2PH_2]_2^{+}$ it is possible to see only the oxidation of phosphorus from +3 to +5 but not the reduction of tin that remains +4. A redox reaction involving halogen transfer is observed when SnI_4 is made to react with Cy_3P and the crystals isolated are $[SnI_3]^-[Cy_3PI]^+$ and $[SnI_5]^-[Cy_3PI]^+$. When $SnCl_4$ reacts with the phosphines, the reactions follow the same mechanism already explained. However, in this case, no salts have been isolated although proofs of mechanism followed are given by formation of $SnCl_2$ and $(RP)_4$, the product of the coupling halophosphines $ClP(H)_{2-n}R_n$. In one single occasion, when $SnCl_4$ and Cy_3P are the reagents involved in the reaction, formation of the adduct $SnCl_4{\cdot}PCy_3$ was achieved. This product has been tested as single–source precursor for CVD use. Although films are not thick enough for a quantitative analysis, SEM shows presence of both Sn and P.

It has been already reported in the Introduction how it is easier for tin to switch from +4 to +2, while germanium forms stable compounds mostly in its +4 state. The difficulty in isolating products such as $Cl_3SnP(H)_{2-n}R_n$ and the tendency of tin(IV) halides to react to give rise to redox reactions in which tin presents +2 as oxidation state is even more accentuated than in the germanium reactions. This characteristic is also noted when $SnCl_2$ reacts with chelated phosphines. The result is the formation of products where tin adopts both the +2 and the +4 oxidation state.

The synthesis of compounds containing the Sn–P and Ge–P bond to be used as precursors for CVD has been successfully achieved employing organogermyl and organotin chlorides ($R_{4-n}MCl_n$, M = Ge and Sn, n = 1–2 and R = Ph, Bu, Et) to react with Ph_2PSiMe_3. Synthesis of Ph_3SnPPh_2 has been also attempted following different procedures. In all the cases, Ph_3SnPP_2 has been produced but the impossibility to separate it from side products has made the synthesis using Ph_2PSiMe_3 the easiest to use. Crystals of the oxidized Ph_3SnPP_2, *i.e.* $Ph_3SnOP(O)PPh_2$, have been also isolated and studied by X–ray diffraction. It has been noted that the compound is not stable in solution, and tends to decompose. Ph_3SnPPh_2 has been used as precursor for the deposition of SnP films and although films are not thick enough for a quantitative analysis, SEM shows presence of both Sn and P. Synthesis of Bu_3SnPPh_2 was possible to achieve only using Ph_2PH and dbu to react with Bu_3SnCl. However, the presence of side products impossible to separate from the main product has prevented its employment as precursor for thin films deposition.

All the organogermyl phosphide synthesized has been proven to be air stable for short periods and have been used as single–source precursor for CVD. While Et_3GePPh_2 shows always a Ge:P ratio of 1:1 at different temperatures, $Et_2Ge(Cl)PPh_2$ has a Ge:P ratio of 1:1 only at 450°C. Increasing temperature (500 and 550°C) the Ge:P ratio changes to 1:1.3 and 1:2.8 respectively. EDAX on the films obtained by Ph_3GePPh_2, instead, shows only presence of phosphorus. All the films produced show presence of a large amount of oxygen derived from a post oxidation reaction.

In terms of future work, formation of adducts using $SnCl_2$ with primary, secondary and tertiary phosphines could be investigated as only two works are reported at the beginning of the 1970s.[92,121] The same reactions could be attempted using GeI_2, in particular those involving primary and secondary phosphines, as the only few attempts reported involve the synthesis of tertiary phosphine adducts GeX_2.[89-92] Reaction of GeI_2 with chelating phosphines can also be challenged.

Further works should also concentrate on the synthesis of precursors obtained using organogermanium or organotin halides with Ph_2PSiMe_3 that have proven to give stable M–P bonds and can be utilized as precursor for CVD. A series of organogemanium and organotin chloride, ranging from di to tri and from methyl to phenyl can be purchased, while R_2PSiMe_3 are not commercially available except when R = Ph. Changing the organic group present in the precursors has been proven to influence the volatility and the purity of the precursors themselves and can be also used to study the effect on the stoichiometric ratio in the films.

An area of study worth pursuing is the reaction between $R_2Sn(NMe_2)_2$ and chelating phosphines of the type $R(H)PCH_2CH_2P(H)R$.

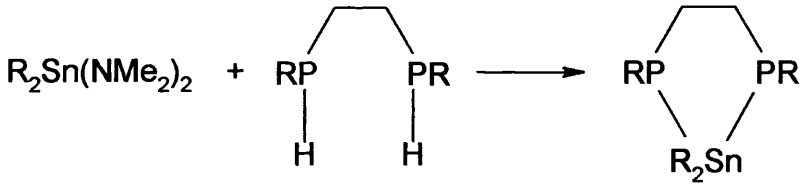

The compound synthesized should be more stable due to the chelating effect of the phosphines, hence it would be a suitable precursor for films depositions.

Also, major improvements could be made by varying the conditions (substrate and precursor temperature, gas flow rate, precursor concentration) to obtain films with a suitable thickness. Deposition using organotin phosphides should be reattempted in order to get thicker films, and employment of different glass substrates could be taken into consideration to minimize the quantity of precursor needed to obtain a sufficient thick film.

APPENDICES

APPENDIX ONE

Reagents

Reagents employed for reactions have been obtained commercially and used without further purification. All reactions have been carried out with fresh dry solvents, produced from distillation under an inert atmosphere and took place in glassware flamed to remove moisture.

Instrumentation

Microanalysis

Carbon, hydrogen and nitrogen elemental analyses were performed using an Exeter Analytical CE 440 analyzer.

Infra – Red Spectroscopy

Infra-red spectra were recorded as nujol (liquid paraffin) mulls between NaCl plates. Measurements were taken using a Nicolet 510P FT–IR spectrometer within the range 4000 – 600 cm^{-1} with a medium slit width and a peak resolution of 4.0 cm^{-1}.

Nuclear Magnetic Resonance Spectroscopy

^{1}H, ^{13}C, ^{31}P and ^{119}Sn NMR spectra were recorded on a Bruker Avance 300 MHz FT–NMR spectrometer.

X – Ray Diffraction (XRD)

Data were collected on Nonius KappaCCD diffractometer. Full matrix anisotropic refinement was implemented in the final least–squares cycles throughout. All data were

collected for Lorentz and polarization and some for extinction. Structure determination and refinement was achieved using the SHELX suite of programs and drawings were produced using ORTEP. Details of individual structure determination are given in Appendix Four, save on CD incorporated with the Thesis.

Scanning Electron Microscopy (SEM)

SEM was carried out using a JEOL JSM T330 scanning electron microscope operating at an accelerating voltage ranging from 4 to 15 kV. Films were sputtered with carbon in order to avoid charging and to improve the secondary electron image quality.

Energy Dispersive X – Ray Analysis (EDAX)

Film thickness estimates using EDAX techniques were performed on a Jeol Superprobe instrument operating at an accelerating voltage of 5kV or 10 kV with a beam current of 5×10^{-8}A or 5×10^{-9}A.

Mössbauer Spectroscopy

Mössbauer spectra were recorded on a Constant Acceleration Mössbauer Spectrometer (Cryophysics) fitted with a 10mCi calcium metasstannate–119m source (Amersham Int.) and operated in sawtooth mode. Spectra were run at 78K with liquid nitrogen as the cooling source. Samples were run as finely ground powders or frozen liquids. Isomer shift are relative to SnO_2.

Thermal Gravimetric Analysis (TGA).

TGA spectra have been recorded with a Perkin Elmer TGA 7 Thermogravimetric Analyzer connected to a personal computer via TEC 7/DX Thermal Analysis Instrument controller. The TGA furnace allows operations from 300 to 1000°C under a N_2 atmosphere. It is a small, platinum–wound micro furnace that allows rapid heating and cooling rates. A chromel–alumel thermocouple provides accurate sample temperature during analyses. Instrument and data have been elaborated with the Pyris software.

APPENDIX TWO

Chemical Vapor Deposition Reactor

The CVD apparatus used in this study has been assembled as a general screening rig for the use in this and other related projects. The system consists of a horizontal cold wall reactor with associated gas lines and electrical heater controls. The reactor contains two separate systems, a heated bubbler assembly (APCVD) and an ultrasonic nebuliser system (AACVD). For the purposes of this study only the ultrasonic nebuliser system (AACVD) was employed and hence will be discussed in detail. A schematic of the reactor system is shown in figure 8.1

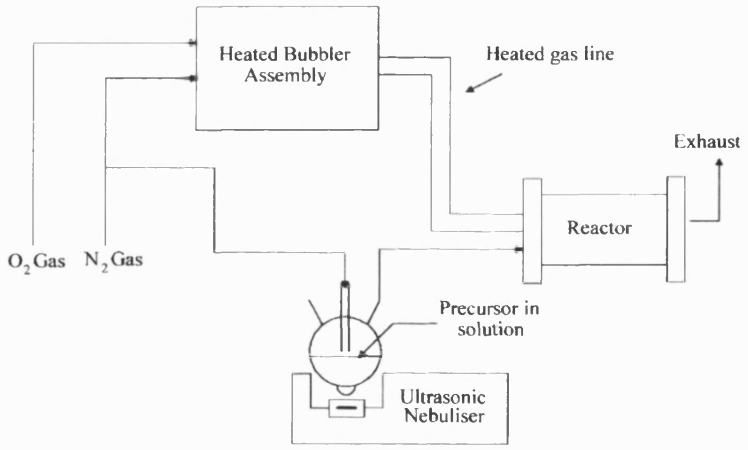

Fig. 8.1 The CVD apparatus.

The nebulizer system used for AACVD is an ultrasonic humidifier from Pifco Health (model No 1077) bought from Argos (Fig. 8.2). The piezoelectric transducer, situated in the reservoir containing water, transmits ultrasound through the water and the glass flask into the solution containing the precursor. The distance between the piezoelectric transducer and the flask is approximately 3–4 cm. The water in the reservoir is replaced every 30 minutes in order to cool the transducer.

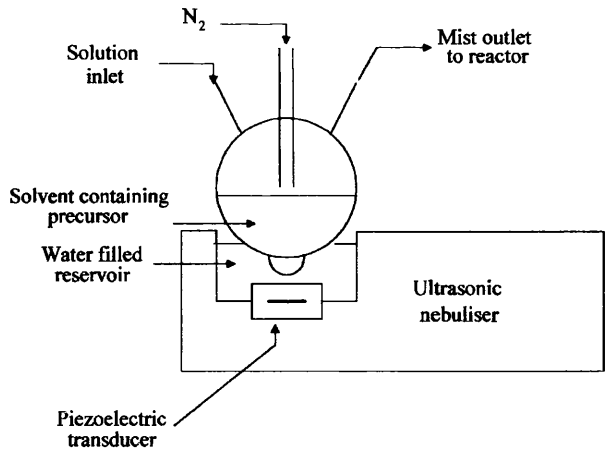

Fig. 8.2 The ultrasonic nebuliser system.

The precursor solution is injected into the flask, which is under an inert atmosphere and placed on the nebulizer. The aerosol of fine droplets created (droplet size: 0.2–5 μm) can be controlled via two controls, the mist output (MO) and the humidity level (HL). The resulting aerosol is then swept out of the flask by a flow of argon and transported to the CVD reactor through a baffle to promote laminar flow.

The CVD reactor chamber where decomposition takes place is 8 mm high, 40 mm wide and 300 mm long. The ceiling tile and walls consist of quartz plates. The glass substrate is positioned on a large graphite susceptor, which is heated by three Watlow firerod cartridge heaters. The temperature of the graphite block is maintained by a Watlow series 965 controller, which monitors the temperature by means of thermocouples positioned inside the block. The graphite susceptor is held inside a large quartz tube (330 mm long, 100 mm diameter) suspended between stainless steel flanges upon which many of the electrical and gas line fittings are fixed. Air–tight seals are provided by 'Viton' O–rings. A schematic of the CVD reactor chamber is shown in figure 8.3.

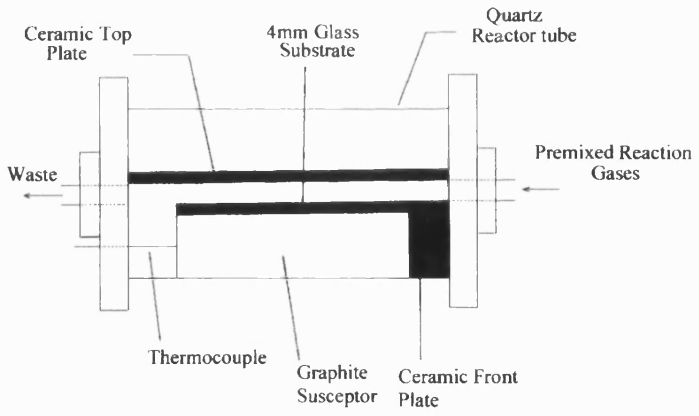

Fig 8.3 The CVD reactor chamber.

For the LPCVD experiments a different reactor was employed and a schematic of the apparatus is shown in figure 8.4. The precursor sample to be decomposed is placed at the bottom end of the quartz tube reactor and the tube is then inserted in to the cylindrical heater, which heats the precursor. The quartz tube reactor also contains the glass substrate and a thermocouple.

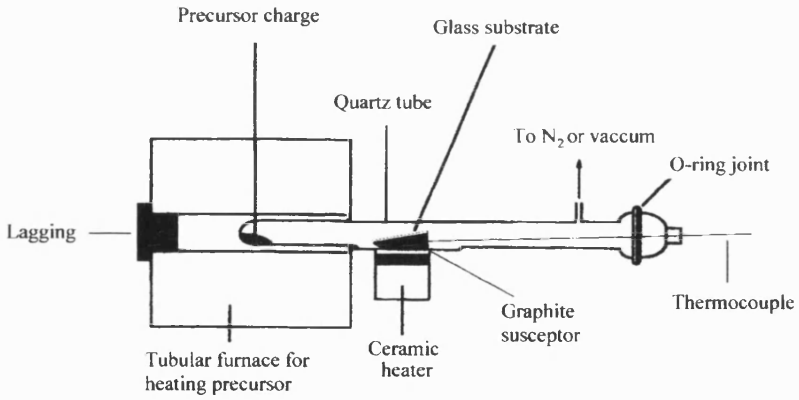

Fig. 8.4. The low pressure CVD reactor.

The glass substrate is positioned outside of the cylindrical heater, and heated conductively by a ceramic heater placed underneath. The temperature is monitored and controlled via a thermocouple and the whole reactor is connected to a Schlenk line to allow for the application of vacuum and backfill of argon.

All glass substrates were cleaned in an identical manner prior to use. The cleaning routine was as follows:

a) The glass was washed thoroughly with water and detergent;
b) Then washed thoroughly with copious amounts of distilled water;
c) The substrate was finally washed with acetone and allowed to dry.

The glass substrate was always prepared prior to a deposition experiment and on completion of screening each precursor the nebuliser (AACVD), reactor tube (LPCVD) and any associated pipework were thoroughly cleaned in an Acid/Base bath followed by acetone to prevent unwanted contamination in films deposited from subsequent precursors.

APPENDIX FOUR

Crystallographic Analysis and Structural Refinement for Compounds Synthesized in This Thesis

All crystallographic data are included in the CD attached at the end of this thesis.

CD Table of Contents:

(**1**)	$[GeCl_3]^-[CyPH_3]^+$	**K01kcm21**
(**6**)	$[GeCl_3]^-[Ph_2PH_2]^+$	**K01kcm19**
(**12**)	$SnCl_4{\cdot}[Ph_2P(O)CH_2CH_2P(O)Ph_2]$	**K01kcm40**
(**15**)	$SnCl_4{\cdot}[P(O)Ph_2]_2$	**H01kcm2**
(**18**)	$[SnI_4]^=[CyPH_3]_2^+$	**K02kcm28**
(**19**)	$[Sn_3I_{12}]^{6-}[Ph_2PH_2]_6^+$	**K02kcm20**
(**20**)	$[SnI_6]^=[Ph_2PH_2]_2^+$	**H02kcm4**
(**21**)	$[SnI_3]^-[Cy_3PI]^+$	**K03Kcm13**
(**22**)	$[SnI_5]^-[Cy_3PI]^+$	**H02kcm2**
(**24**)	$[Cy_3PH]^+[SnCl_5{\cdot}THF]^-$	**H01kcm7**
(**25**)	$[H_2O{\cdot}SnBr_4(O)PCy_3]{\cdot}2THF$	**H02kcm13**
(**27**)	$Ph_3SnOP(O)PPh_2$	**K00kcm30**

REFERENCES

1 C. Y. Ting, *J. Vac. Sci. Technol.*, 1982, **21**, 14.
2 J. C. Haygarth, *Thin Solid Films*, 1980, **72,**, 51.
3 J. S. Liu, *Solar Energy Mater. Res. Bull.*, 1986, **13**, 399.
4 W. D. Munz, D. Hoffman, and K. Harting, *Thin Solid Films*, 1982, **96**, 79.
5 R. L. Ripley, *J. Less. Comm. Met*, 1962, **4**, 496.
6 V. Wazer, *Phosphorous and its Compounds*, 1958, **1**.
7 V. B. Chernogorenko, S. V. Muchnik, K. A. Lynchak, and Z. A. Klimax, *Mater. Res. Bull.*, 1981, **16**, 1.
8 M. Fujii, I. H., and S. Motojima, *J.Crystal Growth*, 1996, **166**, 99.
9 W. S. Sheldrick, *Stereochemistry of Penta and Hexacoordinated Derivates of Phosphorus. Topic.Current.Chem*, 1978, **1**, 73.
10 D. Hellwinkel, *Hexacoordinated Derivates of Phosphorus. Organic Phosphorus Compounds*, 1973, **3**.
11 J. I. G. Cadogan, *Phosphorus Radicals. Adv.Free Rad.Chem.*, 1968, **2**, 203.
12 A. L. Hector and I. P. Parkin, *J.Mater.Chem.*, 1994, **4**, 279.
13 I. P. Parkin, *J.Mater.Chem.*, 1993, **3**, 689.
14 N. Schonberg, *Acta Chem Scand.*, 1954, **8**, 229.
15 T. Ludstrom and P. O. Snell, *Acta Chem Scand.*, 1967, **21**, 1343.
16 R. F. Jarvis, R. M. Jacubinas, and R. B. Kaner, *Inorg. Chem.*, 2000, **39**, 3243.
17 K. A. Gingerich, *Nature*, 1963, **200**, 877.
18 S. Motojima, T. Wakamatsu, and K. Sugiyama, *Less Common Metals*, 1981, **82**, 379.
19 K. Komaki, *Japan Koka Tokkyo KokonJP02150067.*
20 H. Su, Y. Xie, B. Li, X. Liu, and Y. Qian, *J. Solid State Chem.*, 1999, **146**, 110.
21 J. L. Vossen and W. Kern, *Thin Film Processes*, 1978, 259.
22 W. S. J. Rees, *CVD of Nonmetals*, 1996.
23 H. W. Markstein, *EP&P*, 1977, 31.
24 K. K. Schuegraf, *Handbook of thin - film deposition processes and techniques*, 1988, 81.
25 M. Langlet, *Thin Solid Films*, 201, 398.
26 M. Langlet, E. Senet, J. L. Deschanvres, G. Delabouglise, F. Weiss, and J. C. Joubert, *J. Less. Comm. Met*, 1989, **151**, 399.
27 P. O'Brien, N. L. Picket, and D. J. Otway, *Chem. Vap. Deposition*, 2002, **8**, 237.
28 T. Kodas and M. Hempden-Smith, *The Chemistry of Metal CVD*, 1994.
29 D. C. Bradley, R. C. Mehrotra, and P. D. Gaur, *Metal Alkoxides*, 1978.
30 D. C. Bradley, *Chem. Rev.*, 1989, **89**, 1317.
31 A. Purdy, A. Berry, R. Holm, M. Fetunel, and D. Gaskill, *Inorg. Chem.*, 1989, **28**, 2799.
32 S. Thompson, D. Cole-Hamilton, D. Gilliland, M. Hitchman, and J. Barnes, *Adv. Mater. Opt. Electron*, 1992, **1**.
33 M. Hitchman, S. Shamlian, D. Gilliland, D. Cole-Hamilton, J. Nash, S. Thompson, and S. Cook, *J. Mater. Chem.*, 1995, **5**, 47.
34 A. C. Jones, *J.Mater.Chem.*, 2002, **12**, 2576.

[35] J. M. Olson, S. R. Kurtz, and A. E. Kibbler, *J.Crystal Growth*, 1988, **89**, 131.
[36] N. Brianese, F. Ossola, M. Porchia, G. Rossetto, P. Zanella, and O. J. Williams, *Chem. Mater.*, 1991, **3**, 225.
[37] W. B. Duncan and O. H. Dermont, *Inorganic Materials*, 1993.
[38] A. Miehr, O. Ambacher, W. Rieger, T. Metzger, E. Born, and R. A. Fisher, *Chem. Vap. Deposition*, 1996, **5**, 51.
[39] R. Nomura, K. Miyawaky, T. Toyosaki, and H. Matsuda, *Chem. Vap. Deposition*, 1996, **5**, 174.
[40] J. Cheon, D. S. Talaga, and J. I. Zink, *J. Am. Chem. Soc.*, 1997, **119**, 163.
[41] G. Shang, K. Kunze, M. J. Hampden - Smith, and E. N. Duesler, *Chem. Vap. Deposition*, 1996, **2**, 242.
[42] M. Bochmann, *Chem. Vap. Deposition*, 1996, **2,**, 85.
[43] P. O'Brien and R. Nomura, *J. Mater. Chem.*, 1995, **5**, 1761.
[44] R. A. Baldwin, E. E. Foos, R. L. Wells, P. S. White, A. L. Rheingold, and G. P. A. Yap, *Organometallics*, 1995, **15**, 5035.
[45] P. Doppelt and T. H. Baum, *Chem. Mater.*, 1995, **7**, 2217.
[46] S.-G. Shyu, J.-S. Wu, S.-H. Chuang, K.-M. Chi, and Y.-S. Sung, *J. Chem. Soc., Chem. Commun.*, 1996, 2239.
[47] T. S. Lewkebandara, J. W. Proscia, and C. H. Winter, *Chem. Mater.*, 1995, **7**, 1053.
[48] J. D. Kennedy and W. McFarlane, *Rev. Silicon, Germanium, Tin, Lead Compd.*, 1974,, **1**, 235.
[49] J. T. Scheper, K. C. Jayaratne, L. M. Liable-Sands, G. P. A. Yap, A. L. Rheingold, and C. H. Winter, *Inorg. Chem.*, 1999, **38**, 4354.
[50] R. Leutenecker, B. Fröschle, and P. Ramm, *Microelectron. Eng.*, 1997, **37/38**, 397.
[51] I. M. Watson and A. J. Connor, *Thin Solid Films*, 1991, **L21**, 196.
[52] V. Koenig, *Surf. Coat. Technol.*, 1987, **33**, 91.
[53] H. A. Johansen, *Surv. Prog. Chem.*, 1977, **8**, 57.
[54] R. M. Fix, G. Gordon, and D. H. Hoffman, *J. Am. Chem. Soc.*, 1990, 7833.
[55] R. G. Gordon, D. M. Hoffman, and U. Riaz, *Chem. Mater.*, 1992, **4**, 68.
[56] C. J. Carmalt, C. A., R. D. Culp, R. A. Jones, Y.-M. Sun, B. Fitts, S. Whaley, and H. W. Roesky, *Inorg. Chem.*, 1997, **36**, 3108.
[57] Y. Sasaki and M. Hirohashi, *Denki Kagaku Ouobi Kogyo Butsuri Kagaku*, 1995, **52**, 203.
[58] C. Blackman, C. J. Carmalt, S. A. O'Neill, I. P. Parkin, L. Apostolico, and K. C. Molloy, *J. Mater. Chem.*, 2001, **11**, 2408.
[59] C. S. Blackman, C. J. Carmalt, I. P. Parkin, L. Apostolico, K. C. Molloy, A. J. P. White, and D. J. Williams, *J. Chem. Soc., Dalton Trans.*, 2002, 2702.
[60] C. Blackman, C. J. Carmalt, S. A. O'Neill, I. P. Parkin, L. Apostolico, and K. C. Molloy, *Applied Surf. Sci.*, 2003, **211**, 2.
[61] C. S. Blackman, C. J. Carmalt, T. D. Manning, S. A. O'Neill, I. P. Parkin, L. Apostolico, and K. C. Molloy, *Chem. Vap. Deposition*, 2003, **1**, 9.
[62] H. J. Haugan, W. Yu, S. T. Lee, A. Petrou, B. D. McCombe, K. S. Brewer, J. F. Lees, and O. T. Beachley, *J. Cryst. Growth*, 2002, **244(2)**, 157.
[63] C. Blackman, C. J. Carmalt, S. A. O'Neill, I. P. Parkin, L. Apostolico, and K. C. Molloy, *Materials Letters.*, 2003, **57**, 2634.
[64] R. Binions, C. S. Blackman, C. J. Carmalt, S. A. O'Neill, I. P. Parkin, K. C. Molloy, and L. Apostolico, *Polyhedron*, 2002, **21**, 1943.
[65] R. Binions, C. J. Carmalt, and I. P. Parkin, *Polyhedron*, 2003, **22**, 1683.
[66] D. A. Atwood, A. H. Cowley, R. A. Jones, and M. A. Mardones, *J. Organomet. Chem.*, 1993, 449.

[67] R. Hoevel, N. Brianese, A. Brauers, P. Balk, M. Zimmer, M. Hostalek, and L. Pohl, *J. Cryst. Growth*, 1991, **107**, 355.
[68] J. A. J. Glass and S. J.T., *Thin Solid Films*, 1998, **315**, 86.
[69] G. I. Rusu, *Phys. Status Solidi A*, 1971, **4**, 755.
[70] K. E. Lee, C. K. Lowe-Ma, and K. T. Higa, *Materials Research Society Symposium Proceedings*, 1993.
[71] C. W. Hill, G. B. Stringfellow, and L. P. Sadwick, *J. Cryst. Growth*, 1997, **181**, 321.
[72] R. L. Wells, M. F. Self, A. T. McPhail, S. R. Aubuchon, R. C. Woundenberg, and J. P. Jasinski, *Organometallics*, 1993, **12**, 2832.
[73] S. W. Choi, G. Lucovsky, and K. J. Backmann, *Journal of Vacuum Science & Technology, B: Microelectronics and Nanometer Structures*, 1992, **10**, 1070.
[74] R. E. Treece, G. S. Macala, and R. B. Kaner, *Chem. Mater.*, 1992, **4**, 9.
[75] A. H. Cowley, P. R. Harris, R. A. Jones, and C. Nunn, *Organometallics*, 1991, **10**, 652.
[76] R. A. Heineche, I. P. Llewellyn, and G. Scarsbrook, *J. Vac. Sci. Technol. A-Vac. Surf. Films*, 1989, **7(3)**, 1099.
[77] K. Komaki, *Japanese patent JP2*, 1990, **248**, 79.
[78] W. Biltz, M. Heimbrecht, and M. Zumbusch, *Z. Anorg. U. Allgem. Chem.*, 1934, **242**, 237.
[79] P. Jolibois, *C. R. l'Academie. Sci., Ser. II Univers*, 1910, **150**, 106.
[80] K. Hirose, G. A. Medvedkin, T. Ishibashi, T. Nishi, and K. Sato, *J. Cryst. Growth*, 2002, 237.
[81] M. S. Omar, *Mater. Res. Bull.*, 1990, **25(6)**, 691.
[82] P. H. M. van Loosdrecht, M. M. Maior, S. B. Molnar, Y. M. Vysochanskii, P. J. M. van Bentum, and H. van Kempen, *Physcal ReviewB: Condensed Matter and Material Physics*, 1993, **48(9)**, 6014.
[83] P. K. Ajmera and H. Y. Shin, *Report*, 1988, 59.
[84] U. D. Scholz and W. Jeitschko, *J. Solid State Chem.*, 1987, **67(2)**, 271.
[85] D. W. Bullett and W. G. Dawson, *Solid State Commun.*, 1986, **60(9)**, 767.
[86] B. Eisenmann, H. Jordan, and H. Schaefer, *Z. Anorg. U. Allgem. Chem.*, 1986, **532**, 74.
[87] S. Furuseth and H. Fjiellvaag, *Acta Chem Scand.*, 1985, **A39(8)**, 537.
[88] V. V. Sobolev, V. E. Grachev, and A. D. Smirnova, *Phys. Status Solidi B*, 1985, **2**, 128.
[89] R. B. King, *Inorg. Chem.*, 1963, **2**, 199.
[90] N. G. Bokii, Y. T. Struchkov, S. P. Kolenisnov, I. S. Rogozhin, O. M. Neferov, and I. Akad, *Nauk SSSR, Ser. Khim.*, 1975, 812.
[91] M. Karnop, W. W. du Mont, P. G. Jones, and J. Jeske, *Chem. Ber.*, 1997, **130**, 1611.
[92] W. W. du Mont, B. Neudert, G. Rudolph, and H. Schumann, *Angew. Chem., Int. Ed. Engl.*, 1976, **15**, 308.
[93] I. R. Beattie and G. A. Ozin, *J. Chem. Soc. A*, 1970, 370.
[94] D. K. Frison and G. A. Ozin, *Can. J. Chem.*, 1973, **50**, 2697.
[95] W. W. du Mont, *Z. Anorg. Allg. Chem.*, 1979, **85**, 458.
[96] W. W. du Mont, H. J. Kroth, and H. Schumann, *Chem. Ber.*, 1976, **109**, 3017.
[97] F. Ruthe, W. W. du Mont, and P. G. Jones, *Chem. Comm.*, 1997, 1947.
[98] S. M. Godfrey, I. Mushtaq, and R. G. Pritchard, *J. Chem. Soc., Dalton Trans.*, 1999, 1319.
[99] W. W. du Mont and H. Schumann, *J. Organomet. Chem.*, 1977, **128**, 99.

[100] C. Couret, J. Escudie, H. Ranaivonjatovo, and J. Satgé, *Organometallics*, 1986, **5**, 113.
[101] J. Escudie, C. Couret, H. Ranaivonjatovo, and J. Satgé, *J. Chem. Soc., Chem Comm.*, 1984, **24**, 1621.
[102] R. C. Dobbie, P. D. Gosling, and B. P. Straughan, *J. Chem. Soc., Dalton Trans.*, 1975, 2368.
[103] J. C. J. Bart, *Acta Crystallogr., Sect. B: Struct. Sci.*, 1969, **25**, 762.
[104] S. P. Kolesnikov, V. I. Shiryaev, and O. M. Nefedov, *Izv. Akad. Nauk Gruz. SSR, Ser. Khim.*, 1966.
[105] Nakamoto, *Infrared and Raman Spectra of Inorganic and Coordination Compounds*, 1963.
[106] D. J. Bottomley, M. Iwami, Y. Uehara, and S. Ushioda, *J. Vac. Sci. Technol. A-Vac. Surf. Films*, 1999, **17**, 698.
[107] T. G. Hibbert, M. F. Mahon, K. C. Molloy, I. P. Parkin, and L. S. Price, *J. Mater. Chem.*, 2001, **11**, 469.
[108] V. A. Chauzov, Y. N. Studnev, L. S. Rudnitskaya, and A. V. Fokin, *J. Gen. Chem. USSR, Eng. Trans.*, 1989, **59**, 1143.
[109] D. Messer, *Z. Naturforsch., B: Chem. Sci.*, 1978, **33**, 366.
[110] C. Aubauer, K. Davidge, T. M. Klapötke, and P. Mayer, *Z. Anorg. Allg. Chem.*, 2000, **626**, 1783.
[111] G. Fritz and G. Poppenburg, *Angew. Chem.*, 1960, **72**, 208.
[112] H. Schumann, H. Hopf, and M. Schmidt, *J.Organometallic Chem.*, 1964, **2**, 159.
[113] H. Schumann, M. Schmidt, and P. Schwabe, *J.Organometallic Chem.*, 1964, **1**, 366.
[114] K. A. Hooton and F. Glockling, *Proc.Chem. Soc.*, 1963, 146.
[115] E. H. Brooks, F. Glockling, and K. A. Hooton, *J. chem. Soc.*, 1965, 4283.
[116] H. Schumann and H. Benda, *Chem. Ber*, 1971, **104**, 333.
[117] H. Schumann and W. W. Du Mont, *Chem. Ber*, 1975, **108**, 2261.
[118] H. Schumann, P. Schwabe, and O. Stelzer, *Chem. Ber*, 1969, **102**, 2900.
[119] D. Dakternieks, B. F. Hoskins, and C. L. Rolls, *Aust. J. Chem.*, 1986, **39**, 1221.
[120] R. Batchelor and T. Birchall, *J. Am. Chem. Soc.*, 1982, **104**, 674.
[121] J. D. Donaldson and D. G. Nicholson, *Inorg. Nucl. Chem. Letters*, 1969, **6**, 151.
[122] N. Ohkaku and K. Nakamoto, *Inorg. Chem.*, 1973, **12**, 2240.
[123] R. Rivest, S. Singh, and C. Abraham, *Can. J. Chem.*, 1967, **45**, 3137.
[124] A. J. Carty, T. Hinsperger, L. Mihichuk, and H. D. Sharma, *Inorg. Chem.*, 1970, **9**, 2573.
[125] D. Cunningham, M. J. Frazer, and J. D. Donaldson, *Inorg. Phys. Theor.*, 1971, 2049.
[126] J. Philip, M. A. Mullins, and C. Curran, *Inorg. Chem.*, 1968, **7**, 1895.
[127] J. F. Malone and B. E. Mann, *Inorg. Nucl. Chem. Letters*, 1972, **8**, 819.
[128] R. Colton, D. Dakternieks, and C. A. Harvey, *Inorg. Chim. Acta*, 1982, **1**, 61.
[129] G. G. Mather, G. M. McLaughlin, and A. Pidcock, *J. Chem. Soc. Dalton Trans.*, 1973, 1823.
[130] G. Pelizzi, C. Pelizzi, and K. C. Molloy, *Main Group Metal Chem.*, 1988, **10**, 353.
[131] N. Bricklebank, S. M. Godfrey, C. A. McAuliffe, and R. Pritchard, 1994, J. Chem. Soc., Chem. Comm., 695.
[132] F. Kunkel, K. Dahnicke, H. Goesmann, and D. Fenske, *Z. Naturf., Teil B*, 1995, **50**, 848.
[133] C. Furlani, G. Mattogno, G. Polzonetti, P. Mauersberger, E. Rivarola, and A. Silvestri, *Inorg. Chim. Acta*, 1982, 121.

134 D. Dakternieks, H. Zhu, and E. R. Y. Tiekink, *Main Group Metal Chemistry*, 1994, **17**, 519.
135 N. N. Greenwood and A. Timnick, *Journal of the Chemical Society (A)*, 1971, 676.
136 J. D. Donaldson, *Prog. Inorg. Chem.*, 1967, **8**, 287.
137 L. R. Smith and J. L. Mills, *J. Am. Chem. Soc.*,1204, **98**,1976.
138 B. M. Yamin, O. B. Shawkataly, H.-K. Fun, and K. Sivakumur, *Acta Crystallogr., Sect. A: Found. Crystallogr.*, 1996, **C25**, 1966.
139 D. Tuleda, J. D. Tornero, A. Monge, and A. J. Sanchez-Herencia, *Inorg. Chem.*, 1993, **32**, 3928.
140 D. B. Mitzi, *Chem. Mater.*, 1996, **8**, 791.
141 R. G. Dickinson, *J. Am. Chem. Soc.*, 1923, **45**, 958.
142 D. B. Mitzi, D. R. Medeiros, and P. R. L. Malefant, *Inorg. Chem.*, 2002, **41**, 2134.
143 Z. Xu, D. B. Mitzi, C. D. Dimitrakopoulos, and K. R. Maxcy, *Inorg. Chem.*, 2003, **42**, 2031.
144 Z. Xu, D. B. Mitzi, and D. R. Medeiros, *Inorg. Chem.*, 2003, **42**, 1400.
145 D. B. Mitzi, C. A. Felld, W. T. A. Harrison, and A. M. Guloy, *Nature*, 1994, **369**, 467.
146 J. Guan, Z. Tang, and A. M. Guloy, *Chem. Comm.*, 1999, 1833.
147 D. B. Mitzi, S. Wang, C. A. Feild, C. A. Chess, and A. M. Guloy, *Science*, 1995, **267**, 1473.
148 J. A. C. Allison and F. G. Mann, *J. Am. Chem. Soc.*, 1949, 2915.
149 D. B. Mitzi, K. Liang, and S. Wang, *Inorg. Chem.*, 1998, **37**, 321.
150 S. Wang, D. B. Mitzi, C. A. Feild, and A. M. Guloy, *J. Am. Chem. Soc.*, 1995, **117**, 5297.
151 G. R. Willey, T. J. Woodman, R. J. Deeth, and W. Errington, *Main Group Metal Chemistry*, 1998, **21**, 583.
152 Bruker, Balashova, and Soborovskii, *Dokl. Bulg. Akad. Nauk*, 1960, **4**, 843.
153 Kuchen and Buchwald, *Ber. Bunsen-Ges. Phys. Chem.*, 1959, **92**, 227.
154 I.G.M. Campbell, G. W. A. Fowles, and L. A. Nixon, *J. Chem. Soc.*, 1964, 1389.
155 M.R. Hague and J. Prince, *Proc.Chem. Soc.*, 1962, 300.
156 D. Dakternieks and C. L. Rolls, *Inorg. Chim. Acta*, 1989, **161**, 105.
157 R. Colton and D. Dakternieks, *Inorg. Chim. Acta*, 1988, **148**, 31.
158 A. Slvestri, E. Rivarola, and R. Barbieri, *Inorg. Chim. Acta*, 1977, **23**, 149.
159 D. Hanssgen, H. Aldenhoven, and M. Nieger, *Chem. Ber*, 1990, **123**, 1837.
160 H. Schumann and L. Rosch, *J. Organomet. Chem.*, 1973, **55**, 257.
161 D. Hanssgen, H. Aldenhoven, and M. Nieger, *J. Organomet. Chem.*, 1989, **367**, 47.
162 T. L. Breen and D. W. Stephan, *Organometallics*, 1997, **16**, 365.
163 T. L. Breen and D. W. Stephan, *J. Am. Chem. Soc.*, 1995, **117**, 11914.
164 D. Hanssgen, T. Oster, and M. Nieger, *J. Organomet. Chem.*, 1996, **526**, 59.
165 A. Elvers, F. W. Heinemann, B. Wrackmeyer, and U. Zenneck, *Chem.Eur.J.*, 1999, **5**, 3143.
166 H. Schumann, P. Schwabe, and M. Schmidt, *Inorg. Nucl. Chem. Letters*, 1966, **2**, 309.
167 V. G. Engelhardt, *Z. Anorg. Allg. Chem.*, 1972, **387**.
168 H. Schumann, H. Kopf, and M. Schmidt, *Chem. Ber*, 1964, 2395.
169 H. Schumann and M. Schmidt, *Angewandte Chemie. Internat. Edit*, 1965, **4**, 1007.
170 H. Schumann and G. Rodewald, *J. Organomet. Chem.*, 1980, **190**, 53.
171 K. C. Molloy, F. A. K. Nasser, C. L. Barnes, D. van der Helm, and J. J. Zuckermann, *Inorg. Chem.*, 1982, **21**, 960.
172 J. G. Masters, F. A. K. Nasser, M. B. Hossain, A. P. Hagen, D. van der Helm, and J. J. Zuchermann, *J. Organomet. Chem.*, 1990, **385**, 39.

[173] M. G. Newton, I. Haiduc, R. B. King, and C. Silvestru, *Journal of Chemical Society, Chem. Comm.*, 1993, 1229.
[174] H. G. Horn and K. Sommer, *Spectrochim. Acta, Part A*, 1971, **27**, 1049.
[175] H. Schumann, G. Rodewald, J. L. Lefferts, and J. J. Zuchermann, *J. Organomet. Chem.*, 1980, **190**, 53.
[176] H. Schumann and L. Rosch, *Chem. Ber*, 1974, **107**, 854.


Packard Bell
CD-R
52x Speed
700MB
80 minutes
SnapBake
Polyfile CD Pocket
Write with soft tip pen only. Do not scratch. Avoid exposure to heat or direct sunlight.